DEVELOPMENT OF A SMART SENSING SYSTEM FOR EARLY DETECTION OF OSTEOPOROSIS

By

NASRIN AFSARIMANESH

A thesis submitted to Macquarie University
for the degree of
Doctor of Philosophy
School of Engineering

May 2018

MACQUARIE
University
SYDNEY·AUSTRALIA

To my parents

Parvin Mohabatkar

Reza Afsarimanesh

and

To my husband

Ghobad Shafiei Sabet

STATEMENT OF CANDIDATE

I certify that the work in this thesis has not previously been submitted for a degree nor has it been submitted as part of the requirements for a degree to any other university or institution other than Macquarie University.

I also certify that the thesis is an original piece of research and it has been written by me.

In addition, I certify that all information sources and literature used are indicated in the thesis.

.....

Nasrin Afsarimanesh

Acknowledgements

First, I would like to express my deepest and sincerest gratitude to my supervisors, ***Professor Subhas Mukhopadhyay*** and ***Professor Marlena Kruger*** for their excellent support, advice and encouragement through my research. This work would not have been possible without their great knowledge and patient guidance.

I am grateful to all of those with whom I have had the pleasure to work during this project at Massey University, New Zealand. I would especially like to thank Asif Zia, who helped me to understand and progress with my project during the initial months of my PhD candidature. I would also like to thank Diana Leticia Cabrera Amaro, Krishanthi Jayasundera, Gabrielle Plimmer, Niki Murray and John Sykes for their technical assistance.

I am also thankful to the technical and administrative staff from the School of Engineering, Macquarie University for their great support during my research period. I also would like to extend my thanks to Dr Keith Imrie for his valuable suggestions and comments that made significant improvements in my thesis.

Words cannot express my gratitude and appreciation to my parents and siblings- Nasim and Kourosh- for the constant motivation and support they have provided throughout my life. Very special thanks to my husband whose love, patience and encouragement helped me to go through this journey and finish it successfully.

Last but not least, I would like to thank my friends and colleagues, Anindya Nag, Md Eshrat E Alahi, Van Nguyen Thi Phuoc, Shilun Feng, Fifi Zaefarian, Reza Abdollahi, Nazanin Nourifar, Elham Ebrazeh and Elham Khanipour who have always stood beside me and helped me in times of need.

Research Outputs

Publications related to the field of this thesis are as follows.

Journals

1. ***Nasrin Afsarimanesh,*** S. C. Mukhopadhyay and M. Kruger. "Performance Assessment of Interdigital Sensor for Varied Coating Thicknesses to Detect CTX-I", IEEE Sensors Journal, vol. 18, no. 10, pp. 3924-3931, May 2018.
2. ***Nasrin Afsarimanesh,*** M. E. E. Alahi, S. C. Mukhopadhyay and M. Kruger. "Development of IoT-Based Impedometric Biosensor for Point-of-Care Monitoring of Bone Loss", IEEE Journal on Emerging and Selected Topics in Circuits and Systems, March 2018. **DOI:** 10.1109/JETCAS.2018.2819204
3. ***Nasrin Afsarimanesh***, S. C. Mukhopadhyay and M. Kruger. "Sensing Technologies for Monitoring of Bone-Health: A Review", Sensors and Actuators A: Physical, vol.274, pp. 165-178, March 2018.
4. ***Nasrin Afsarimanesh***, M. E. E. Alahi, S. C. Mukhopadhyay, and M. Kruger, "Smart Sensing System for Early Detection of Bone Loss: Current Status and Future Possibilities", Journal of Sensor and Actuator Networks, vol. 7, no. 1, pp. 1-11, February 2018.
5. A. Nag, ***Nasrin Afsarimanesh***, S. Feng. and S. C. Mukhopadhyay, "Strain Induced Graphite/PDMS Sensors for Biomedical Applications", Sensors and Actuators A, vol. 271, pp. 1-14, March 2018.
6. ***Nasrin Afsarimanesh,*** S. C. Mukhopadhyay and M. Kruger. "Molecularly Imprinted Polymer-Based Electrochemical Biosensor for Bone Loss Detection". IEEE Transactions on Biomedical Engineering, vol. 65, no. 6, pp. 1264-1271, June 2018.
7. ***Nasrin Afsarimanesh***, S. C. Mukhopadhyay and M. Kruger. "Biosensors for the Measurement of C-Terminal Telopeptide of Type I Collagen (CTX-I)", Journal of Osteoporosis and Physical Activity, vol 5, no.1, April 2017. **DOI:** 10.4172/2329-9509.1000199
8. ***Nasrin Afsarimanesh***, Asif I. Zia, S. C. Mukhopadhyay, M. Kruger, P. L. Yu, J. Kosel, and Z. Kovacs. "Smart Sensing System for the Prognostic Monitoring of Bone Health". Sensors 16, no. 7, pp. 1-13, June 2016.

Conference Proceedings

1. ***Nasrin Afsarimanesh***, M. E. E. Alahi, S. C. Mukhopadhyay, M. Kruger. "A Novel Electrochemical Biosensor for Bone Turnover Detection Based on Molecular Imprinting Technology", Proceedings of the 11th International Conference on Sensing Technology (ICST), pp. 1-6, Sydney, Australia, 4-6 December 2017.
2. M. E. E. Alahi, ***Nasrin Afsarimanesh,*** S. C. Mukhopadhyay, L. Burkitt. "Development of the Selectivity of Nitrate Sensors Based on Ion Imprinted Polymerization Technique", Proceedings of the 11th International Conference on Sensing Technology (ICST) , pp. 1-6, Sydney, Australia, 4-6 December 2017.
3. ***Nasrin Afsarimanesh***, M. E. E. Alahi, S. C. Mukhopadhyay, M. Kruger, P. L. Yu. "Development of Molecular Imprinted Polymer Interdigital Sensor for C-Terminal Telopeptide of Type I Collagen", Proceedings of the 10th International Conference on Sensing Technology (ICST), pp. 143-147, Nanjing, China, 11-13 November 2016.
4. M. E. E. Alahi, ***Nasrin Afsarimanesh***, S. C. Mukhopadhyay, L. Burkitt, P. L. Yu, "Highly Selective Ion Imprinted Polymer based Interdigital Sensor for Nitrite Detection", Proceedings of the 10th International Conference on Sensing Technology (ICST) , pp. 30-34, Nanjing, China, 11-13 November 2016.
5. ***Nasrin Afsarimanesh***, S. C. Mukhopadhyay, M. Kruger, P. L. Yu, J. Kosel. "Sensors and Instrumentation towards early detection of Osteoporosis". Proceedings of the IEEE: International Instrumentation and Measurement Technology Conference (I²MTC), pp. 1394-1399, Taipei, Taiwan. 23-26 May 2016.
6. ***Nasrin Afsarimanesh***, A. I. Zia, S. C. Mukhopadhyay, M. Kruger, P. L. Yu, J. Kosel. "Development of a Sensing System to detect C-telopeptide of Type-I Collagen". Proceedings of the International Conference on Sensing Technology (ICST), pp. 629-633, Auckland, New Zealand, 8-10 December, 2015.
7. Asif Iqbal Zia, ***Nasrin Afsarimanesh***, Anindya Nag, Li Xie, S. C. Mukhopadhyay, Pak Yu, Ibrahim Al-Bahadly, Jürgen Kosel. "Improved Detection Limits for Phthalates by Selective Solid-phase Micro-extraction". Proceedings of the International Conference on Sensing Technology (ICST), pp. 803-808, Auckland, New Zealand, 8-10 December, 2015.

Book chapters

1. M. E. E. Alahi., A. Nag, Nasrin ***Afsarimanesh***, S. C. Mukhopadhyay, and J. K. Roy, "A simple Embedded Sensor: Excitation and Interfacing", Advanced Interfacing Techniques for Sensors, Smart Sensors, Measurement and Instrumentation series of Springer-Verlag, vol. 25, pp. 111-138, 2017.
2. ***Nasrin Afsarimanesh***, S. C. Mukhopadhyay, M. Kruger, P. Yu, "Sensing System for Bone Health Monitoring", in Sensors for Everyday Life, Smart Sensors, Measurement and Instrumentation series of Springer-Verlag, pp. 1-19, 2016.

Google scholar

https://scholar.google.com.au/citations?user=LtmkIUYAAAAJ&hl=en

Awards

1. Awarded "WiMED Student Prize" Macquarie University of 1500 AUD.
2. Awarded "Student Travel Grant" for I2MTC 2016 in the amount of 750 USD.
3. Awarded second-place runner up, **"**A smart Sensing System for Early Detection of Osteoporosis", IEEE Post Graduate Presentations. 20th Oct 2015. Massey University, Palmerston North, New Zealand.

Seminars

1. Presented at the 11th International Conference on Sensing Technology (ICST) 2017, Sydney, Australia, 4-6 November 2017.
2. Presented at the IEEE IMS NSW Chapter Annual Workshop, Sydney, Australia, 22 November 2017.
3. Presented at the 10th International Conference on Sensing Technology (ICST) 2016, Nanjing, China, 11-13 November 2016.
4. Presented at the International Instrumentation and Measurement Technology Conference (I²MTC) 2016, Taipei, Taiwan. 23-26 May 2016
5. Presented at the 9th International Conference on Sensing Technology (ICST) 2015, Auckland, New Zealand, 8-10 December 2015.
6. Nasrin Afsarimanesh. "A smart Sensing System for Early Detection of Osteoporosis". IEEE Post Graduate Presentations. 20th Oct 2015. Massey University, Palmerston North, New Zealand.

Abstract

Early detection of any disease is essential for an efficient treatment. Bone loss can be detected and monitored by regular measurement of serum or urine C-terminal telopeptide of type 1 collagen (CTx-I). Therefore, rapid, sensitive, accurate, portable and low-cost point-of-care devices are highly desirable. In this research, we have proposed a selective, sensitive, quick and inexpensive Internet of Things (IoT)-based device for the quantification of CTx-I levels in serum. A capacitive interdigital sensor with multi-sensing-electrode configuration was employed to perform the experiments. Initially, natural antibodies were used to introduce selectivity for the target molecule. In spite of the high selectivity and sensitivity of the proposed system, there were some limitations in using natural antibodies. Natural antibodies are very expensive, sensitive to harsh environmental conditions and have limited stability. In order to overcome these limitations, the interdigital sensor was coated with artificial antibodies, prepared by molecular imprinting technology. Electrochemical impedance spectroscopy was used to evaluate the resistive and capacitive properties of the sample solutions. A microcontroller-based system was developed for the measurement of the level of CTx-I in serum and for data transmission to an IoT-based cloud server. The data can be provided to the medical practitioner and a detailed investigation can start for early detection and treatment. The developed sensing system responded linearly in a range of 0.1 ppb to 2.5 ppb, which covers the normal reference range of CTx-I in serum, with a limit of detection (LOD) of 0.09 ppb. The results demonstrated that the proposed portable biosensing system could provide a rapid, simple and selective approach for CTx-I measurement in serum. Sheep serum samples were tested using the proposed system and the validation of the results was done using an enzyme-linked immunosorbent assay (ELISA) kit.

Contents

Acknowledgements ..... **iii**

Research Outputs ..... **iv**

Abstract ..... **vii**

Glossary ..... **xiii**

List of Figures ..... **xv**

List of Tables ..... **xix**

Introduction **1**

1.1 What is Osteoporosis? 2

1.2 Osteoporosis Facts and Statistics 3

1.3 Osteoporosis Diagnosis 5

1.4 Motivation 6

1.5 Objectives 6

1.6 Research Contributions 7

1.7 Thesis Outline 8

Literature Review **11**

2.1 Introduction 12

2.2 Bone Structure 13

2.3 Biochemical Markers of Bone Turnover 14

2.3.1 Biochemical Markers of Bone Formation 15

2.3.2 Biochemical Markers of Bone Resorption 16

2.4 Analytical Methods for the Measurement of Bone Turnover Markers 20

2.4.1 Enzyme-Linked Immunosorbent Assay 20

2.4.2 Radioimmunoassay 21

2.4.3 High-Performance Liquid Chromatography 22

2.5 Current Advancements in Bone Biosensors 24

2.5.1 Biomechanical Sensors 24

2.5.2 Biomarker-based Sensors 30

2.5.3 Multiplex Assays 33
2.5.4 EIS-based sensor 33
2.6 Chapter Summary 35

Planar Interdigital Sensors and Electrochemical Impedance Spectroscopy 37
3.1 Operating Principle of Interdigital Sensors 38
3.2 Novel Planar Interdigital Sensors 40
3.2.1 Sensors Fabrication 41
3.3 Electrochemical Impedance Spectroscopy (EIS) 43
3.4 Experimental Setup 47
3.5 Chapter Summary 50

Antigen-antibody-based Sensor for CTx-I Detection 51
4.1 Introduction 52
4.2 ELISA-based Experiments 52
4.2.1 Materials and Chemicals 53
4.2.2 Assay Procedure 53
4.2.3 Results 55
4.3 Ag-Ab-based Biosensor 56
4.3.1 CTx-I Measurement in Known Samples 57
4.3.2 Data Analysis Using Non-linear Least-Square Curve Fitting 59
4.3.3 Multivariate Chemometric Analysis 61
4.3.4 CTx-I Measurement in Unknown Samples using the Ag-Ab-based Biosensor 64
4.4 Chapter Summary 65

MIP-based Sensor for CTx-I Detection 67
5.1 Introduction 68
5.2 General Principle of Molecular Imprinting Technology 68
5.2.1 MIP Categories 70
5.2.2 Effects of Monomers, Cross-linker, Porogenic Solvents and Initiator in MIP 71
5.2.3 Preparation Methods of MIP 75
5.3 Materials and Methods 75
5.3.1 Materials and Apparatus 75

5.3.2 Preparation of Artificial Antibodies using Molecular Imprinting Technology ……76
5.3.3 Preparation of the Functionalised Biosensing Surface ……77
5.3.4 Preparation of the CTx-I Samples……78
5.3.5 Experimental Measurements……78
5.4 Results and Discussions……78
5.4.1 SEM Characterisation ……79
5.4.2 Sorption Studies of CTx-I to MIP and NIP ……79
5.4.3 EIS Measurement and Analytical Measurement……82
5.4.4 CNLS–based Biosensor Response……84
5.4.5 Measurement of CTx-I in Real Serum Samples using the CNLS–based calibration Curve……87
5.4.6 Single-frequency Reactance–based Biosensor Response ……87
5.4.7 Measurement of CTx-I in Real Serum Samples using Single-frequency-based Calibration Curve……88
5.4.8 Comparison Between the CNLS-based Measurement and Single-frequency Measurement……89
5.5 Performance Assessment of Interdigital Sensor for Varied Coating Thicknesses ……89
5.5.1 Coating the Sensing Surface with Acrylic……90
5.5.2 Coating the Sensing Area with Selective Material ……91
5.5.3 CTX-I Measurement using the Coated Interdigital Sensor……93
5.5.4 Sensitivity of the Coated Sensor and the Saturation Level……95
5.5.5 Dependence of Coating Thickness on Withdrawal Speed and Dipping Time ……98
5.6 Chapter Summary ……99

IoT-enabled Microcontroller-based System……101
6.1 Introduction……102
6.2 Electrochemical Impedance Monitoring using the Microcontroller-based System ……103
6.2.1 Block Diagram of the Point-of-Care System……103
6.2.2 Circuit Diagram of the Proposed System……104
6.2.3 Software Process Flow of the PoC Device ……105

6.3 Results and Discussion 107
6.3.1 Calibration Curve Development from the Proposed System 107
6.3.2 Unknown Sample Measurement 108
6.3.3 IoT Data from the Point-of-care Device 111
6.4 Chapter Summary 111

Conclusion and Future Work 113
7.1 Conclusion 114
7.2 Future Possibilities 114

References 119

Glossary

AC	Alternating Current
ACN	Acetonitrile
AIBN	2,2-azoisobutronitrile
ANN	Artificial Neural Network
AP	Alkaline Phosphatase
BAP	Bone-specific AP
BM	Bone Metastasis
BMBT	Biochemical Markers of Bone Turnover
BMD	Bone Mineral Density
BSP	Bone sialoprotein
C	Capacitance
Ca^{2+}	Calcium ion
C_{dl}	Double-layer capacitance
CNLS	Complex non-linear least-square
CNT	Carbon nanotube
CPE	Constant Phase Element
Cr	Chromium
CTx-I	C-terminal telopeptide of type-I collagen
DC	Direct Current
DDS	Direct Digital Synthesis
DPD	Deoxypyridinoline
DXA	Dual-energy X-ray absorptiometry
ECLIA	Electrochemiluminescence
EGDMA	Ethylene glycol methacrylate
EIS	Electrochemical Impedance Spectroscopy
ELISA	Enzyme-linked immunosorbent assay
FRF	Frequency-response function
GF	Gauge Factor
GGHL	Glycosyl-galactrasyl-hydroxylysine
GHL	Galactrasyl-hydroxylysine
HPLC	High-Performance Liquid Chromatography
ICTP	Carboxy-terminal crosslinked telopeptide of type I collagen
IDE	Integrated Development Environment
IIP	Ion Imprinted Polymers
IoT	Internet of Things
ITA	Itaconic acid
LOD	Limit of Detection

MAA	Methacrylic acid
MEMS	Micro-Electro-Mechanical Systems
MeOH	Methanol
MIP	Molecular Imprinted Polymer
MMP	Matrix metalloptoteinase
MUT	Material Under Test
NIP	Non-imprinted polymer
NTx-I	N-terminal telopeptide of type-I collagen
OC	Osteocalcin
OHP	Hydroxyproline
OPG	Osteoprotegerin
PC	Principlal Component
PDMS	Poly-dimethyl-siloxane
PoC	Point of care
PTH	Parathyroid hormone
PYD	Pyridinoline
QCM	Quartz-crystal microbalance
R	Resistance
RANKL	Receptor activator of NF-kB ligand
R_{ct}	charge transfer resistance
RIA	Radioimmunoassay
R_s	Solution resistance
SAM	Self-assembled monolayer
SEM	Scanning electron microscope
Si	Silicon
SiO2	Silicon Dioxide
SPR	Surface Plasmon Resonance
SSID	Service Set Identifier
SWCNT	Single-wall carbon nanotubes
TRACP	Tartrate-resistant acid phosphatase
VACNT	Vertically aligned CNT
WHO	World Health Organization
WIPSS	Wireless Implantable Passive Strain Sensor
X	Reactance
Z	Impedance

List of Figures

Figure 1.1 Depicting healthy bone and osteoporotic bone [1]. 2
Figure 1.2 Proportion of men and women worldwide above a fracture threshold by age calculated in 2010 [3]. 3
Figure 1.3 Proportions of osteoporotic fractures in Australia. 4
Figure 1.4 Dual-energy X-ray absorptiometry (DXA) [11]. 5
Figure 2.1 A graphical representation of bone markers, generated during various stages of bone remodelling. 14
Figure 2.2 Schematic representation of type I procollagen Propeptides [21]. 16
Figure 2.3 Schematic representation of collagenous bone resorption markers [52]. 16
Figure 2.4 Different types of Enzyme-Linked Immunosorbent Assay (ELISA) techniques. 20
Figure 2.5 Radioimmunoassay (RIA) principle. 21
Figure 2.6 Schematic diagram of HPLC instrumentation. 22
Figure 2.7 Block diagram of the IMPACT 3500 system [96]. 25
Figure 2.8 Flexible, highly sensitive strain gauge based on reversible interlocked nanofibers [98]. 26
Figure 2.9 Schematic of the wireless implantable passive strain sensor concept [101]. 27
Figure 2.10 Schematic of the implantable CMOS-MEMS multi-axis stress sensor [109]. 28
Figure 2.11 Schematic of the experimental setup developed for monitoring bone decalcification using a fiber Bragg-grating sensor [112]. 29
Figure 2.12 Schematic illustration of a label-free CTx-I biosensor developed by Yun et al. [115]. 31
Figure 2.13 Schematic illustration of biosensing surface preparation and sample testing of the immunosensor developed by Ramanathan et al. [119]. 32

Figure 3.1 Transition from the parallel-plate capacitor to a planar capacitor. 38
Figure 3.2 Geometric structure of conventional planar Interdigital sensor. 39
Figure 3.3 Electric field formed for different pitch lengths [129]. 39
Figure 3.4 Schematic excitation patterns for multi-sensing-electrode interdigital sensors. 40
Figure 3.5 1-5-25 and 1-11-25 configurations of novel interdigital sensors. 41
Figure 3.6 Silicon wafer sensors fabricated using MEMS technology. 42
Figure 3.7 Fabrication process of novel interdigital sensors. 43
Figure 3.8 Phase shift in current signal with reference to the applied voltage. 44
Figure 3.9 Nyquist plot obtained from EIS measurements. 46
Figure 3.10 Block diagram of the measurement system, including power supply, planar interdigital sensor, measurement instrument and auto measurement. 47
Figure 3.11 Experimental setup of the measurement system including the LCR meter and interdigital sensor. 48
Figure 3.12 The front panel of a high precision HIOKI IM3536 LCR Meter (Japan) [153]. 49
Figure 4.1 Flow chart of ELISA procedure. 54
Figure 4.2 The standard curve plotted from the ELISA results. 55
Figure 4.3 SEM image of streptavidin agarose-coated sensing surface, showing streptavidin agarose coating on the gold electrodes. 56
Figure 4.4 Graphical illustration of the steps required to prepare the sensing surface for CTx-I sensing. 57
Figure 4.5 (a) Imaginary part (reactance) of the impedance vs frequency; (b) Real part of the impedance vs frequency. 58
Figure 4.6 Imaginary part (reactance) of the impedance vs frequency. 59
Figure 4.7 Proposed equivalent circuit by CNLS with a parallel combination of a constant-phase element (CPE1) and a charge-transfer resistance (R2) in series with the solution resistance (R1). 60
Figure 4.8 (a) Principal Component Analysis score plot (PC1-PC2); (b) Principal Component Analysis loadings plot (PC1-PC2). 62
Figure 4.9 (a) Partial Least-Square Regression model to regress on CTx-I concentration (red colour is for calibration and the blue colour is for the cross-validation model), (b) regression vector of Partial Least-Square Regression model showing 710 Hz as the most discriminating frequency. 63

Figure 4.10 The reference calibration curve for the sensitivity of the sensor vs. concentration evaluated at 710 Hz. 65

Figure 5.1 General principle of molecular imprinting technology. A template molecule (*T*) is mixed with functional monomers (*M*) and a cross-linker (*CL*) forming a self-assembled complex (*1*). The polymerisation of the resulting system produces a highly cross-linked structure including imprinted sites (*2*). Finally comes the extraction of the template living cavities that can selectively recognise and bind the target molecule (*3*) 69

Figure 5.2 Chemical structure of common functional monomers used in non-covalent molecular imprinting [186]. 72

Figure 5.3 Common cross-linkers used in non-covalent molecular imprinting [186]. 73

Figure 5.4 Chemical structure of some initiators used in non-covalent MIP [186]. 74

Figure 5.5 Schematic diagram of the biosensing surface preparation for CTx-I recognition. 77

Figure 5.6 (a) SEM image of MIP-coated biosensing surface and (b) SEM image of the MIP-coated sensor to show the thickness of the coating layer. 79

Figure 5.7(a) Uptake kinetics of CTx-I to MIP and NIP, and (b) Isotherms for static adsorption capacity of CTx-I to MIP and NIP. 81

Figure 5.8 Nyquist plot for various concentrations of CTx-1 molecules. 82

Figure 5.9 Imaginary part of impedance (Reactance) vs. frequency for various concentrations of CTx-1 molecules. 83

Figure 5.10 Real part of impedance (Resistance) vs frequency for various concentrations of CTx-1 molecules. 83

Figure 5.11 Reactance value for five times reading to show the consistency of the biosensor. 84

Figure 5.12 The Nyquist plot and its corresponding Randle's model estimated by CNLS analysis. 85

Figure 5.13 CNLS-based calibration curve, representing changes in R_{ct} for various concentrations of CTx-I. 86

Figure 5.14 Single-frequency reactance-based calibration curve, representing changes in reactance X to various concentrations of CTx-I measured at 319 Hz. 88

Figure 5.15 Graphical illustration of dip-coating technique [220]. 90

Figure 5.16 SEM image of acrylic-coated sensor to show the coating layer. 91

Figure 5.17 SEM image of MIP-coated sensor to show the coating layer. 92

Figure 5.18 (a) Selective layer development and (b) Coated sensor. 92
Figure 5.19 Measurement of CTx-I samples by acrylic-coated sensor with various coating thicknesses: (a) 30 µm, (b) 65 µm, (c) 100 µm, and (d) 145 µm 93
Figure 5.20 Measurement of CTx-I samples by MIP-coated sensor with various coating thicknesses: (a) 40 µm, (b) 75 µm, (c) 130 µm, and (d) 165 µm. 94
Figure 5.21 Calibration curves for the acrylic-coated sensor with different coating thicknesses: (a) 30 µm, (b) 65 µm and (c) 100 µm. 95
Figure 5.22 Calibration curves for the MIP-coated sensor with different coating thicknesses: (a) 40 µm, (b) 85 µm and (c) 130 µm. 96
Figure 5.23 Sensitivity of the MIP-coated sensor and the acrylic-coated sensor. 97
Figure 5.24 Saturation level of the coated sensor. 97
Figure 5.25 Speed-dependent thickness of the coated sensor. 98
Figure 5.26 Time-dependent thickness of the coated sensor. 99
Figure 6.1 Complete Block diagram of the point-of-care system. 104
Figure 6.2 Circuit diagram of the proposed point-of-care device. 105
Figure 6.3 Software flow of the point-of-care device for CTx-1 calculation and transfer to the IoT cloud server 106
Figure 6.4 First prototype of the point-of-care system**.** 107
Figure 6.5 Calibration standard of the PoC device. 108
Figure 6.6 Comparison between the PoC results and the ELISA results. 110
Figure 6.7 Correlation analysis between the proposed PoC device and a standard ELISA kit for CTx-I measurement. 110
Figure 6.8 Real-time data from developed point-of-care device. 111
Figure 7.1 Schematic representation of Ca^{+2}- IIP method. 116
Figure 7.2 Schematic diagram of the proposed sensor array for simultaneous measurement of CTx-I, creatinine and calcium in urine. 116
Figure 7.3 Schematic diagram of the possible smart toilet for continuous monitoring of bone-loss. 117

List of Tables

Table 1.1 T-score ranges for different categories of bone density according to WHO [15]. 5

Table 2.1 Biochemical markers of bone turnover. 19

Table 2.2 Comparison of most commonly used analytical methods for the measurement of bone turnover markers. 23

Table 2.3 Some of the existing bone biosensors and their characteristics. 34

Table 3.1 Geometric design parameters for four types of Interdigital sensors. 40

Table 3.2 Specification overview of HIOKI IM3536 LCR meter. 49

Table 4.1 Comparison between the known concentrations and measured concentrations using the ELISA kit. 55

Table 4.2 Equivalent Circuit Parameters. 61

Table 4.3 Unknown sample measurement and validation with standard ELISA method. 65

Table 5.1 Summary of different preparation methods of MIP. 76

Table 5.2 Equivalent circuit parameters for different CTx-I concentrations. 85

Table 5.3 Determination of CTx-I concentration in real serum samples using the CNLS-based calibration curve. 87

Table 5.4 Determination of CTx-I concentration in real serum samples using the **single-frequency calibration curve.** 88

Table 6.1 Unknown sample measurement and validation with standard ELISA method. 109

1

Introduction

1.1 What is Osteoporosis?

Osteoporosis literally means “porous bones”. It is a disorder of bone which causes bones to become brittle, weak and more likely to fracture. The bone loss happens silently and continuously. Often there are no signs or symptoms of osteoporosis until a fracture happens. That is why it is often called the “silent disease”. Figure 1.1 depicts the status of a normal bone and an osteoporotic bone. Osteopenia is an intermediate state of bone loss in which the bone density is between the normal level and osteoporosis.

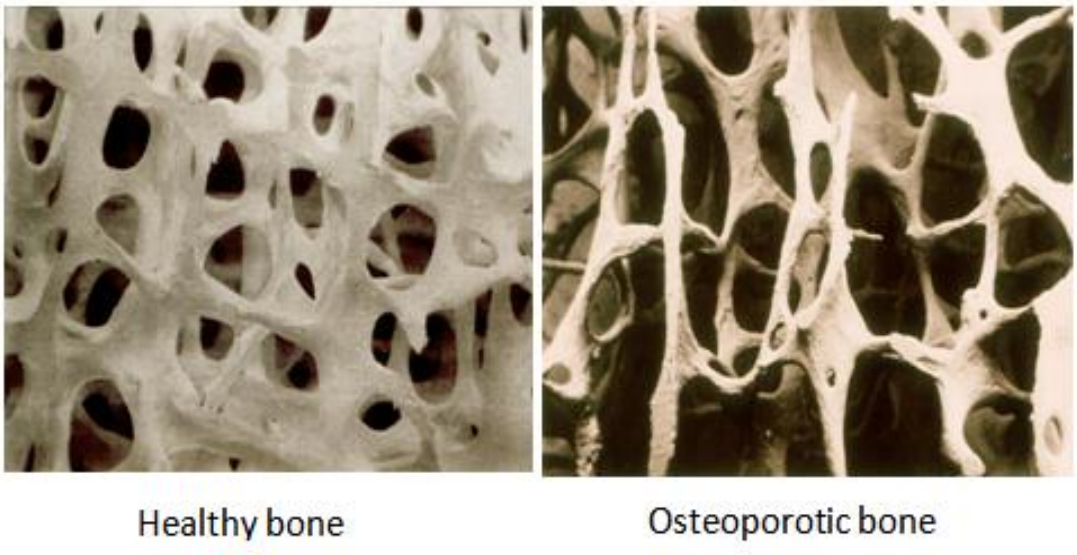

Figure 1.1 Depicting healthy bone and osteoporotic bone [1].

Osteoporosis can affect any bones, but most commonly:

- Hip
- Spine
- Wrist
- Ribs
- Pelvis
- Upper arm

1.2 Osteoporosis Facts and Statistics

The WHO reported that the world's population is rapidly ageing and predicted that the number of people living to 60 years and more will increase from 900 million to 2 billion between 2015 and 2050 [2]. A consequence of this increase is an increase in the number of people who suffer from serious health disorders such as osteoporosis.

In an article published in 2015, Odén et al. estimated that 158 million people in the world, over the age of 50, are at risk of developing osteoporosis, based on the data collected in 2010. Moreover, they evaluated that this number will double by 2040 [3]. According to this article, the proportion (%) of men and women worldwide above the fracture threshold obtained in 2010 is given in Figure 1.2. In this study the increased with age was not indicated in males but increased continuously with age in females. In the range of 50 to 54 years, 12% crossed the threshold and this increased continuously with age to 30% in the age category of 80 to 84 years.

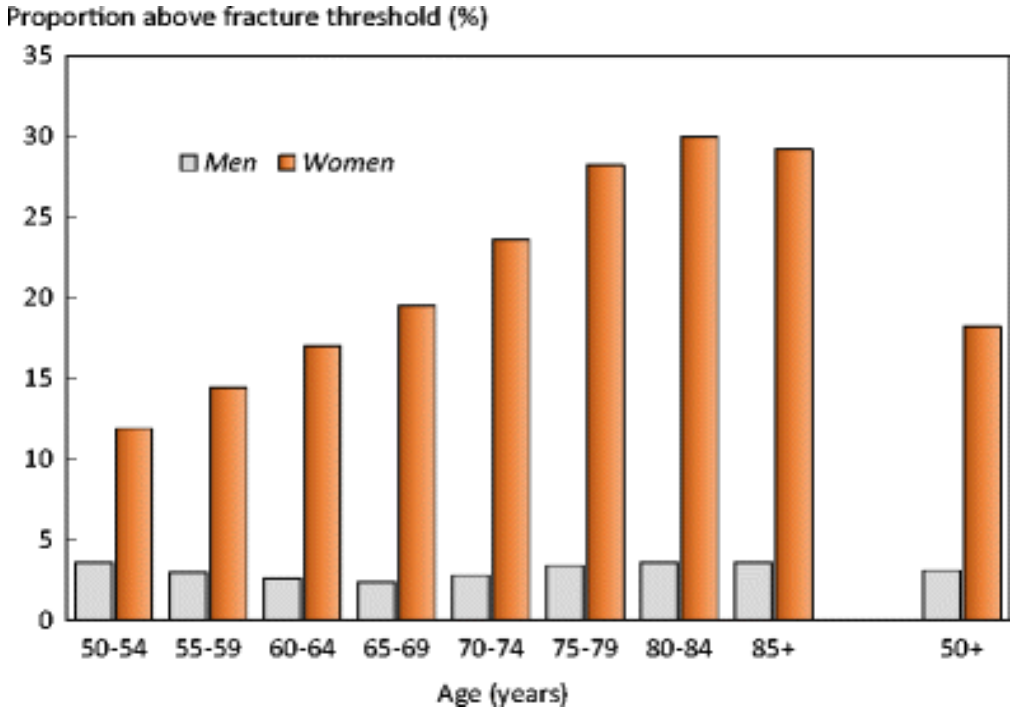

Figure 1.2 Proportion of men and women worldwide above a fracture threshold by age calculated in 2010 [3].

Osteoporosis in Australia- Almost two million Australians (nearly 10% of the population) have an osteoporosis-related problem, and 75% of them are women. 1 in 2 Australian women will experience a fracture related to osteoporosis after age 60 [4]. Among all the osteoporotic fractures in Australia, nearly half are fractures of the spine followed by fractures of the hip and wrist as shown in Figure 1.3.

In terms of economic impact, it is estimated the direct cost on osteoporosis in 2008-2009 will be $306 million [5]. A broader study conducted by Osteoporosis Australia estimated the direct and indirect expenditure on osteoporosis in Australia to be $2,754 million in 2012 [6].

It is reported that [6] that 4.74 million people in Australia over 50 years of age (nearly 66% of the people over 50) are suffering from osteoporosis or osteopenia, where 22% of them have osteoporosis and 78% have osteopenia. It is predicted that, by 2022, there would be 6.2 million Australians over 50 with osteoporosis or osteopenia, which is a 31% increase from 2012.

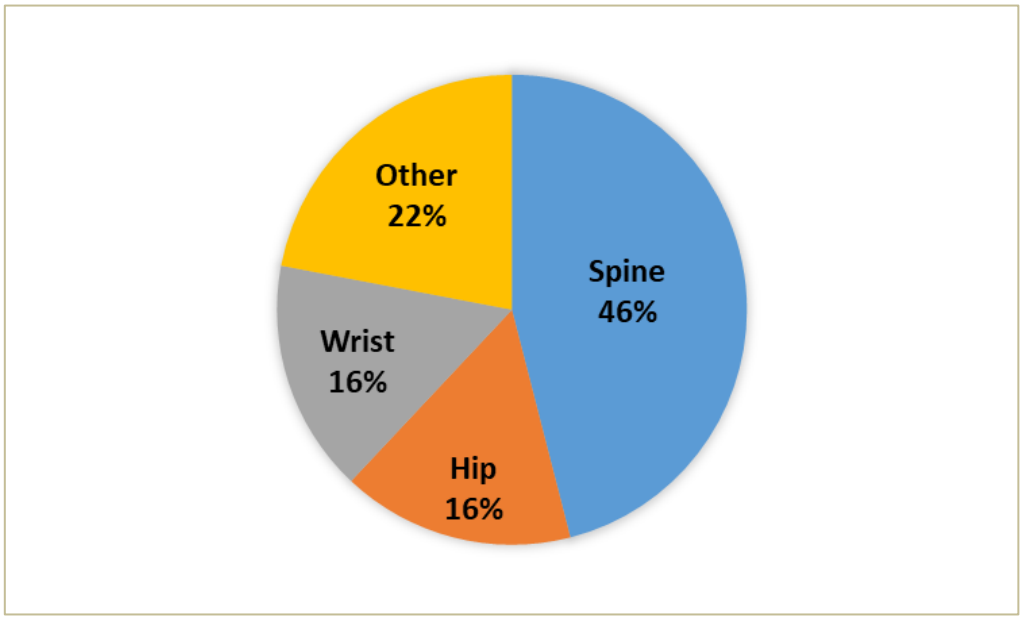

Figure 1.3 Proportions of osteoporotic fractures in Australia.

1.3 Osteoporosis Diagnosis

Dual-energy X-ray absorptiometry (DXA) [7] is the most reliable way and the gold standard technique to measure bone mineral density (BMD) [8]. DXA scans can be used to diagnose osteoporosis and monitor the effect of therapy. This method uses dual X-ray beams at high and low photon energies [9]. A certain amount of X-ray transmission is blocked by bone. Dense bones allow less of X-rays to pass through them and get to the detector. This data is sent to a computer which calculates a T-score of the average density of the bones. The T-score is a comparison of a person's bone density with that of a healthy 30-year-old of the same sex. A low T-score shows that the bone is less dense than it should be [10]. T-score ranges are specified in Table 1.1.

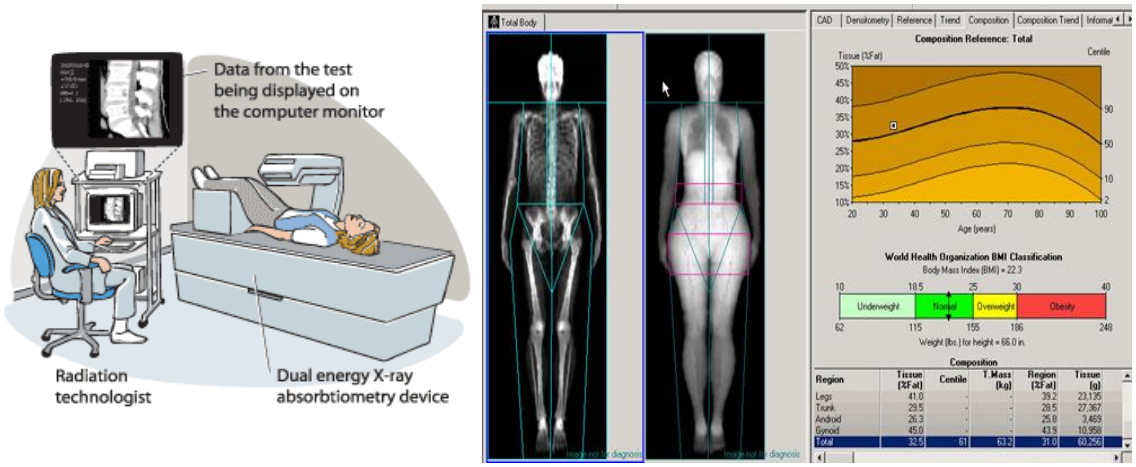

Figure 1.4 Dual-energy X-ray absorptiometry (DXA) [11].

In spite of the excellent reliability of the DXA method, there is a major limitation in this technique. As changes in bone mineral density (BMD) are very slow, it takes more than two years for DXA to be able to detect changes in BMD, while changes in biochemical markers may be identified after only a few weeks [12]. Thus, measurement of BMD along with the detection and measurement of biochemical markers such as CTx-I can aid in monitoring the disease and improve the response to treatment.

There are different types of biochemical markers of bone turnover in serum and urine, which are discussed in detail in Chapter 2. Among all of them, measurements of urinary and serum CTx-I are the most accurate and sensitive tests [13, 14].

Table 1.1 T-score ranges for different categories of bone density according to WHO [15].

T-SCORE RANGES	
Normal bone density	-1.0 to 0
Bone density for osteopenia	-2.5 to -1
Bone density for osteoporosis	-2.5 or less

1.4 Motivation

The impact of osteoporosis is far greater than that of many other serious health problems, like breast and prostate cancers. Statistically, one in three women and one in five men over 50 years of age will experience osteoporotic fractures in their life. The symptoms of osteoporosis are not evident at early stages, so early detection is the key factor for efficient osteoporosis management. It is also crucial for opportune recognition and treatment of people who are at risk of developing osteoporotic fractures. Thus, early detection can highly reduce the risk of future fractures by starting treatment at early stages of the disease when it is more beneficial. The therapies provided at the right time can manage osteoporosis only if it is identified at an early stage [16, 17]. The main reasons that motivated me towards the development of a smart sensing system for bone-loss monitoring can be summarised as follows:

- The limitations of the available methods for early detection of osteoporosis,
- Lack of a domestic PoC device which can be used by any person for a regular check-up, and
- The huge costs related to Measurement of bone health.

1.5 Objectives

The objective of this research is to design, fabricate and implement a portable smart sensing system for early detection of bone loss by characterisation and quantification of a biochemical marker (CTx-I) in blood that is:

- Robust, efficient and low cost,

- Highly selective and quicker than the available techniques,
- User-friendly, and
- Easy to use in the point-of-care environment with a minimum of training.

The selectivity of the analyte CTx-I would be included on the sensing area of a MEMS-based interdigital sensor. After pipetting the test sample on the selective sensing surface, Electrochemical Impedance Spectroscopy (EIS) technique would be used to measure the electrochemical properties of the test sample, which is proportional to the concentration of the target molecule. In order to develop a portable PoC device, an IoT-enabled embedded system would be designed and developed, which can measure the CTx-I level in the test sample and transfer it to an IoT-based cloud server.

1.6 Research Contributions

The main contribution of this work is the development of a smart sensing system which is able to detect CTx-I molecules in serum samples. The smart sensing system is dependent on the design and development of a smart sensor that can selectively quantify the target molecule. Low cost and robustness of the developed system are the significant features that make the system unique.

The major contributions of this research can be summarised as follows:

1 Use the most suitable sensor that allows a penetration depth of the fringing electric field, enough to enable bulk-sample testing. Characterise the sensor and find the optimum frequency range. Our group members worked with the King Abdullah University of Science and Technology (KAUST), Saudi Arabia to fabricate the sensor used in this research.

2 Develop and customise a suitable technique to induce selectivity for CTx-I molecules in the smart sensing system.

3 Explore and apply an antigen-antibody technique to induce selectivity of CTx-I to the system using the natural antibodies.

4 Develop and tailor artificial antibodies for CTx-I molecules in order to overcome the limitations of using natural antibodies.

5 Design and implement an IoT-enabled microcontroller-based system in order to develop a portable PoC device for simple measurement of CTx-I.
6 Analyse the performance of the developed smart sensing device and validate it using a reference method (ELISA).

1.7 Thesis Outline

The thesis is divided into seven chapters, as follows:

Chapter 1

This chapter includes an introduction to osteoporosis, its diagnosis methods and the importance of PoC devices in early detection and management of osteoporosis.

Chapter 2

This chapter gives a literature overview on the available biochemical markers of bone turnover and focuses on the recent advancements in bone biosensing technologies for monitoring bone biochemical markers, as well as the biomechanical assessment of bone.

Chapter 3

In this chapter, the operating principle of a planar interdigital sensor is explained and a basic theory of Electrochemical Impedance Spectroscopy (EIS) is discussed. An experimental setup is introduced which can fetch the information from the test sample and convert it into an electrical signal for further analysis.

Chapter 4

The original work of the researcher starts from chapter 4. This chapter reports the details of the steps involved in the design and development of an antigen-antibody-based biosensor for detection and measurement of CTx-I in serum. In this phase of the work, natural antibodies are used to induce selectivity in the sensing system.

Chapter 5

This chapter explains the detailed procedure of creating artificial antibodies using Molecular Imprinted Polymers (MIPs). A novel sensing technique for the recognition of

CTx-I by combining electrochemical impedance spectroscopy and MIP technology was also explained in this chapter. Moreover, the role of the coating thickness on the sensitivity of the planar interdigital sensors has been investigated.

Chapter 6

In this chapter the design and implementation of a portable IoT-enabled microcontroller-based PoC device is discussed. The device is able to measure the concentration of CTx-I in serum and transfer the data to an IoT-based cloud server.

Chapter 7

This chapter gives a general conclusion of the research work and future prospects of the reported work.

2

Literature Review

Publication pertaining to this chapter:

- ***N. Afsarimanesh***, S. C. Mukhopadhyay and M. Kruger. "Sensing Technologies for Monitoring of Bone-Health: A Review", **Sensors and Actuators A: Physical**, Vol.274, pp. 165-178, March **2018.**
- ***N. Afsarimanesh***, S. C. Mukhopadhyay and M. Kruger. "Biosensors for the Measurement of C-Terminal Telopeptide of Type I Collagen (CTX-I)**", Journal of Osteoporosis and Physical Activity**, vol 5, no.1, April **2017**.

2.1 Introduction

Bone metabolism is a dynamic remodelling procedure, including the resorption of old bone and the formation of new bone. The activity of osteoclasts, osteoblasts and osteocytes significantly affects the resorption, formation and maintenance of bones, respectively [18-20]. Bone resorption and bone formation are normally kept in a good balance and this balance is controled and modulated through the activity of the steroid hormones and local mediators such as cytokines [21]. Osteoporosis usually occurs when bone loss outruns the formation of new bone [22].

Bone strength can be dependent on different biomechanical factors such as force, displacement and energy absorption and is affected by bone size, shape and properties of bone tissue. Biomechanical assessment of these factors verify the biomechanical properties of bone, such as strength, toughness, stifness, fatigue and creep properties. Biomechanical assays can be employed at various loading conditions such as shear, tention and binding, and different techniques can be used to assess biomechanical performance of bone [23, 24].

The diagnosis of osteoporosis is normally made using a measurement of bone mineral density (BMD). Currently, dual-energy X-ray absorptiometry (DXA) is the gold standard to assess the BMD and bone remodelling procedure. However, BMD studies have undeniable limitations. The technology is costly and requires at least 2-3 years to observe bone loss. Thus, an instantaneous measurement of bone metabolism is essential [12, 25, 26].

Biochemical markers of bone turnover can provide a real-time evaluation of the bone remodelling process and can be used in the management and monitoring of bone diseases such as osteoporosis [27].

In this chapter, an overview of the available biomarkers of bone turnover will be introduced and existing biosensors for the monitoring of bone strength, as well as the bone mechanism, will be discussed.

2.2 Bone Structure

Bone is a metabolically living tissue that is subjected to continuous remodelling, the process of replacing old bone tissues by new tissues. During childhood and early adult years, bone formation occurs faster than bone resorption, so bones become denser, heavier and larger. This condition will continue until the age of 30 when bones reach their maximum density and strength (peak bone mass). The bone condition will be relatively stable during the ages of 30-45 and after that bone resorption begins to exceed bone formation.

In women, bone loss is fastest in the first years after menopause [28] and this is one of the main causes of developing low bone mass or osteoporosis. The hormone changes that occur in the menopause directly affect the bone density. The female hormone estrogen is essential for healthy bones. After the menopause, the level of estrogen falls and this can lead to a rapid decrease in bone density.

Bone is composed of bone cells and bone matrix. Bone cells are responsible for bone production and maintenance and the activity of bone cells can highly affect the process of bone remodelling. Osteoblasts are responsible for bone formation and its subsequent mineralization. Once they form bone matrix, the osteoblasts will be surrounded by the mineralized matrix and buried in the substance of the bone. Through this process, osteoblasts convert to osteocytes. On the other hand, osteoclasts are very large cells responsible for bone resorption and are placed on the bone surface [29].

Type I collagen is the main structural protein bone that form almost 94% of the organic bone matrix. During the process of bone remodeling it broken down to small fragments, release into circulation, and can be measured as biomarkers of bone loss.

Figure 2.1 shows a graphical representation of bone structure and the markers generated during various stages of bone remodeling. Biochemical markers Bone formation contain osteoblastic enzymes or are the consequence of active osteoblasts. Most of bone resorption markers are consequence of type I collagen breakdown, noncollagenous bone matrix proteins or osteoclastic enzymes. Moreover, different regulators of bone cells' function and bone turnover could also be used as biomarkers [30].

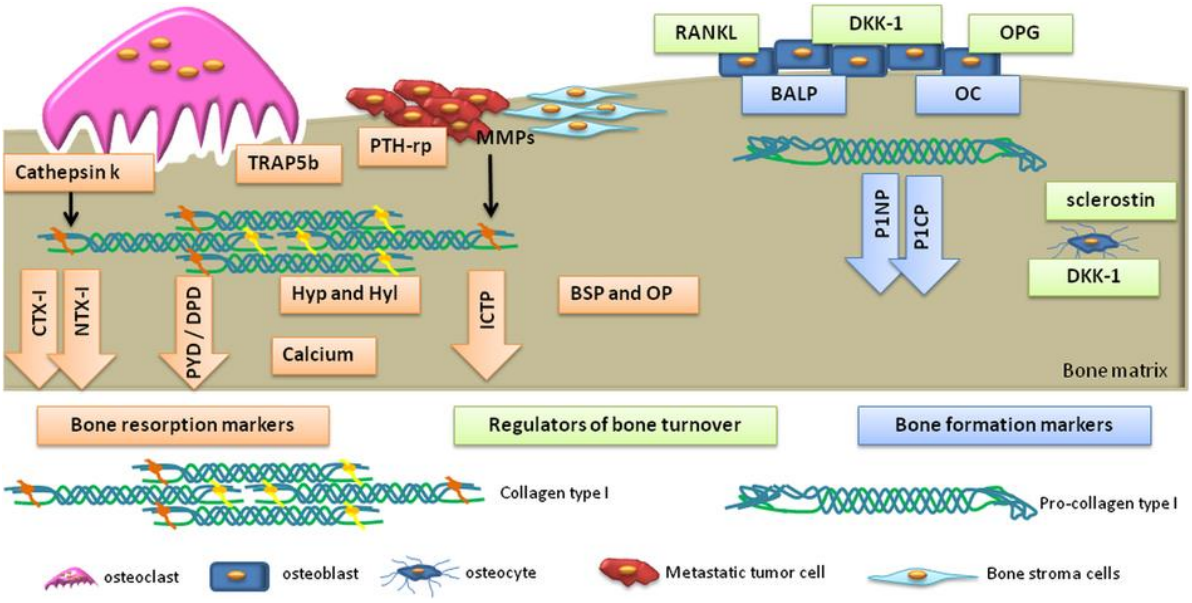

Figure 2.1 A graphical representation of bone markers, generated during various stages of bone remodelling. Blue boxes and arrows indicate bone formation markers. Orange boxes and arrows indicate bone resorption markers and green boxes indicate regulators of bone remodelling. During the process of bone remodelling, osteoblasts generate receptor activator of NF-kB ligand (RANKL) and osteoprotegerin (OPG) which control differentiation of osteoclasts. Osteoclastic function is assessed by the measurement of its lysosomal enzymes: cathepsin K and TRAP5b. The degradation of bone collagen type-I releases CTx-I and NTx-I, (PYD, DPD and Hyp/Hyl). During the process of bone resorption, calcium and enzymes from the bone matrix such as BSP and OP are produced. Bone formation is a process corresponding to the release of BALP and OC-specific osteoblast enzymes. Osteoblasts deliver to the extracellular space collagen type I as procollagen type-I molecules; then, its terminals are cleaved releasing P1NP and P1CP. With DDK-1 and sclerostin being present, the Wnt is regulated and as a result, osteoblastic differentiation is restrained. In bone metastasis (BM), matrix metalloptoteinases (MMPs) are generated by bone stromal cells and bone metastatic cells. These proteases can reduce collagen type-I producing carboxy-terminal crosslinked telopeptide of type I collagen (ICTP) [30].

2.3 Biochemical Markers of Bone Turnover

Bone markers, generated during various stages of remodelling, indicate any variations in bone remodelling. Biochemical markers of bone turnover (BMBT) are fragments of bone-tissue enzymes or proteins, usually measured in blood or urine, and indicate the bone

metabolism [31-33]. BMBT are usually classified into two main categories: biochemical markers of bone formation and biochemical markers of bone resorption.

2.3.1 Biochemical Markers of Bone Formation

Alkaline Phosphatase (AP)

Alkaline Phosphatases (APs) are enzymes in the cell membranes of osteoblasts. The total AP consists of different isoforms, produced from several tissues: liver, bone, intestine and kidney [34-36]. Bone-specific AP (BAP) is produced by osteoblasts during the bone formation process and therefore is a significant biomarker of bone formation action. Clinically, measurement of BAP is increasingly preferred due to the high specificity [37-39]. BAP levels in men stay comparatively stable throughout their life, whereas BAP levels in women rise around menopause [40]. BAP measurement assays are prevalent, widely accessible and commonly used in clinical assessment of osteoporosis treatments [41-43].

Osteocalcin (OC)

Osteocalcin (OC) is a comparatively small non-collagenous protein comprising of vitamin K and glutamic acid residues, produced by osteoblasts and odontoblasts [44-46]. The lowest OC levels in men are observed in the mid years and increase afterwards in life. The levels of OC in women follow the same pattern to BAP levels with a notable growth in the premenopausal time [40, 47]. OC is counted as a particular biomarker of osteoblast activity [48, 49]. After being released from osteoblasts, the largest part of the newly produced OC integrates to the bone matrix. A small fragment is released into the circulation where it can be measured by immunoassays [50, 51].

Propeptides of type I procollagen (PICP & PINP)

The peptides of procollagen type I are extracted from type I collagen. Type I collagen forms 90% of the organic matrix of bone and is produced as a procollagen molecule. This molecule includes amino-terminal as well as carboxy-terminal peptides (PICP and PINP). These peptides are divided and released into the circulation and therefore can be considered as markers of bone formation. Figure 2.2 depicts the schematic representation of type I procollagen propeptides.

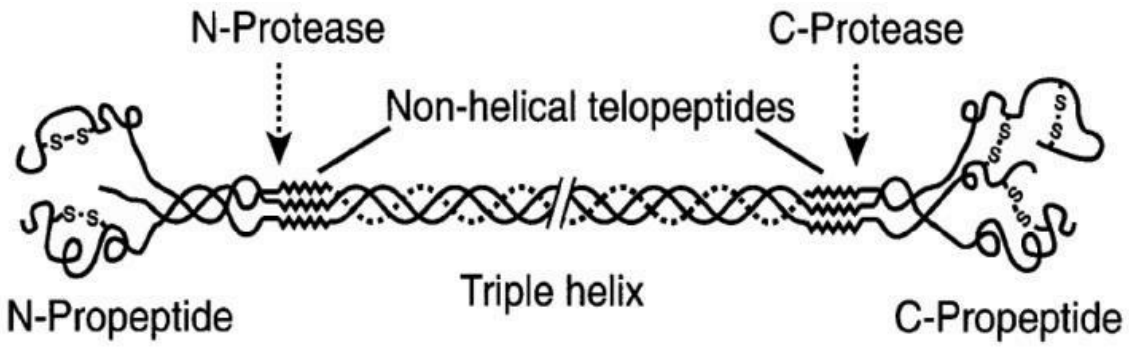

Figure 2.2 Schematic representation of type I procollagen Propeptides [21].

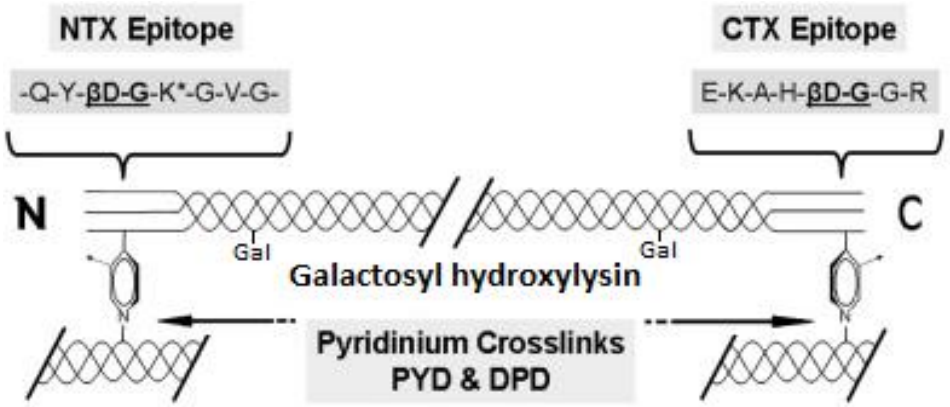

Figure 2.3 Schematic representation of collagenous bone resorption markers [52].

2.3.2 Biochemical Markers of Bone Resorption

Excluding tartrate-resistant acid phosphatase, most of the bone resorption markers are produced from bone collagen, as shown in Figure 2.3. Recently, the non-collagenous markers of bone resorption such as bone sialoprotein and osteoclast-derived have been studied as well [21].

Hydroxyproline

Hydroxyproline (OHP) is an amino acid produced from the post-translational hydroxylation of proline. It forms 13-14% of the total amino acid content of collagen and is also found in some other tissues such as skin and cartilage [53]. The majority of bone

OHP is fragmented to free amino acids that are processed by the kidney and then oxidized by the liver, therefore only 10-15 % releases into the urine. About 90% of OHPs are in the form of peptides, a small amount is in the free form, and the rest is found in the form of polypeptides [54, 55].

Hydroxylysine-Glycosides

Hydroxylysine-Glycosides is another amino acid existing in collagen, which is formed during the post-translational process of collagen and is more specific to bone than OHP. The advantage of Hydroxylysine-Glycosides over OHP is that it is not affected by diet [53]. Hydroxylysine-glycosides are available in two forms, glycosyl-galactrasyl-hydroxylysine (GGHL) and galactrasyl-hydroxylysine (GHL) [56, 57]. During the collagen breakdown process, GHL and GGHL are delivered into the circulation and can be quantified in urine [58]. However, it is reported that it is a less valid bone resorption marker because of its biological variability [59].

Collagen crosslinks molecules

Pyridinoline (PYD) and Deoxypyridinoline (DPD) crosslinks are developed in the time of extracellular maturation of collagen and are released into the circulation during the process of bone resorption. They crosslink the collagen peptides and mechanically strengthen the collagen molecule (Figure 3) [60, 61]. PYD can be found in bone, cartilage, vessels and ligaments, while DPD is merely found only in bone and dentin, and either of them is available in skin and other sources. Therefore, DPD is considered as a more sensitive marker than PYD [62]. As bone turnover occurs at a higher rate than in cartilage, vessels and ligaments, the PYD and DPD present in urine and serum are mostly derived from the bones. Therefore PYD and DPD are among the best markers of bone resorption [27, 63].

Cross-linked telopeptides of type I collagen

Cross-linked telopeptides of collagen are the most widely used markers of bone resorption [64]. They are derived from the aminoterminal (N-terminal) and the carboxyterminal (C-terminal) of type I collagen and named NTx-I and CTx-I, respectively [65]. They are cleared by the kidney, so can be quantified in serum as well as in urine. Different immunoassays have been developed for the measurement of NTx-I and CTx-I in serum and urine [66]. Recent investigations on these immunoassays have suggested that

they are more suitable for assessing bone resorption. Moreover, the studies on the bone resorption markers show that urine NTx-I and serum CTx-I are more sensitive than DPD in monitoring the anti-osteoclastic therapies [67, 68].

Bone Sialoprotein

Bone sialoprotein (BSP) is a phosphorylated glycoprotein, which forms 5-10% of the non-collagenous bone matrix [69]. BSP has been found in mineralized tissues such as bone and dentine. It is found in osteoblasts, odontoblasts and osteoclast-like and cancerous cell lines [69, 70]. BSP has been shown to be important in cell-matrix-adhesion procedures and is able to evaluate osteoclast-mediated bone resorption [71].

Tartrate-resistant acid phosphatase

Tartrate-resistant acid phosphatase (TRACP) is a heterogeneous group of enzymes that belongs to the group of acid phosphatases [72]. Two forms of TRACP are released into the circulation, TRACP5a and TRACP5b. These isoforms have similar structures but the difference is in the optimum pH and carbohydrate contents. Moreover, TRACP5a is derived from macrophages while TRACP5b is produced from osteoclasts [53, 62, 73]. During the process of bone resorption, TRACP5b is released from osteoclasts and contributes to the degradation of the bone matrix. Thus, it can be used to study the function of osteoclasts [74]. Kidney activity or dietary components have no influence on the level of TRACP5b [75].

Cathepsin K

There are different isoforms of cathepsins. Cathepsin K is a part of the cysteine protease group, which is able to cleave the helical as well as telopeptide parts of type I collagen [76, 77]. Cathepsin K is secreted from osteoclasts and plays a significant role in bone resorption [78]. At present, Cathepsin K inhibitors are used as a treatment for osteoporosis [79]. While cathepsin K is potentially an effective biomarker of bone resorption, additional investigations are required before it can be used commercially [80].

Biochemical markers of bone turnover are reviewed in Table 2.1 [30].

Table 2.1 Biochemical markers of bone turnover.

Marker	Symbol	Source	Analytical Method
Markers of bone formation			
Bone-specific Alkaline Phosphatase	BAP	Serum	Colorimetric
Osteocalcin	OC	Serum	ELISA
C-terminal propeptide of type I procollagen	PICP	Serum	ELISA, RIA
N-terminal propeptide of type I procollagen	PINP	Serum	ELISA, RIA
Markers of bone resorption			
Hydroxyproline	OHP	Urine	Colorimetric, HPLC
Hydroxylysine-Glycosides	Hyl-Glyc	Urine	HPLC, ELISA
Pyridinoline	PYD	Urine, Serum	HPLC, ELISA
Deoxypyridinoline	DPD	Urine, Serum	HPLC, ELISA
Aminoterminal cross-linked telopeptide of type I collagen	NTx-I	Urine, Serum	ELISA, CLIA, RIA
Carboxyterminal cross-linked telopeptide of type I collagen	CTx-I	Urine, Serum	ELISA, RIA
Bone Sialoprotein	BSP	Serum	ELISA, RIA
Tartrate-resistant acid phosphatase	TRACP	Serum	Colorimetric, ELISA, RIA
Cathepsin K		Serum	ELISA

2.4 Analytical Methods for the Measurement of Bone Turnover Markers

Currently, ELISA, RIA and HPLC are the most commonly used analytical methods for the detection and measurement of biochemical markers of bone turnover.

2.4.1 Enzyme-Linked Immunosorbent Assay

Enzyme-linked Immunosorbent Assay (ELISA) is able to detect very low concentrations of antigens or antibodies in a biological fluid through a colour variation. In the ELISA method, enzyme-labelled antigens and antibodies are used for the detection of target molecules. Alkaline phosphatase and glucose oxidase are the most commonly used enzymes [81, 82]. ELISA has been widely used in peptide and protein detection [83].

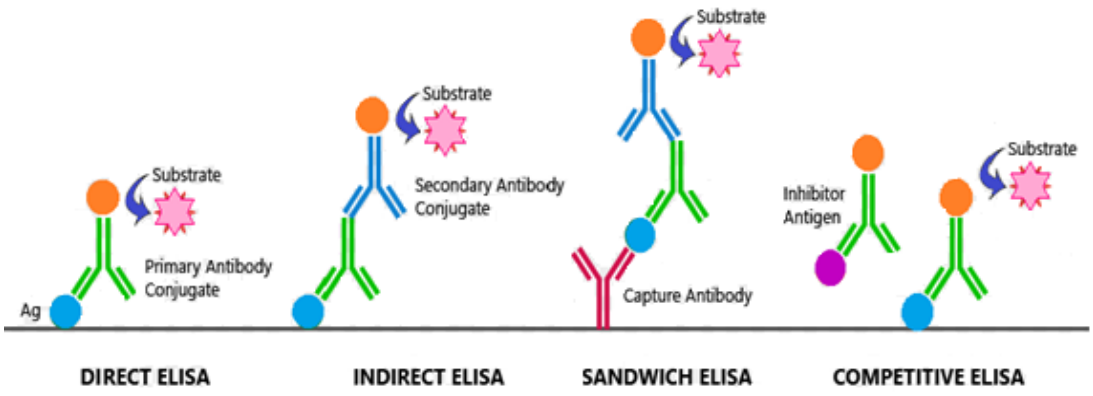

Figure 2.4 Different types of Enzyme-Linked Immunosorbent Assay (ELISA) techniques.

Enzymatic immunoassays are either homogenous or heterogeneous. In the homogenous method there is no washing step, so it is easy to use, however it is costly and not very sensitive. In the heterogeneous method, after forming an antigen-antibody complex, the complex is bound to the walls of a microtitre plate. After that, anything except the antigen-antibody complex is removed through washing steps. Thus, heterogeneous methods are more popular than the homogeneous ones due to their high sensitivity [81, 84].

Four different types of ELISA (direct, indirect, sandwich and competitive) have been developed to enhance the measurement specificity of various types of substrates (Figure 2.4).

2.4.2 Radioimmunoassay

Radioimmunoassay (RIA) is one of the most sensitive methods to detect antigens or antibodies [85]. RIA operates based on competitive binding of radiolabeled antigen and unlabeled antigen to an antibody.

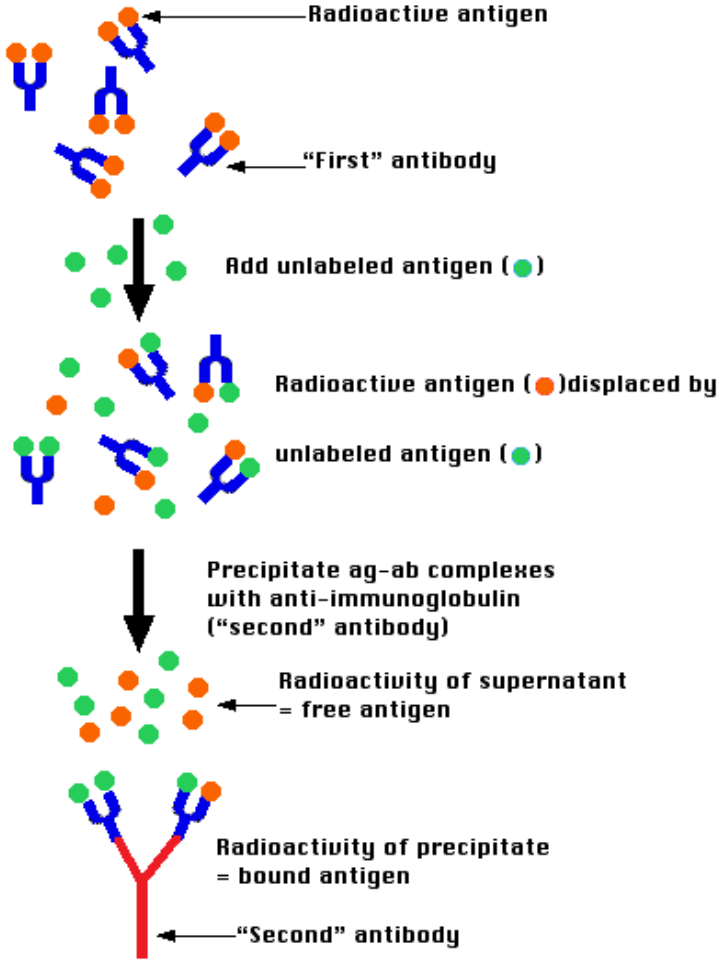

Figure 2.5 Radioimmunoassay (RIA) principle.

The antibody cannot differentiate labeled antigens from unlabeled ones; therefore, the two types of antigen compete for the binding sites of the antibody. Due to an increase in the concentration of unlabeled antigen, the number of labeled antigens displacing from the binding sites increases. In order to verify the concentration of antigen in the test sample,

the reduction in the concentration of the radiolabeled antigen attached to antibody in the test sample is estimated. Gamma- and beta- emitting isotopes are usually used for labeling the antigen [85]. Though the RIA method is very sensitive and more reliable than ELISA [86], however the use of radioactivity in this method makes it very expensive and hazardous for human health and for the environment [87]. The RIA principle is shown in Figure 2.5.

2.4.3 High-Performance Liquid Chromatography

High-Performance Liquid Chromatography (HPLC) is a powerful and accurate quantitative and qualitative separation technique which is mainly used to detect a single or multiple particles in pharmaceutical and biological samples. HPLC employs a column that contains the stationary phase, an injector that introduces the sample into the mobile phase, a pump that drives the mobile phase through the column and detector, and a detector that indicates the retention time of the particles. The retention time, which is an identifying characteristic of a particle, is the time at which a particular molecule elutes from the column. The most common types of detectors are UV-spectroscopy, electrochemical, florescence and mass spectrometric [88, 89].

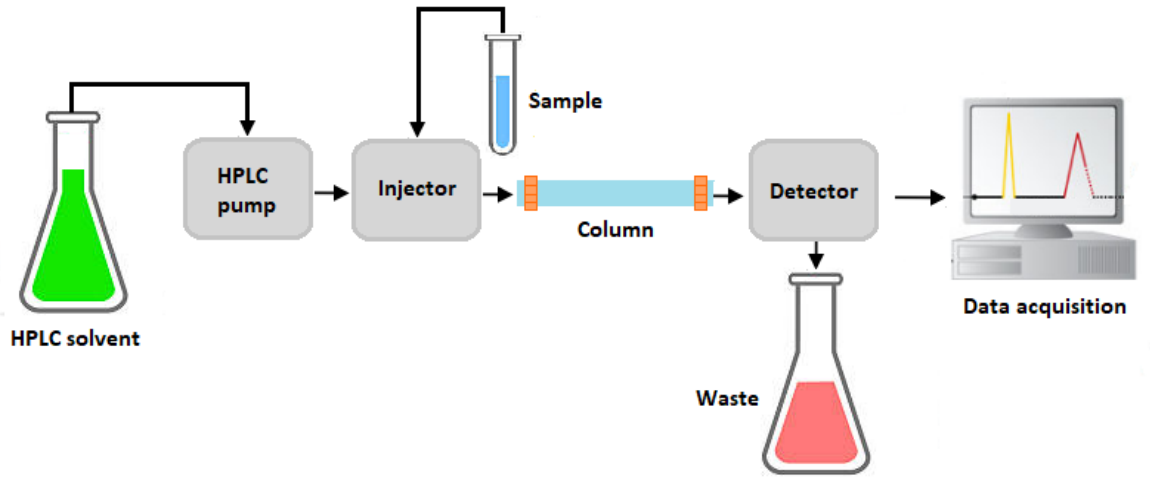

Figure 2.6 Schematic diagram of HPLC instrumentation.

Depending on the stationary phase system, there are various types of HPLC: normal phase, reverse phase, size-exclusion and ion-exchange HPLC. Figure 2.6 shows the schematic diagram of HPLC instrumentation. It contains a pump, injector, column, detector and data acquisition system. As the separation occurs in the column, it is considered to be one the most important parts of the HPLC system.

Table 2.2 gives a comparison of the most commonly used analytical methods for the detection and measurement of biochemical markers of bone turnover.

Table 2.2 Comparison of most commonly used analytical methods for the measurement of bone turnover markers.

Method	Biomarker	Advantages	Disadvantages
Enzyme-linked Immunosorbent Assay (ELISA)	• OC • PICP • PINP • Hyl-Glyc • PYD • DPD • NTX-I • CTX-I • BSP • TRACP • Cathepsin K	• Highly specific • Highly sensitive • No radiation hazards • Minimal reagents are required	• Sample preparation is complicated • Results may not be absolute • Requires technical expertise • Kits are commercially available, but expensive
Radioimmunoassay (RIA)	• PICP • PINP • NTX-I • CTX-I • BSP • TRACP	• Highly specific • Highly sensitive	• Radiation hazards • Requires technical expertise • Requires special arrangements to store radioactive material. • Requires special arrangements for radioactive waste disposal.
High-Performance Liquid Chromatography (HPLC)	• OHP • Hyl-Glyc • PYD • DPD	• High resolution • High speed • Highly sensitive • Highly accurate • Automated • Measurement of multiple components in a single analysis.	• Costly equipment. • complex equipment • Requires technical expertise

2.5 Current Advancements in Bone Biosensors

Recently, technological advancements in biosensors have permitted assessment of the biomechanical quality as well as the metabolic status of bone. These investigations and improvements have been enhanced the operation of available biosensors and developed fast, reliable and highly sensitive point-of-care devices [64, 90, 91]. However, development of a low-cost device which can be used outside the laboratories is under investigation. According to the available reviews, bone biosensors can be categorized as biomechanical sensors or biomarker-base sensors [90, 91].

2.5.1 Biomechanical Sensors

Dual-energy X-ray absorptiometry (DXA) and sonography are the most commonly available methods to measure BMD [91, 92]. In spite of the high accuracy, these techniques are expensive and require bulky devices [93-95]. Moreover, they cannot provide a real-time assessment of the biomechanical status of bone. One of the most significant advantages of bone biomechanical sensors is that they are able to indicate the bone status in real time, whereas the available techniques detect the bone problem that is already occurred [91].

Therefore, various biomechanical sensors were developed to study bone strength in an easier way than the available methods [96-105]. The IMPACT 3500 project introduced a system for measuring implant strain. This work showed the medical applicability of detecting the implants deformation as an important element to assess rehabilation exercises, to monitor useful overloads and predicting implant failure and observing the healing procedure. In this method, a resistive 5 kΩ strain gauge was used to measure the implant strain. The strain gauge in a Wheatstone-bridge format was connected to an amplifier to get an output proportional to the strain. Figure 2.7 shows the block diagram of the system used in this project [96].

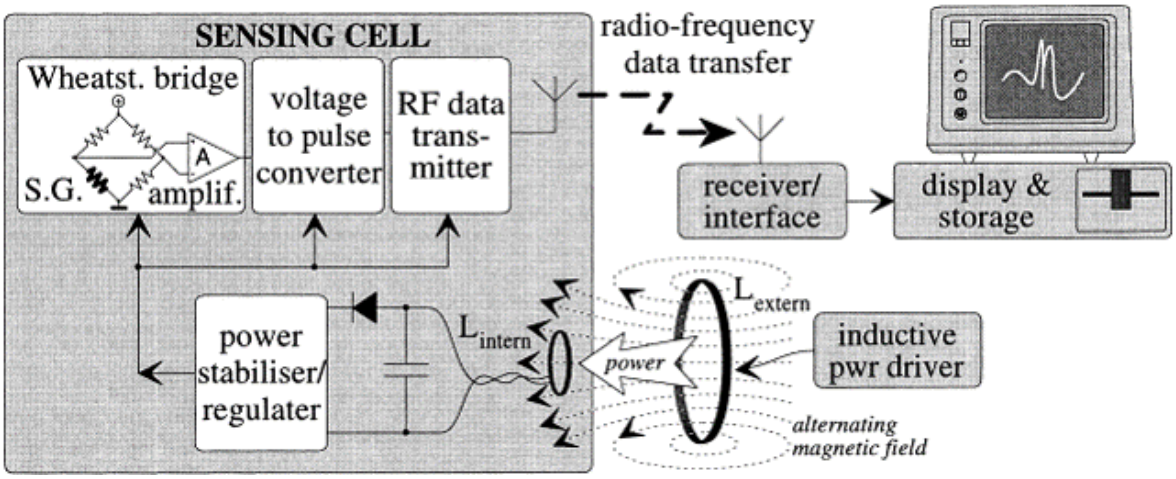

Figure 2.7 Block diagram of the IMPACT 3500 system [96].

Wen et al. discussed a micro-fabricated strain gauge that could be used on live bones. In this research, a thin-film strain gauge was enclosed in a poly-dimethyl-siloxane (PDMS) membrane. The aim of this research was to develop a flexible, implantable sensor array for monitoring surface strain on live bone. They used a new method to enhance the mechanical robustness of the sensor. By replacing the conventional lift-off by wet etching method to pattern the thin metal film, a miniaturized sensor was developed. The results showed that the proposed strain gauge is more accurate than the commercial ones [97].

In 2012, Pangen et al. designed a flexible, highly sensitive strain-gauge sensor, which enables the recognition of pressure, shear and torsion. In this device, two layers of silicon nanohairs were bounded between two flexible PDMS supports (500 μm thickness). The silicon nanohairs were coated by Pt and the fiber arrays were repeated over a 9×13 cm2 area (Figure 2.8). Changes in the electrical resistance were recorded as a function of strain for pressure, shear and torsion. To estimate the capability of the sensor to work as a strain gauge, the gauge factor (GF) of the device was determined over an area of 4×5 cm2 by gradually increasing the strain up to 2% for pressure, 4% for shear and 5% for torsion. Pressure responses were analysed using a computer-based user interface and a force with a piezoelectric position to apply a pressure of 550 Pa with a frequency of up to 10 Hz. The sensor showed high sensitivity, repeatability and reproducibility [98].

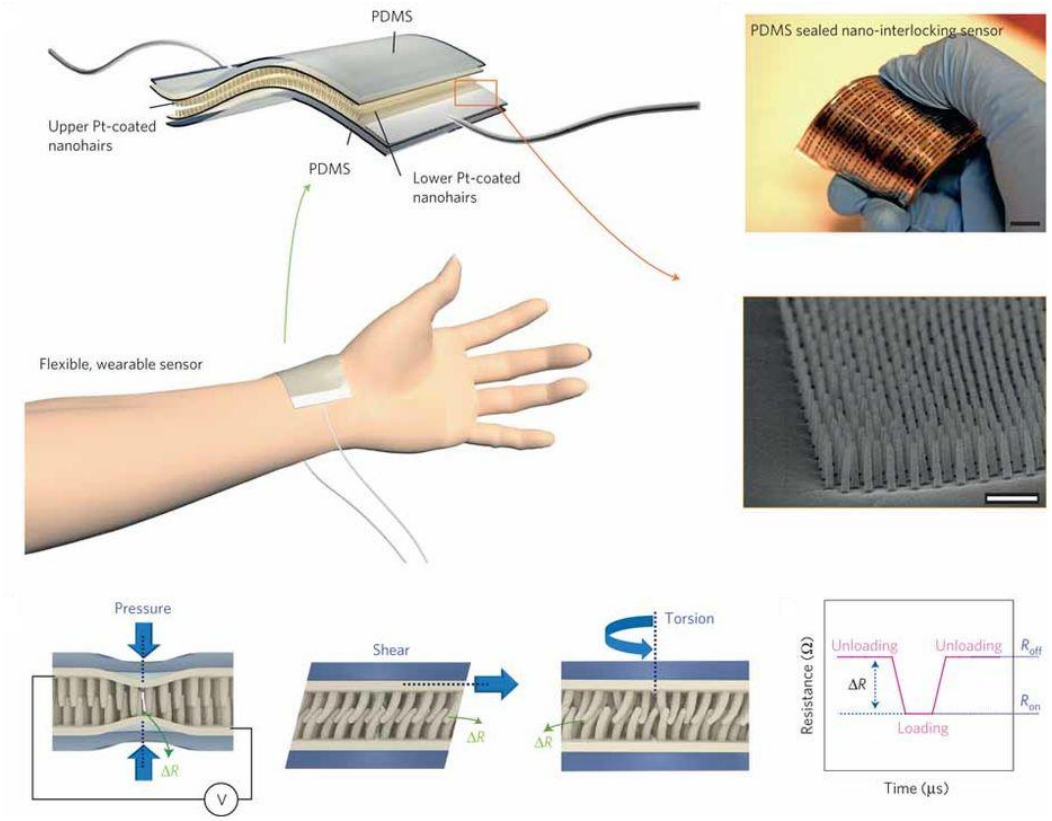

Figure 2.8 Flexible, highly sensitive strain gauge based on reversible interlocked nanofibers [98].

A nanotube film strain-sensing system was developed by Dharap et al. in order to introduce a new sensor that can be used in multi-directional location sensing. This sensing system was based on single-wall carbon nanotubes (SWCNT) for strain sensing on the macro scale. The results indicated a nearly linear relationship between the voltage across the CNT film and the strain in the film, showing the capability of such films for multi-directional and multi-location strain sensors [106].

Vibration response of bone tissues has also been investigated. In this regard, NASA introduced OsteoSonic for detecting bone and joint damage using a vibrational analysis of bone tissue [107]. Likewise, Nogata et al. described a method for estimating bone strength using ultrasound signals [108]. Later, in 2010, an ultrasound-based wireless implantable passive strain sensor (WIPSS) was designed to monitor the deformation of implants. The sensor's operating principle was based on hydro-mechanical effects (Figure 2.9). A strain resolution of 1.7 ± 0.2 × 10-5 was obtained using the developed sensor [101].

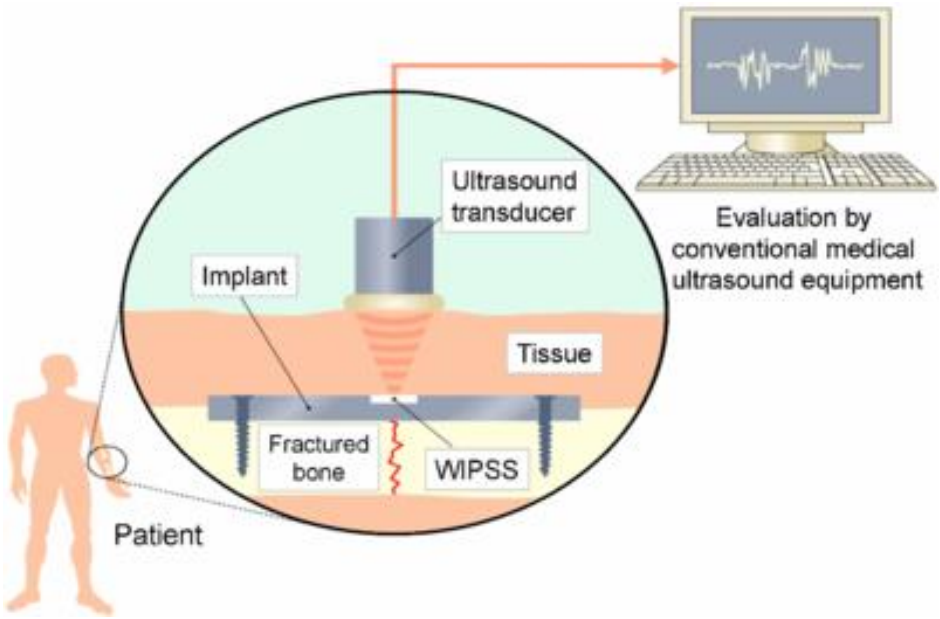

Figure 2.9 Schematic of the wireless implantable passive strain sensor concept [101].

Piezoelectric sensors have been shown to give reproducible results for variations in the mechanical properties of bone. Bender et al. explained the use of piezoelectric sensors for monitoring capsule formation near soft-tissue implants. Later, a piezoelectric ceramic (PZT) biosensor was designed for evaluation of the mechanical parameters of bones. In this method, two PZT patches were connected to the bone; one was used as the actuator and the other as the sensor. The excitation of the actuator was done by applying an ac signal that excited the bone and the variations were sensed using the sensor patch. The developed biosensor could measure changes in the mechanical parameters of bone using changes in the frequency-response function (FRF). It was claimed that the method could be used for monitoring the healing process of bones after surgery [102]. Hsieh et al. designed a contact-type piezoresistive micro-shear-stress sensor for measuring the sheer stress of a knee prosthesis. The sensor was designed based on a micro-electro-mechanical system (MEMS) which contained two X-ducers that transform the stress into a voltage. A sensitivity of 0.13 mV/mA-MPa for a 1.4 N shear force range was achieved using the developed sensor shear [99]. Alfaro et al. presented an ultra-miniature multi-axis implantable sensor to measure bone stress at a micro-scale level. The device was fabricated by CMOS-MEMS technology and comprised of an array of piezoresistive sensor pixels to monitor the stress at the interface of the MEMS chip and bone (Figure 2.10) [109, 110].

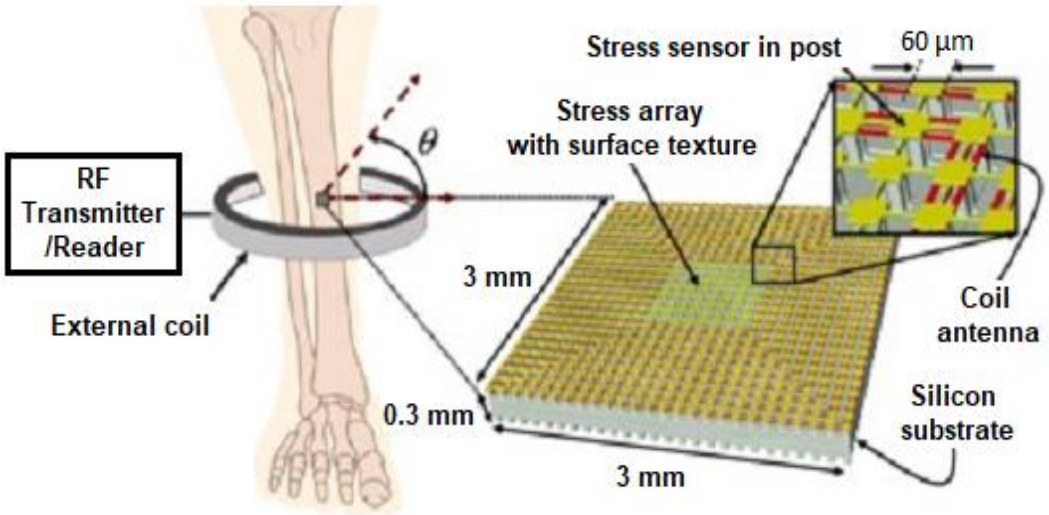

Figure 2.10 Schematic of the implantable CMOS-MEMS multi-axis stress sensor [109].

Recently, researchers have paid more attention to optical sensors due to their quick response, high sensitivity, real-time monitoring capability, immunity to EM interference and biocompatibility [111]. Optical Bragg grating fibres are widely used for the measurements of strain in different applications. Fibre Bragg grating are diffracting components printed in the core of an optical fiber. They act as selective filters of light and reflect in the fiber core the spectral elements of a propagating packet according to the Bragg relation $\lambda = 2n\Lambda$ where λ is the wavelength, n is the core mean reflective index and Λ is the spatial period of the refractive index modulation. If the fiber Bragg grating is strained across the fibre axis, Λ is changed. As a result, the Bragg wavelength is shifted, which indicates a measure of strain. Fresvig et al. proposed an alternative method to the strain gauge for bone deformation monitoring in which the use of fiber optic Bragg grating sensors was evaluated. The measurements were performed on an acrylic tube as well as on a sample of human femur diaphysis. Four optical fiber sensors were used for the measurements and four strain gauges were used as a reference method to validate the results. However, no notable difference was detected between the two measurement devices, neither in the acrylic tube measurement nor in the human sample measurement [105]. Later Mishra et al. proposed a fiber Bragg-grating sensor to estimate bone decalcification. In this research, the three-point bending method was used to strain the bone and the equivalent Bragg wavelength shift was recorded (Figure 2.11). Two identical animal bone samples were selected, one slightly decalcified. The strain response of both the samples was taken to

investigate the effect of calcium loss and deterioration with time. The strain response gave a direct demonstration of the level of calcium present in the bone [112]. Singh et al. introduced a model of photometric biosensor based on a microbending technique to measure the bone strength. An Artificial Neural Network (ANN) based test model was used to optimize the fiber optic biosensor to measure strain in orthoapplications using MATLAB. The performance of the developed model was evaluated by changing the number of layers as well as the number of neurons of the network. The proposed model with 96% performance accuracy could be considered for detecting the onset of osteoporosis [113].

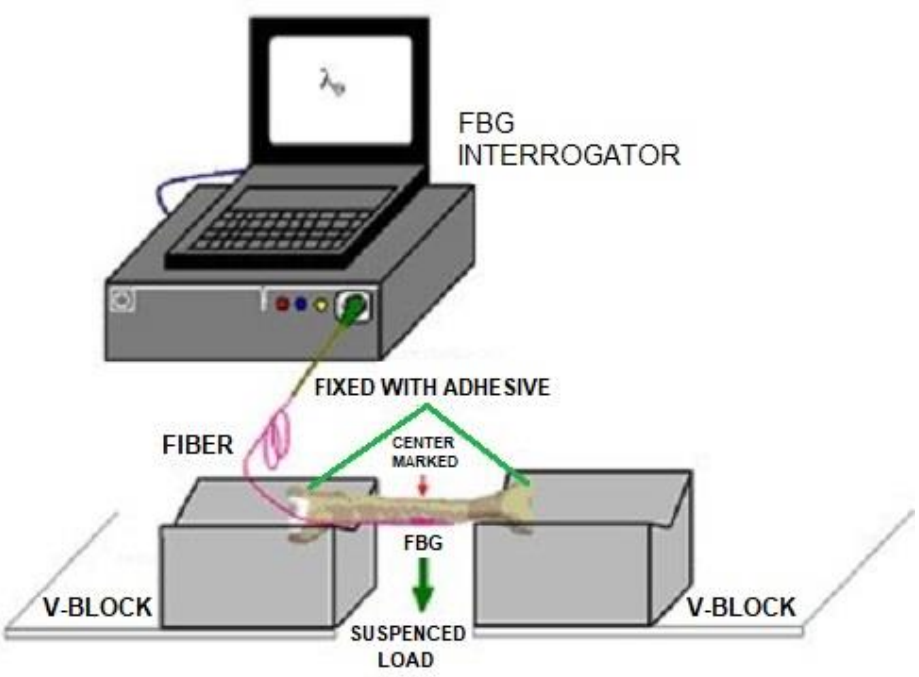

Figure 2.11 Schematic of the experimental setup developed for monitoring bone decalcification using a fiber Bragg-grating sensor [112].

Sirivisoot et al. developed a biodegradable biosensor for monitoring orthopaedic tissue growth [100]. This biosensor was able to sense and recognize the regrowth of bone. The sensor was made of anodized titanium, carbon nanotubes (CNTs) and a biodegradable polymer that degrades once bone grows, and CNTs could measure conductivity variations as new bone forms. Parallel multiwall CNTs were prepared from the pores of the anodized titanium using the chemical vapour deposition process. CNTs are widely used in

orthopaedic applications due to their unique electrical, mechanical, and biological properties.

2.5.2 Biomarker-based Sensors

While BMD measurements using biomechanical sensors can evaluate the process of bone remodelling by providing information on bone strength, biochemical markers of bone turnover can reflect the status of bone metabolism by indicating the condition of bone matrix components. The available research shows that biochemical markers of bone turnover are also in some cases helpful to enhance the estimation of an individual's risk of fractures. Hence, the use of biomechanical sensors for BMD assessment combined with biomarker-based measurements can greatly improve the assessment of bone-loss in patients with or without osteoporosis and the response to medication [114]. During the last decades, different biosensors have been developed to detect and measure the level of biochemical markers of bone turnover [115-119].

Caglar et al. developed a glass-PDMS microchip-based sensor for calcium-ion determination in serum. The sensor employed arsenazo III attached to the surface of polymeric beads. Variations in the reflectance indicated the presence of calcium. The sensor could be reused by washing it in HCl solution. The developed microchip sensor showed good results in clinical testing of calcium ions in serum [116].

Chung et al. invented a quartz-crystal microbalance (QCM) biosensor to assess the concentration and function of TRAP in blood. In this method, when the TRAP 5a, TRAP 5b or the total TRAP in blood samples captured by the antibodies are immobilized on the cantilever surface, the extra weight causes a position deflection in the cantilever beam, which was then measured using an optical detection plate [92].

An electrochemical biosensor was developed by Khashayar et al. for determination of Osteocalcin (OC) in serum. The corresponding antibody was immobilized on gold electrodes to measure the electrochemical response of Oc. The detection limit of 0.65 ng/ml was calculated. Electrochemiluminescence (ECLIA) was used to validate the results; there was a high correlation between ECLIA and the developed biosensor [120].

Zhang et al. presented a simple, sensitive and label-free electrochemical method for studying ALP activity based on the difference of the surface charge of electrodes. Phosphorylated peptides were immobilized on the surface of gold electrodes to make negatively charged self-assembled monolayers (SAMs) that helped the access of the

positively charged [Ru $(NH3)_6]^{3+}$ probes to the electrode surface. The proposed method avoided the need for costly bio-reagent labeled nanoparticles for output amplification and complex operation [121].

Lung et al. proposed another method for bone loss monitoring. In their proposed method, they used Surface Plasmon Resonance (SPR) technology to detect urinary NTx as a bone-loss marker. The results demonstrated that the SPR method could be used as an alternative method for NTx measurement, as it showed a good correlation with ELISA [122].

In recent years, different biosensing methods have been developed for the detection and measurement of CTx, as one of the most sensitive biochemical markers of bone loss. Yun et al. designed a label-free biosensor for the detection of CTx-I. They used a SAM of dithiodipropionic acid on the surface of gold electrodes. Streptavidin and biotinylated antibody were then immobilized on the SAM layer. Finally, Electrochemical Impedance Spectroscopy (EIS) was employed to measure the concentration of CTx-I in different samples. A limit of detection of 50 ng/ml was achieved using the proposed method. Figure 2.12 shows a schematic representation of the developed CTx-I biosensor [115].

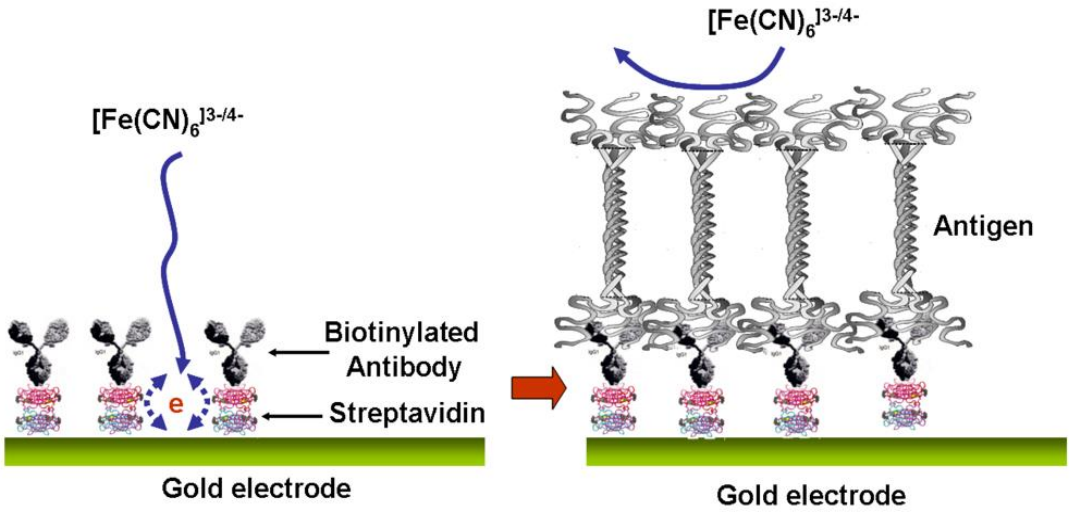

Figure 2.12 Schematic illustration of a label-free CTx-I biosensor developed by Yun et al. [115].

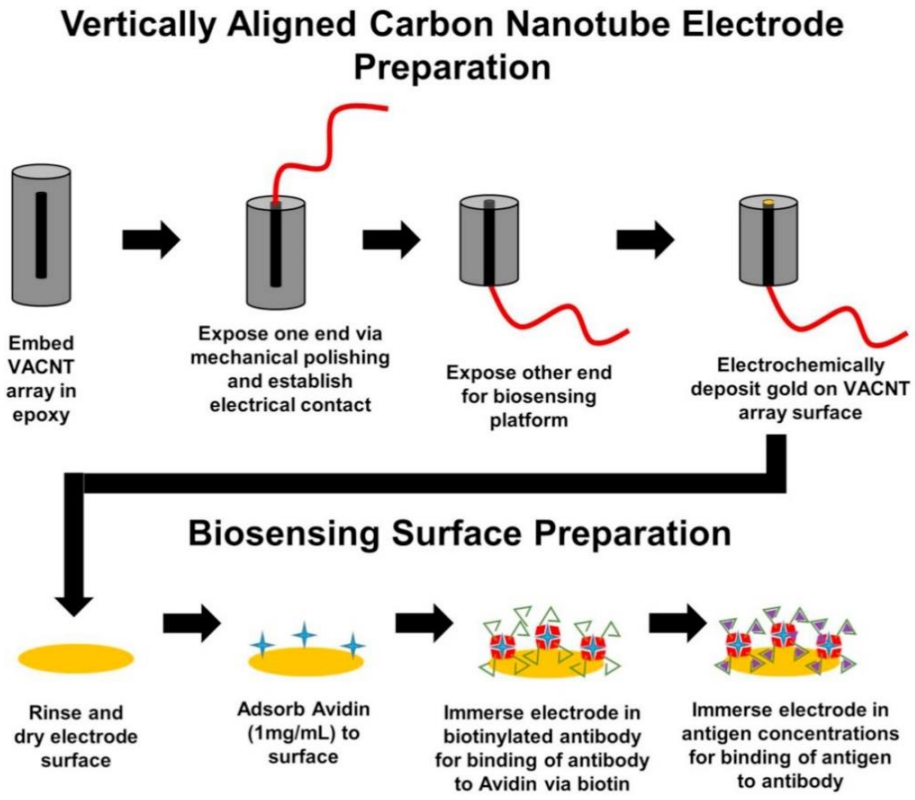

Figure 2.13 Schematic illustration of biosensing surface preparation and sample testing of the immunosensor developed by Ramanathan et al. [119].

Ramanathan et al. reported an impedimetric immunosensor, based on gold-coated carbon nanotube (CNT) control arrays for CTx-I detection. Extra-long vertically aligned CNT (VACNT) posts were used to fabricate the electrodes. Gold nanoparticles were then electrodeposited on the tips of the electrodes, which eliminated the need for CNT functionalization. In the next step CTx antibody was immobilized on the gold modified electrodes in order to make the sensor selective for CTx-I. The various stages of VACNT sensor fabrication and biosensing surface preparation are illustrated in Figure 2.13. The EIS technique was used to detect the antigen-antibody phenomenon happening on the surface of the electrode. The immunosensor could measure CTx-I concentrations as low as 0.05 ng/ml [119].

2.5.3 Multiplex Assays

Recently, a few multiplex immunoassays have been developed to simultaneously detect several biomarkers to monitor the process of bone remodelling more accurately [123]. An automated multiplex assay was developed by Claudon et al. for bone turnover markers.

This multiplex assay allowed simultaneous measurement of CTx-I, PINP, OC and parathyroid hormone (PTH) in 20 µL of serum. The automated multiplex immunoassay showed the same analytical precision and better sensitivity compared to the single assays. It can specially be useful when a limited sample volume is available [124]. Khashayar et al. introduced another multiplex assay named Osteokit for bone marker assessment. They used a microfluidic platform to have a simultaneous measurement of OC and CTx-I in serum. The results showed that there is a comparable sensitivity of Osteokit with the conventional method, ECLIA. The total assay time was reported to be 10 min, shorter than the time required by ECLIA [125].

2.5.4 EIS-based sensor

We have developed a sensing method for detection and measurement of CTx-I which works based on Electrochemical Impedance Spectroscopy which is explained in the next chapters. EIS technique has been discussed in detail in chapter 3.

Table 2.3 gives a summary of some of the developed bone biosensors along with their characteristics.

Table 2.3 Some of the existing bone biosensors and their characteristics.

Biosensor	Technology	Invasive/ Non-invasive	Specification especially LoD	Benefits
IMPACT3500 [96]	Strain gauge	Invasive	Elastic range: 300 µs (100-400 µs)	Real-time measurement
Contact-type multi-axial sensor [99]	Piezoresistive micro-shear-stress	Invasive	0.13 mV/(mA-MPa) for a 1.4 N shear force range	Direct evaluation
Biodegradable CNT biosensor [100]	CNT	Invasive	20% improvement in osteoblast adhesion	Biodegradable
WIPSS [101]	Ultrasound	Invasive	Resolution: $1.7 \pm 0.2 \times 10^{-5}$	Biocompatible
Piezoelectric ceramic biosensor [102]	Piezoelectric transducer	Invasive	Damping ratio: 0.035	Direct evaluation
Calcium sensor [116]	Reflectance variations from arsenazo III	Non-invasive	2.68×10^{-5} M	Non-invasive
TRAP biosensor [92]	Electrochemical cantilever	Non-invasive		Non-invasive Highly accurate Low sample volume
CTx-I biosensor [115]	EIS	Non-invasive	50 ng/ml	Non-invasive Lablel-free
Multiplex automated assay [124]	Automated assay (measures P1NP, CTx-I, OC, PTH)	Non-invasive	P1NP: 0.26 µg/l CTx-I: 0.002 µg/l OC: 0.51 µg/l PTH: 0.39 ng/l	Automated Multiple markers
Osteokit [125]	Automated assay (measures OC and CTx-I)	Non-invasive	OC: 1.94 ng/ml CTx-I: 1.39 pg/ml	Automated Multiple markers

2.6 Chapter Summary

Biochemical markers of bone turnover provide important tools for the analysis of bone metabolism. Together with the measurement of bone mineral density using the imaging techniques, biochemical assays have a significant role in the assessment and diagnosis of metabolic bone disorders such as osteoporosis. Different methods and immunoassays are available for bone-health monitoring. The conventional techniques are usually laboratory-based, time-consuming, expensive and complex. In order to control these issues, bone biosensors are being developed. On the other hand, biomechanical sensors have a significant role in monitoring the behavior of bone tissues during the development, aging, responding to treatments and hailing. Different biosensors have been developed for biomechanical assessment of bone, verifying the factors such as strength, toughness, stiffness, fatigue and creep properties. This chapter has provided a review of the available bone biomarkers, emphasizing recent technologies of bone biosensors.

3

Planar Interdigital Sensors and Electrochemical Impedance Spectroscopy

3.1 Operating Principle of Interdigital Sensors

Planar interdigital sensors are made of a comb-like or finger-like periodic pattern of parallel electrodes on a planar substrate. The electrodes are used to form the capacitance related to the electric fields that penetrate into the Material Under Test (MUT) and carry useful information about the properties of the material sample [126]. One of the most important benefits of the planar interdigital sensors is the single-side access to the MUT. This property helps to penetrate the sample with magnetic, electric, or acoustic fields from only one side. The strength of the output signal can be controlled by changing the number of fingers, the area of the sensor, and the spacing between them. The capability of being used for non-destructive testing is another advantage of these sensors, which makes them more useful for online testing and process-control applications [127].

Basically, planar interdigital sensors follow the operating principle of parallel-plate capacitors. Figure 3.1 shows a transition from the parallel-plate capacitor to a planar, fringing-field capacitor, where electrodes open up to provide a single-side access to the MUT. The finger pattern of interdigital sensors is usually replicated many times to increase the signal strength [127] and keep the signal-to-noise ratio in an acceptable range [128]. The configuration of the conventional interdigital sensor is shown in Figure 3.2.

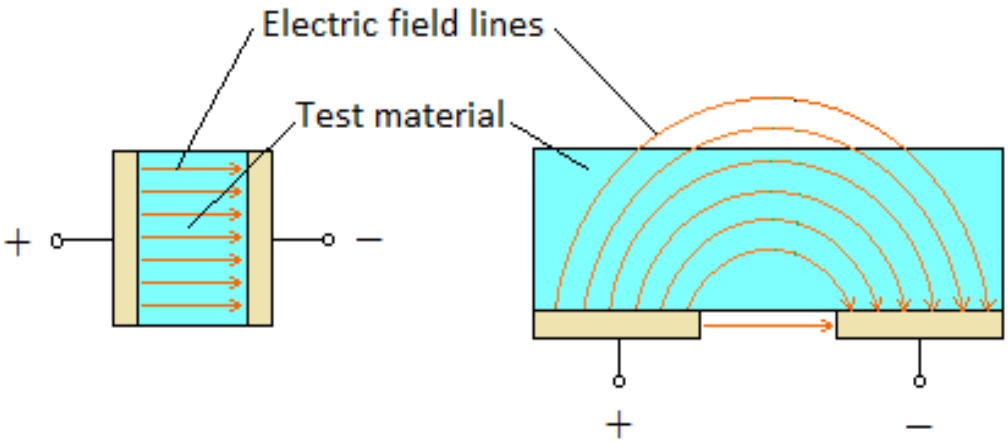

Figure 3.1 Transition from the parallel-plate capacitor to a planar capacitor.

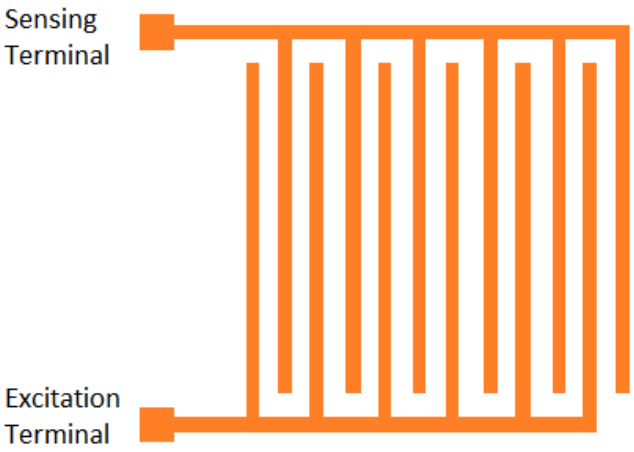

Figure 3.2 Geometric structure of conventional planar Interdigital sensor.

When an AC signal is applied as an excitation voltage to the terminals, an electric field is formed from positive to negative terminal. This electric field bulges through the test sample via the excitation electrode, is received by the sensing electrode, and carries useful information about the properties of the MUT such as impedance, density, chemical material and so on. Figure 3.3 shows the electric field formed between positive and negative electrodes for different pitch lengths- the distance between two consecutive electrodes of the same polarity. As is illustrated in the figure, different pitch lengths (l_1, l_2 and l_3) show different penetration depths. The penetration depth rises by increasing the pitch length, but the electric field will get weak.

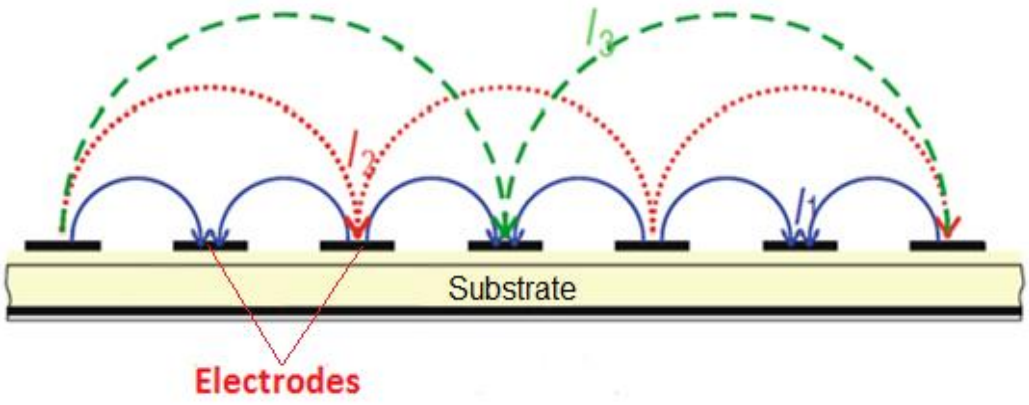

Figure 3.3 Electric field formed for different pitch lengths [129].

3.2 Novel Planar Interdigital Sensors

Novel interdigital sensors are designed with more sensing electrodes than excitation electrodes, in order to increase the penetration depth of the fringing electric field. Different geometries have been studied in the research literature [130-132]. Figure 3.4 shows the excitation pattern for a multi-sensing electrode in interdigital sensor geometry. .

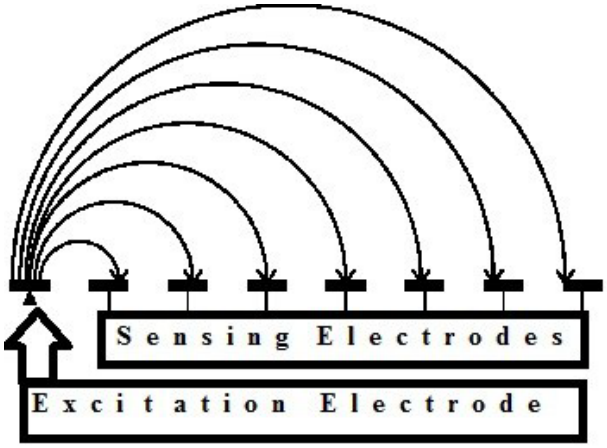

Figure 3.4 Schematic excitation patterns for multi-sensing-electrode interdigital sensors.

The novel interdigital sensors have been fabricated based on different geometric parameters. Table 3.1 shows the geometric parameters of four different interdigital sensors and Figure 3.5 shows the schematic of a 1-5-25 and 1-11-25 configuration of newly designed planar interdigital sensors [133].

Table 3.1 Geometric design parameters for four types of Interdigital sensors.

Sensor Type	Pitch Length (μm)	Number of sensing electrodes	Number of excitation electrodes	Sensing area (mm^2)
1-5-25	25	40	9	6.25
1-5-50	50	30	7	6.25
1-11-25	25	44	5	6.25
1-11-50	50	33	4	6.25

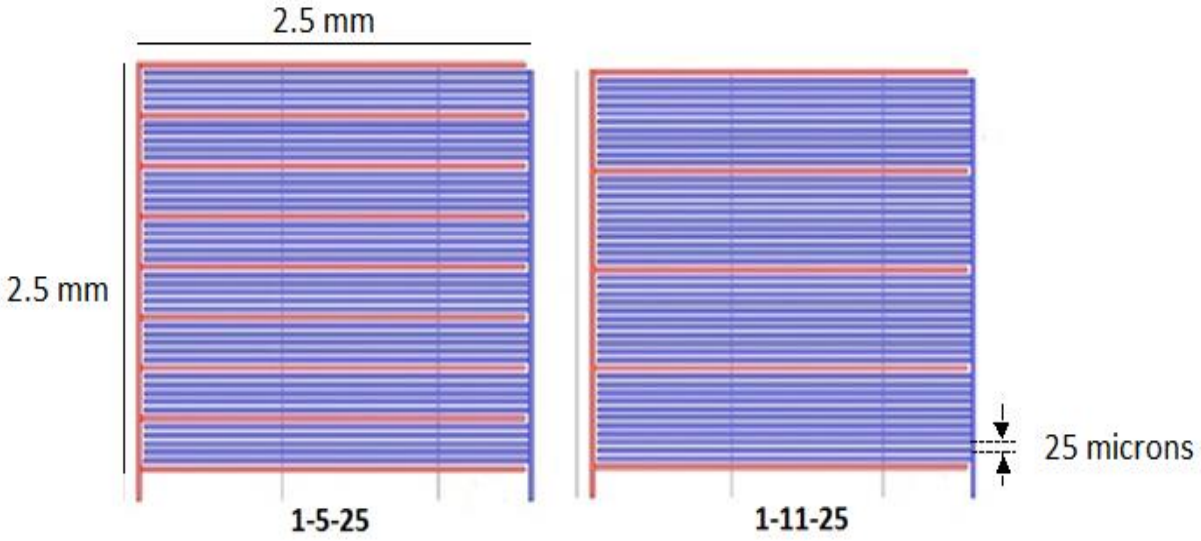

Figure 3.5 1-5-25 and 1-11-25 configurations of novel interdigital sensors.

3.2.1 Sensors Fabrication

The sensors were fabricated at the King Abdullah University of Science and Technology (KAUST), Saudi Arabia as an academic collaboration between the School of Engineering and Advanced Technology, Massey University, New Zealand and KAUST. One of our group members worked with KAUST to fabricate the sensor and in the present work a similar sensor was used to perform he experiments. The fabrication of the sensors was done by etching and photolithography techniques on a single crystal Silicon/Silicon Dioxide (Si/SiO_2) 4-inch (diameter) wafer, 525 µm thick. 36 workable sensors were patterned on one wafer (Figure 3.6) with each sensor having dimensions of 10 mm × 10 mm and a sensing area of 6.25 mm2 (2.5 mm × 2.5 mm).

The patterns were written for a periodic interdigital structure with 11 sensing between two excitation electrodes for a pitch length of 25 µm with the width of electrodes and the sensing area set to values of 25 µm and 2.5 mm × 2.5 mm respectively. The sensors were fabricated using MEMS technology involving the steps of photoresist coating, UV exposed interdigital pattern transfer, plasma etching metal deposition by DC magnetron sputtering and lift-off. Gold was used as the electrode material due to the flexibility in the methods available for its deposition as thin film electrodes. 500 nm of Gold (Au) were sputtered on

top of 20 nm of Chromium (Cr) to provide proper adhesion of the interdigital structures on the substrate. Plasma etching was used to develop the patterns of the electrodes by removing the UV-exposed part from the photolithography step.

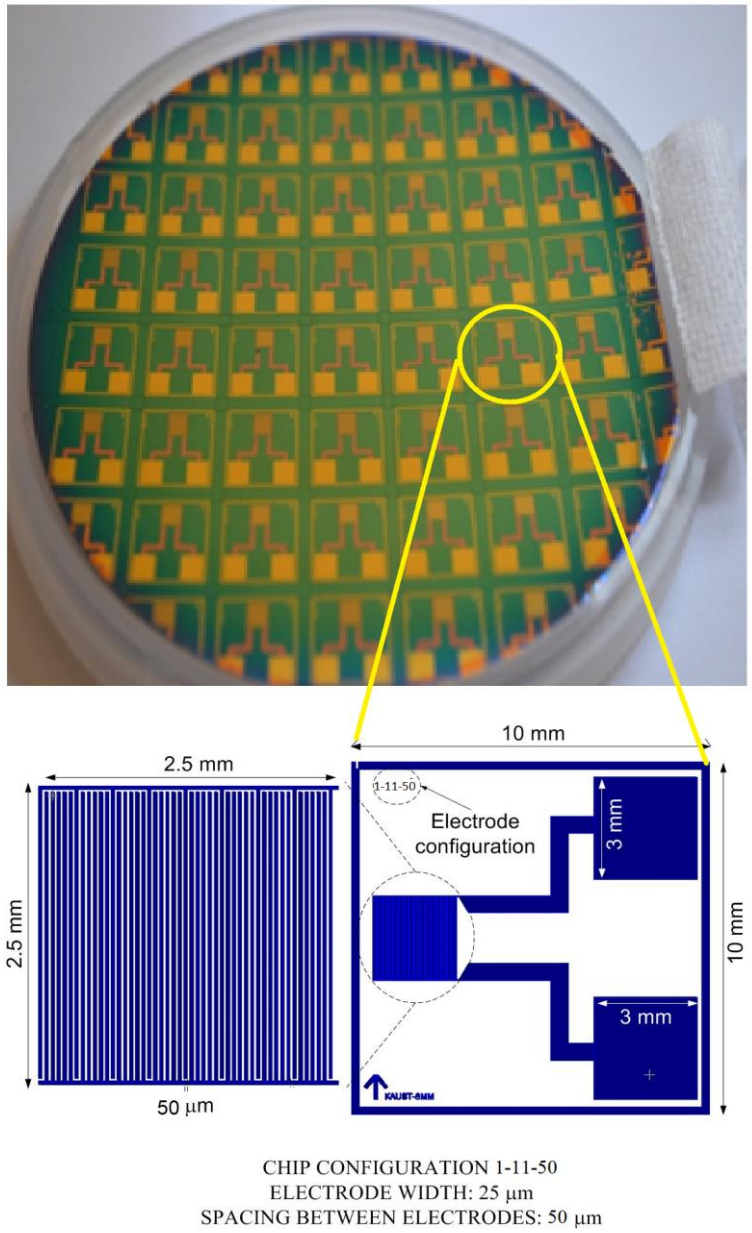

Figure 3.6 Silicon wafer sensors fabricated using MEMS technology.

After that, the bonding pads were opened using a plasma-etching process. Figure 3.7 shows the required steps in the fabrication process of the interdigital sensors. These sensors have several applications in manufacturing processes [134], environmental monitoring

[132, 135-138], humidity and moisture sensing system [139, 140], photosensitive detection [141] and gas sensor [142].

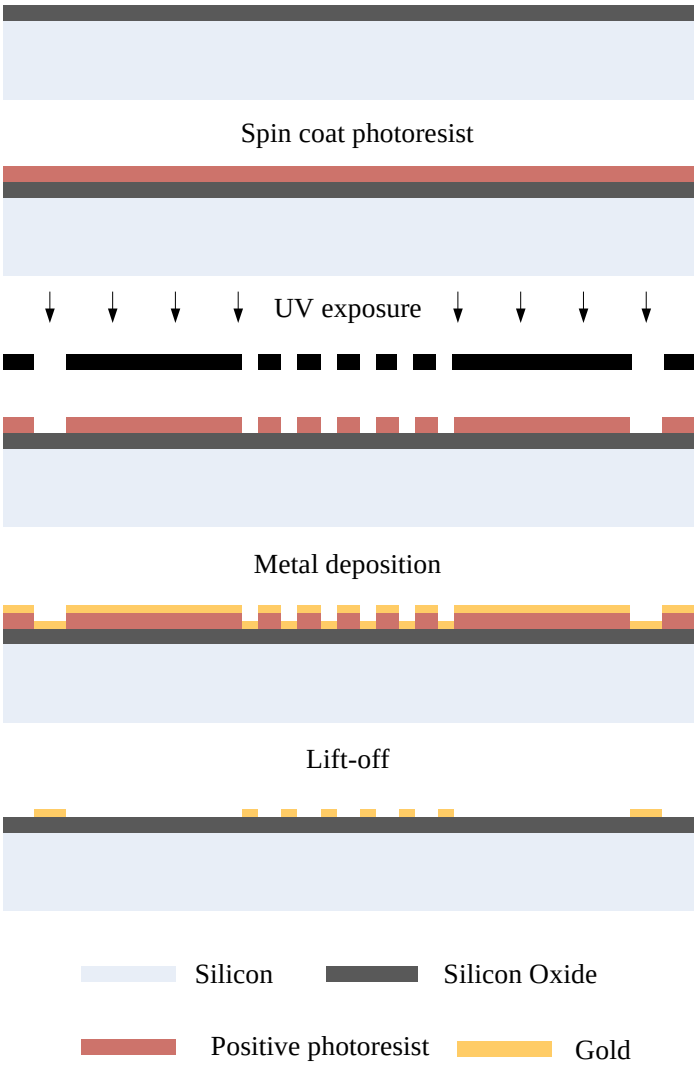

Figure 3.7 Fabrication process of novel interdigital sensors.

3.3 Electrochemical Impedance Spectroscopy (EIS)

Electrochemical Impedance Spectroscopy (EIS) has been one of the most popular and robust measurement techniques in sensor investigations [143, 144]. This technique has been widely used in monitoring of corrosion in materials [145], biomedical applications [146] and measurement of contaminants in food and beverages [136, 147]. EIS is a

powerful method for the measurement of the electrical impedance of an electrochemical system and has a high sensitivity to interfacial phenomena. Therefore, it can be useful for the characterisation of biological materials when they are introduced into a sensing system and create an electrochemical cell [148, 149]. In this method, the impedance of the system as a function of frequency is measured. EIS is actually the reaction of an electrochemical system to the applied AC signal. The real and imaginary parts of the impedance are usually used to represent the response of the system to the applied potential.

Impedance analysis of linear systems is much easier than that of non-linear systems. In EIS measurement experiments, a small AC signal is applied to the cell. With such a low voltage, the system can be considered as a pseudo-linear system. If the system is non-linear, the current response of the system will contain harmonics of the excitation frequency and may be damaged by the harmonics.

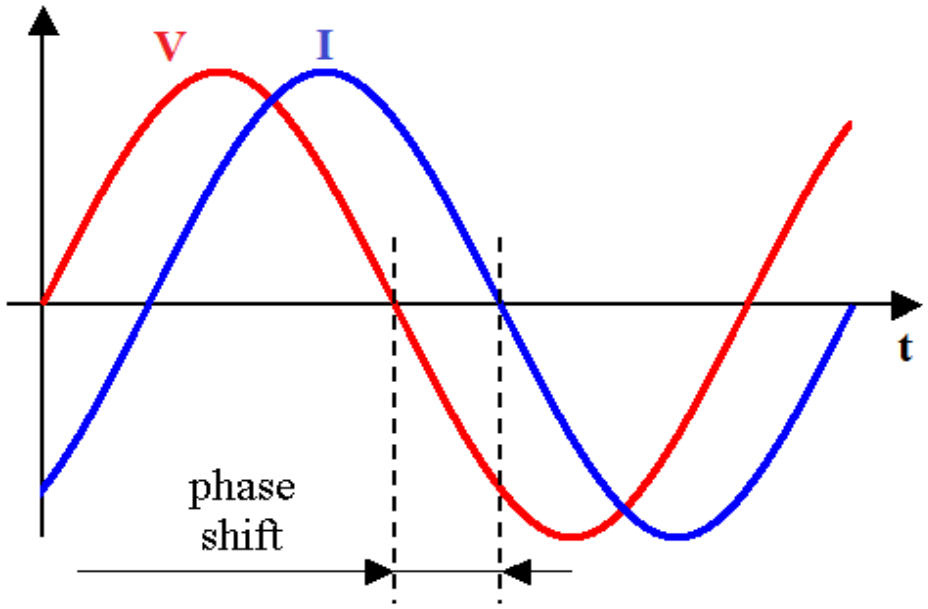

Figure 3.8 Phase shift in current signal with reference to the applied voltage.

A small-amplitude AC voltage is usually applied to an electrochemical cell and the response is a current with a certain amplitude and a phase (θ) with the input voltage. Electrochemical impedance is measured using a low excitation signal so that the cell's response is pseudo-linear. In a linear system, this current response to a sinusoidal excitation

potential will result in a sinusoidal current at the same frequency but shifted in phase as shown in Figure 3.8.

Impedance is defined as the measurement of the ability of a circuit to opposite the flow of electrical current when a voltage is applied. In an AC circuit, impedance is represented as a complex value, which involves a real part (resistance) and an imaginary part (reactance).

The excitation signal can be explained as a function of time

$$E_t = E_0 \sin \omega t \tag{3.1}$$

where E_t is the voltage difference at time t, E_0 is the amplitude of the input signal, and ω is the angular frequency given by ($\omega = 2\pi f$) expressed in radians/second and frequency, f, in hertz. For a linear circuit, the response signal, I_t, has a phase shift θ with amplitude of I_0 which can be expressed by

$$I_t = I_0 \sin(\omega t + \theta) \tag{3.2}$$

The impedance of the system can be calculated by

$$Z = \frac{E_t}{I_t} = \frac{E_0 \sin \omega t}{I_0 \sin(\omega t + \theta)}$$
$$= Z_0 \frac{\sin(\omega t)}{\sin(\omega t + \theta)} \tag{3.3}$$

The impedance, Z, can be expressed in terms of a magnitude Z_0 and a phase shift θ. Equation 3 can also be represented based on the Euler's relationship given by

$$e^{j\theta} = \cos \theta + j \sin \theta \tag{3.4}$$

The impedance, Z, can be expressed in terms of potential, E, and current response, I, given by

$$E_t = E_0 e^{j\omega t} \tag{3.5}$$

$$I_t = I_0 e^{j(\omega t - \theta)} \tag{3.6}$$

Therefore the impedance Z can be calculated by

$$Z(\omega) = \frac{V_t}{I_t} = \frac{V_0 e^{j\omega t}}{I_0 e^{j(\omega t - \theta)}} = Z_0 e^{j\theta} \tag{3.7}$$

$$= Z_0(\cos\theta + j\sin\theta) \tag{3.8}$$

The impedance now is in the form of a real part ($Z' = Z_0 \cos\theta$) and an imaginary part ($Z'' = Z_0 \sin\theta$).

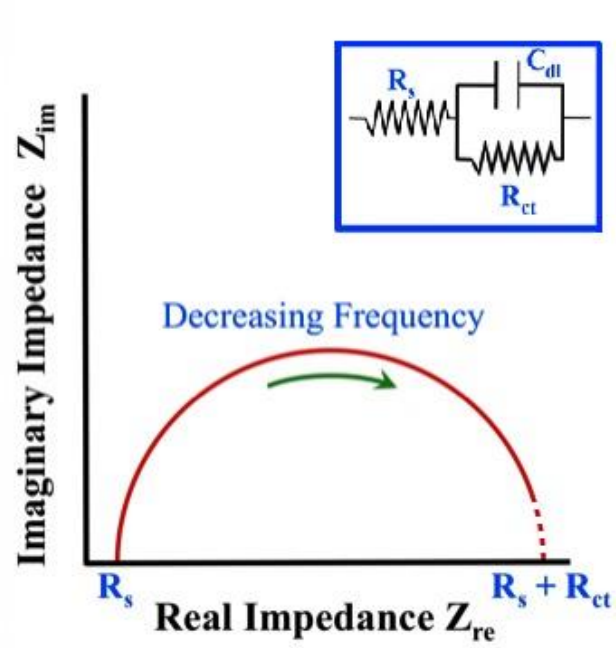

Figure 3.9 Nyquist plot obtained from EIS measurements.

The impedance is normally measured over a wide frequency range and the results are usually represented in the form of a Nyquist plot (Figure 3.9) [150, 151], which can be

useful to deduce some important parameters such as the solution resistance (R_s), charge transfer resistance (R_{ct}) and double-layer capacitance (C_{dl}). It can also give some information about the surface properties, diffusion effects and material properties. R_{ct} can be calculated by extrapolating the semicircle to the Z_{re} axis as illustrated in Figure 3.9. The solution resistance R_s can be calculated by reading the real-axis value at the high-frequency intercept, which is the intercept near the origin of the Nyquist plot. C_{dl} can be calculated using $\omega = 1/R_{ct}\, C_{dl}$ [152].

3.4 Experimental Setup

The experimental setup consisted of a thermometer and a humidity meter, interdigital sensor, material under test and a high-precision LCR meter (HIOKI IM3536 LCR Meter) that was connected to the computer through the USB port. The sensor was connected to the reference and working probes via gold-plated pin connectors. The block diagram of the measurement acquisition system is shown in Figure 3.10 and the experimental setup is given in Figure 3.11.

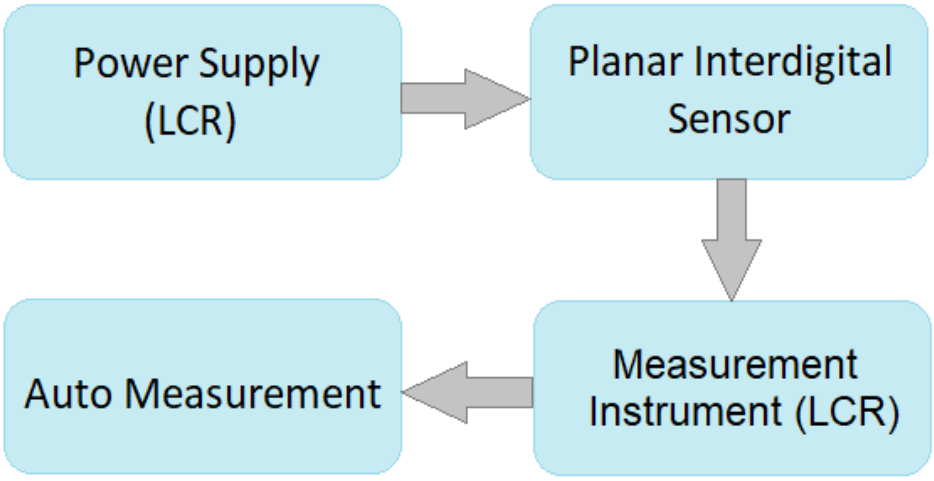

Figure 3.10 Block diagram of the measurement system, including power supply, planar interdigital sensor, measurement instrument and auto measurement.

The HIOKI IM3536 LCR Meter has been used to perform the EIS measurement. It has high accuracy (± 0.05% rdg) and high speed (1 ms fastest time). The LCR meter was used as a power supply as well as the measurement instrument and it was connected to a computer to save data as an Excel file while sweeping through a range of pre-defined frequencies. Figure 3.12. shows the front panel of HIOKI high precision LCR meter IM3536. The technical specifications of the HIOKI IM3536 LCR Meter are given in Table 3.2.

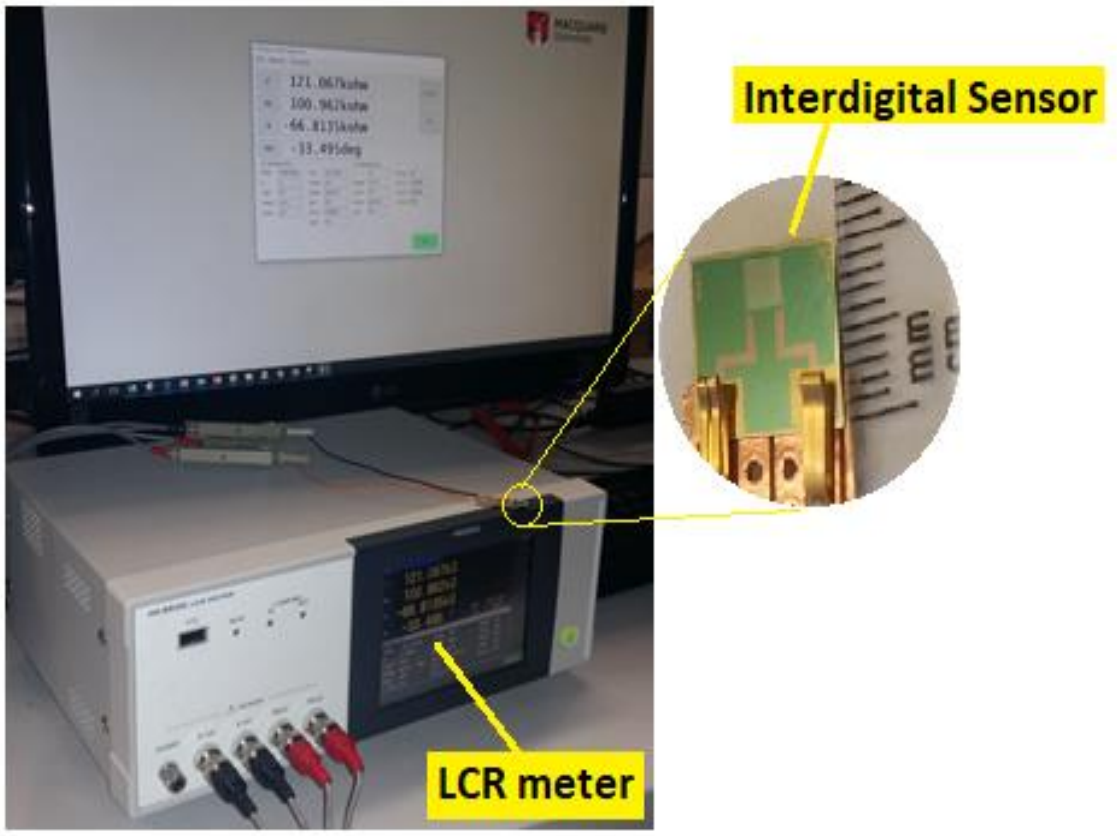

Figure 3.11 Experimental setup of the measurement system including the LCR meter and interdigital sensor.

Figure 3.12 The front panel of a high precision HIOKI IM3536 LCR Meter (Japan) [153].

Table 3.2 Specification overview of HIOKI IM3536 LCR meter.

Frequency range	4 Hz to 8 MHz
Measurement level (V mode, CV mode)	Normal mode: 4 Hz to 1 MHz: 10 mV to 5 V_{rms} (Max. 50 mA) 1.0001 MHz to 8 MHz: 10 mV to 1 V_{rms} (Max. 10 mA) Low-impedance high-accuracy mode: 10 mV to 1 V (Max. 100 mA)
Measurement level (CC mode)	Normal mode: 4 Hz to 1 MHz: 10 µA to 50 mA(Max. 5 V) 1.0001 MHz to 8 MHz: 10 µA to 10 mA (Max. 1 V) Low-impedance high-accuracy mode: 10 µA to 100 mA (Max. 1 V)
Measurement time	Approximately 1 ms
Accuracy range	1 mΩ to 200 MΩ
Measurement parameters	Z, Y, θ, R_S, R_P, X, G, B, C_S, C_P, L_S, L_P, D, Q, R_{dc}, σ, ε

3.5 Chapter Summary

Interdigital sensors are among the most popular periodic electrode structures. Several advantages such as one-side access, control of signal strength, simplified modelling high sensitivity and small size have made them suitable for different applications. EIS is a versatile method that describes the capacitive and resistive characteristics of materials by using a frequency-dependent small-amplitude AC signal. Due to the high sensitivity and simplicity of the technique, it has been widely implemented in biosensor applications using different methods [154]. Interdigital sensors in conjunction with the EIS measurement method has been reported to evaluate environmental monitoring [155], detection of phthalates in juices and water [156], dangerous chemicals in seafood [157], humidity [158] and DNA detection [159]. In this chapter, the operating principle of the planar interdigital sensor has been explained and a basic theory of Electrochemical Impedance Spectroscopy has been discussed. An experimental setup has been introduced which can fetch the information from the test sample and convert it into an electrical signal for further analysis.

4

Antigen-antibody-based Sensor for CTx-I Detection

Publication pertaining to this chapter:

- ***N. Afsarimanesh***, A.I. Zia, S.C. Mukhopadhyay, M. Kruger, Pak-Lam Yu, J. Kosel, and Z. Kovacs. "Smart Sensing System for the Prognostic Monitoring of Bone Health". **MDPI Sensors** 16, no. 7, pp. 1-13, June **2016**.

4.1 Introduction

A receptor that behaves as a sensing element (such as an antibody [160], an enzyme or nucleic acid) plays a significant role in deciding the sensitivity and selectivity of an electrochemical sensor. The selective and specific capturing of the target molecules through the recognition elements is very important to design and develop an efficient biosensor. Thus, developing sensors with good efficiency greatly relies on the use of a selective material to enhance the recognition of the biosensor. Different types of biosensors have been developed by making use of enzymes [160], antibodies [161], membranes [162], carbon nanotubes [162], magnetic nanoparticles and supramolecular assemblies to act as the recognition elements for chemical and biochemical molecules. Various antigen (Ag)-antibody (Ab)-based biosensors have been reported in the literature [115, 119]. In our research, an impedometric antigen-antibody-based biosensor has been developed for the bone-loss monitoring by measuring CTx-I in serum.

4.2 ELISA-based Experiments

The experiments were initiated by using an ELISA kit in order to get some idea about antigen-antibody-based techniques. It was also used to validate the results obtained from the proposed biosensor. As it was explained in Chapter 2, most of the available techniques for the detection and measurement of biochemical markers of bone turnover are based on the ELISA. ELISA is an analytical tool that is widely used in biomedical research for the detection and measurement of a specific antigen in a liquid sample. ELISA uses enzyme-linked antigens and antibodies to detect the target molecule. Very small quantities of antigens such as hormones, proteins, peptides, or antibodies in a liquid sample can be detected using ELISA [163, 164].

The antigen in the liquid phase is coated into the wells of a 96-well microtitre plate that binds to a primary antibody. A secondary, enzyme-linked antibody then detects the antigen by binding the antigen to the antibody. A chromogenic substrate is used to change colour in the presence of the antigen. Finally, the measurement is done using spectrophotometry [165]. Though this method is a standard immunoassay technique and has been commercialised, there are some drawbacks in using ELISA; it is a laboratory-based assay that is time-consuming, expensive and requires several steps and technical expertise. It

involves numerous steps and procedures for incubation, antibodies binding and measurements that require not only the services of highly skilled professionals and an expensive laboratory setup but also involve high costs for testing individual samples, and hence cannot be used for frequent monitoring of CTx-I levels to track changes in bone resorption in an individual.

4.2.1 Materials and Chemicals

The Serum CrossLaps® ELISA kit, a product of the IDS Company (UK), was purchased locally from Abacus ALS, New Zealand. This is a special test to measure the concentration of CTx-I in blood plasma. The kit contained a streptavidin-coated microtitre plate, biotinylated antibody, peroxidase conjugated antibody, six known-concentration antigen solutions, washing buffer, incubation buffer and stopping solution. Known-concentration antigen standards, biotinylated antibody and peroxidase conjugated antibody from the ELISA kit were also used for performing the experiments using the developed sensing system. Streptavidin-agarose was procured from Sigma-aldrich, USA.

4.2.2 Assay Procedure

The antibody solution was prepared 30 minutes before starting the assay by mixing biotinylated antibody, peroxidase conjugated antibody and incubation buffer in the volumetric ratio of 1+1+100. After that, standards and control were pipetted into the wells followed by adding the prepared antibody solution to them. At this stage, a complex between the antigens and antibodies was formed and this complex binds to the streptavidin surface via a biotinylated antibody. After one-step incubation (120±5 min), the wells were emptied and washed 5 times manually with diluted washing buffer.

Then a chromogenic substrate was pipetted into the wells and incubated for 15±2 min in the dark mixing apparatus (300 rpm). Then, the colour reaction was stopped with sulphuric acid. Finally, the measurement was done using the spectrophotometer. The ELISA procedure has been summarised in the form of a flow chart in Figure 4.1.

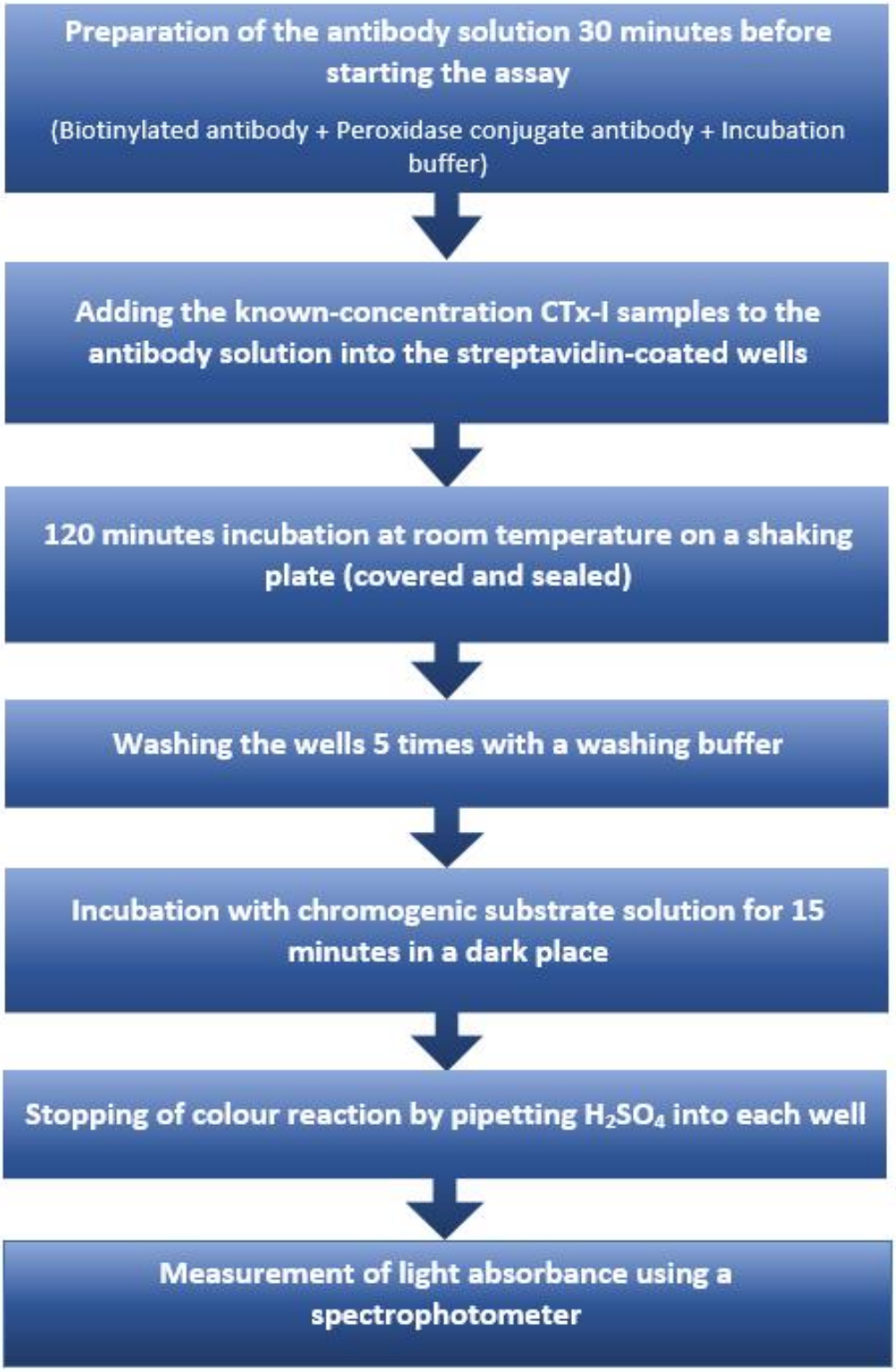

Figure 4.1 Flow chart of ELISA procedure.

4.2.3 Results

The Serum CrossLaps® ELISA kit was used to obtain the standard curve by testing six standards. The concentrations of known samples are zero (control), 0.147, 0.437, 0.798, 1.693 and 2.669 ng/ml. The standard curve obtained from ELISA is given in Figure 4.2. All samples were tested in duplicate and the assay was performed at room temperature. Once the standard curve was obtained the experiments were performed for two unknown samples, obtained from sheep blood. The concentration of CTx-I in the first sample was 0.6514 ng/ml, and in the second sample it was 0.5049 ng/ml. Table 4.1 provides a comparison between the actual and measured concentrations.

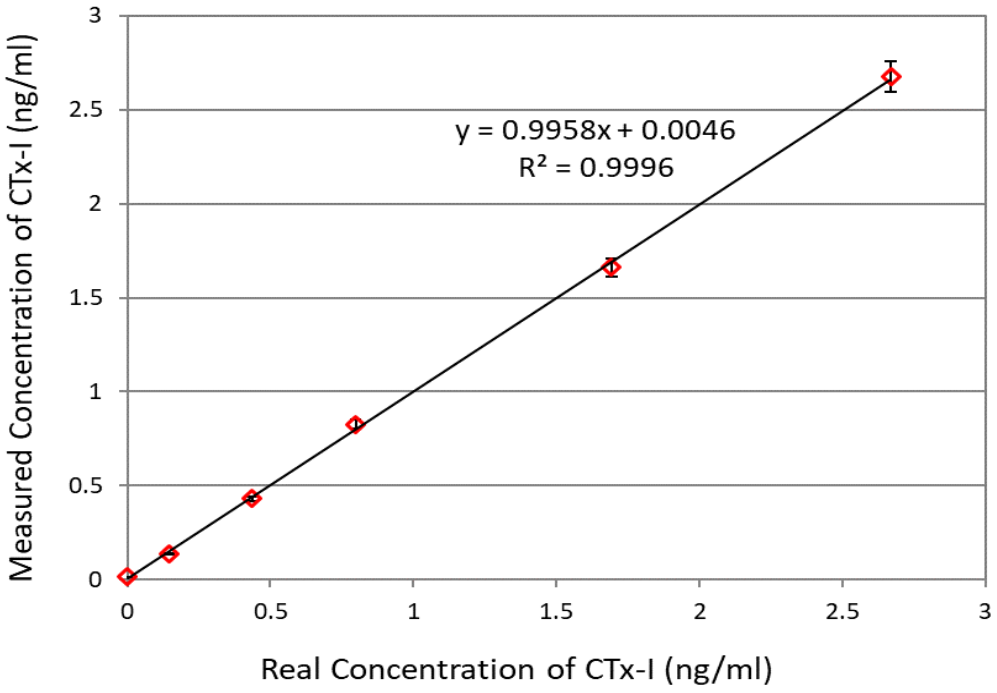

Figure 4.2 The standard curve plotted from the ELISA results.

Table 4.1 Comparison between the known concentrations and measured concentrations using the ELISA kit.

Known concentration	Measured concentration	Error (%)
0.147	0.151	2.63
0.437	0.439	0.62
0.798	0.800	0.16
1.693	1.690	0.15
2.669	2.662	0.25

4.3 Ag-Ab-based Biosensor

In order to develop an efficient smart sensing system for CTx-I detection, the sensor is required to be selective to CTx-I and should be able to capture the CTx-I molecules for the detection and quantification purpose. An Ag-Ab-based technique was used to make the sensor selective for a particular analyte (CTx-I) using the corresponding natural antibodies. Biotinylated antibody, peroxidase conjugated antibody and standard antigens from an ELISA kit were also used for the developed sensing system and streptavidin agarose was purchased from Sigma-Aldrich, USA. The same procedure as ELISA was followed to prepare the antigen-antibody solution.

The bare interdigital sensor was EIS-profiled in air in order to characterise the sensor and to determine the sensitive frequency range for the specific sensor. In the next step, the sensing area of the sensor was spin-coated with 4 µL of streptavidin agarose in order to functionalise the sensing surface [166]. The sensor was dried in a nitrogen atmosphere and later it was characterised again by impedance spectroscopy to determine the change in impedance profile, which was compared to that of the uncoated sensor in order to obtain a reference plot for the individual interdigital sensor.

Figure 4.3 shows the SEM image of a streptavidin agarose-coated sensor. Streptavidin agarose acts as a cross-linker between the gold electrodes/ SiO_2 substrate and biotinylated CTx-I antibodies that are responsible for capturing the analyte from serum or urine samples.

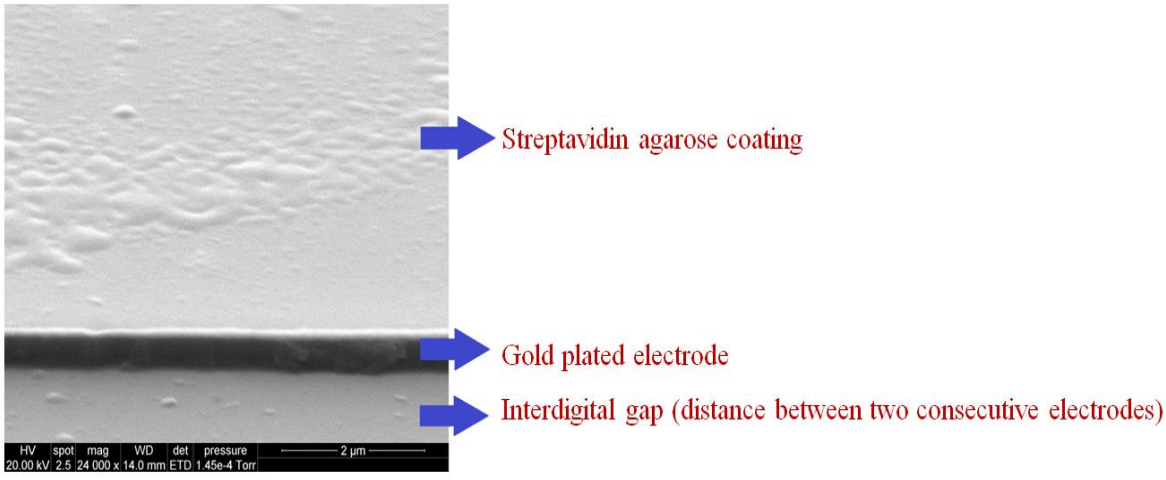

Figure 4.3 SEM image of streptavidin agarose-coated sensing surface, showing streptavidin agarose coating on the gold electrodes.

At the next stage, the antibody-antigen solution was prepared by mixing the antigen, biotinylated antibody and a peroxidase conjugated antibody which are available in the ELISA kit. The prepared solution was then incubated for an hour to allow antibodies to entrap CTx-I molecules from the test sample, before pipetting 8 µL of the solution on the streptavidin-coated sensing surface of the interdigital sensor. Later, one-hour incubation at room temperature was allowed for the streptavidin coating to cross-link the antibody-antigen complex onto the gold interdigital electrodes. The sensor was washed five times using a washing buffer solution and dried under nitrogen at room temperature.

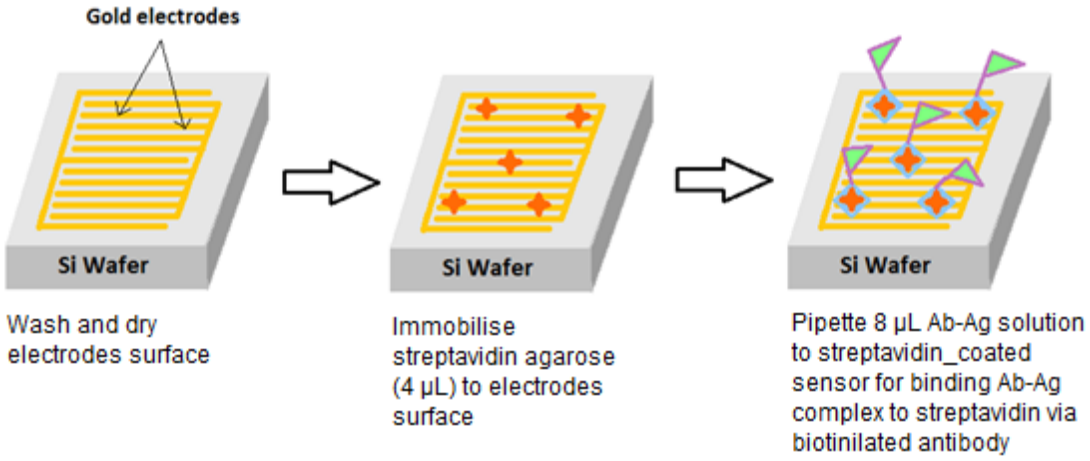

Figure 4.4 Graphical illustration of the steps required to prepare the sensing surface for CTx-I sensing.

4.3.1 CTx-I Measurement in Known Samples

Samples with four known concentrations (0.147 ng/ml, 0.437 ng/ml, 0.798 ng/ml and 1.693 ng/ml) were tested in the developed sensing system. The standard solution with a zero concentration of CTx-I was considered as the control. Experiments were conducted at room temperature (21ºC) at a humidity level of 31%.

Tests on the samples were performed by the developed sensing system immediately after preparing the sample solutions. Figure 4.5 (a) shows the reactance in the frequency domain for all four CTx-I concentrations. As illustrated in this figure, the capacitive reactance (X) shows a drastic variation, especially at lower frequencies between 100 Hz to

750 Hz. with a change in CTx-I concentration that is attributed to the dielectric properties of the sample. The real part of impedance vs frequency for different concentrations of CTx-I is plotted in Figure 4.5 (b).

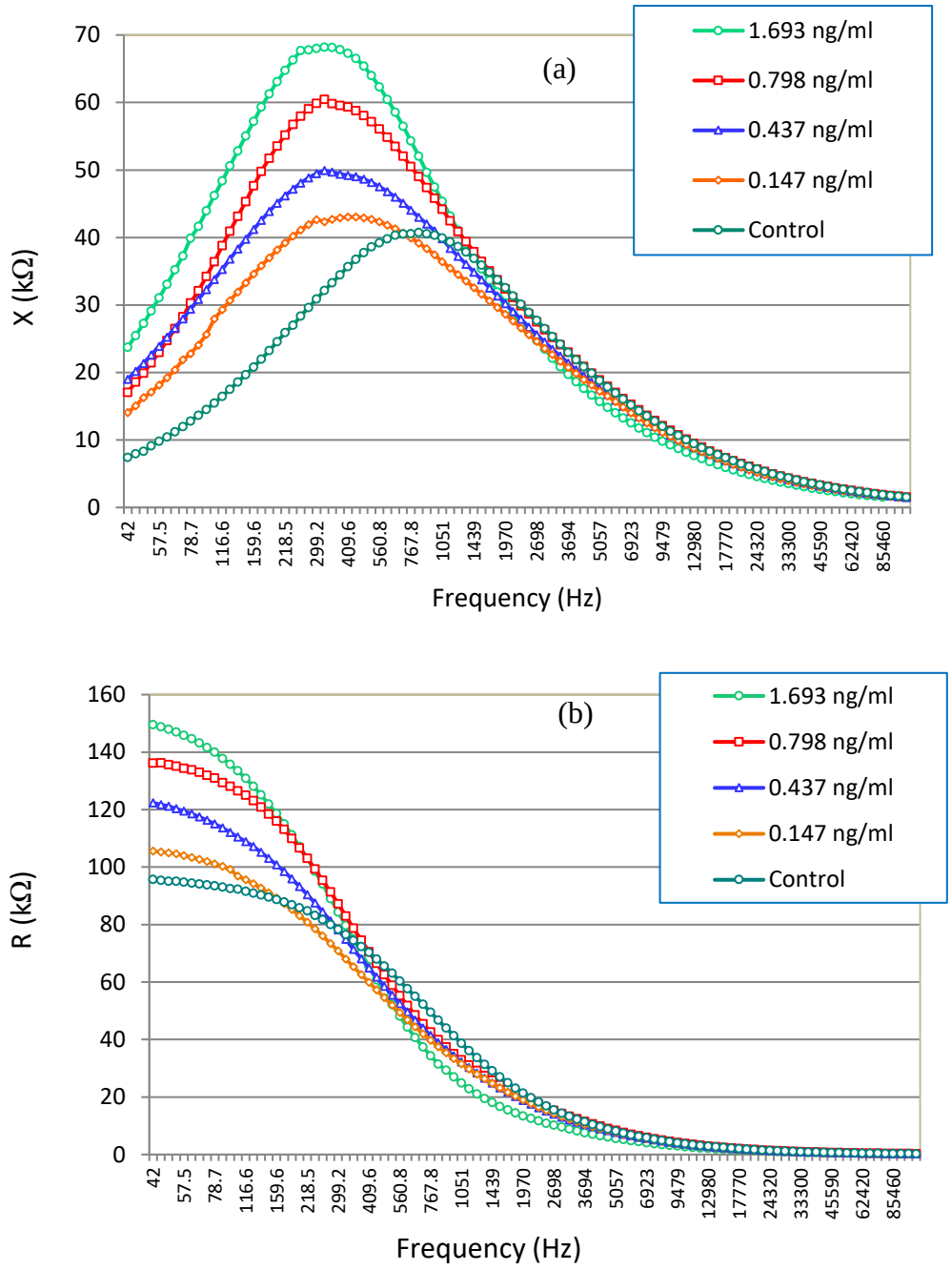

Figure 4.5 (a) Imaginary part (reactance) of the impedance vs frequency; (b) Real part of the impedance vs frequency.

The change in the resistive part of the impedance (R) is seen only at very low frequencies up to 150 Hz, which is mainly due to the ionic properties and faradic current through the sample material. The sensitivity obtained from the reactance part is also higher

than for the resistive part. Therefore, the reactance was used to evaluate the concentration of CTx-I in the sample solutions.

Figure 4.6 shows the Nyquist plot for the impedance spectrum obtained for all four concentrations of CTx-I in a frequency range of 42 Hz to 100 kHz. It was observed that the diameter of the semicircle is increased by increasing the concentration of CTx-I, depicting the increase in charge transfer resistance due to the presence of higher amounts of CTx-I attached to the sensing surface.

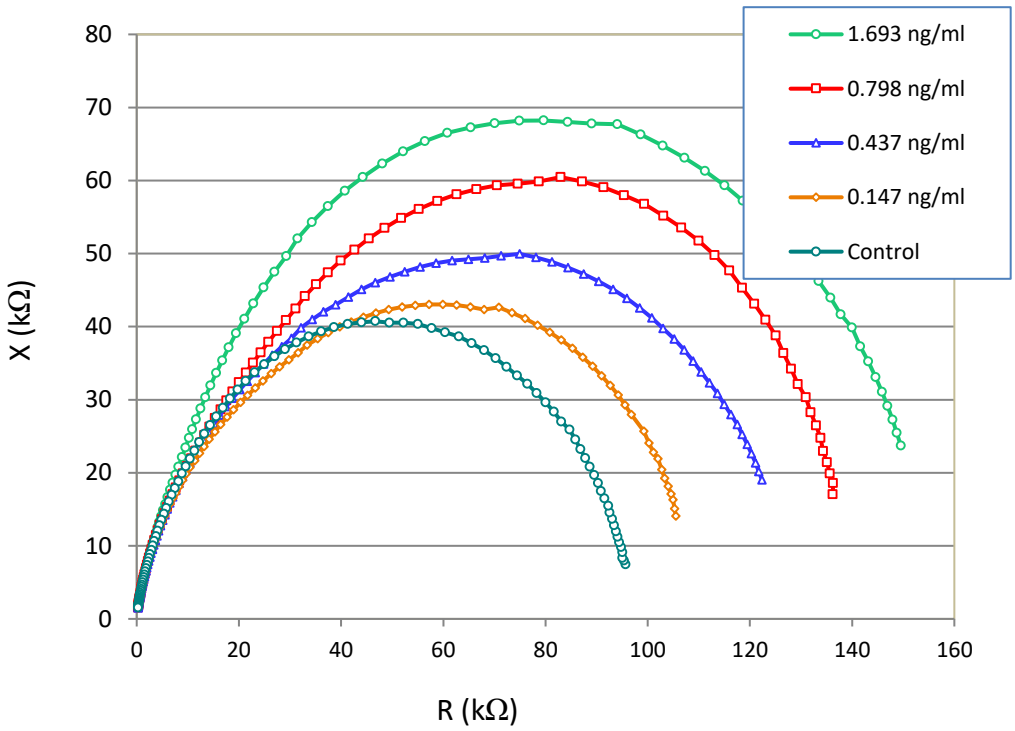

Figure 4.6 Imaginary part (reactance) of the impedance vs frequency.

4.3.2 Data Analysis Using Non-linear Least-Square Curve Fitting

The equivalent circuit was deduced by applying the complex non-linear least-square method (CNLS) that fits the experimentally observed impedance spectrum to theoretically evaluated values for an electrical circuit. It interprets the electrochemical kinetic processes executing inside a chemical cell into its electrical equivalent circuit based on Randle's model [127, 167].

The EIS Spectrum-analyser algorithm was used to estimate the equivalent circuit. The fitted Nyquist plot and the proposed equivalent circuit for the electrochemical processes are given in Figure 4.7, where the points on the graph represent the experimentally observed data and the solid line shows the theoretically fitted response for the equivalent circuit. The equivalent circuit proposed by the complex non-linear least-square curve fitting is a parallel combination of constant phase element (CPE1) and charge transfer resistance (R2) in series with the solution resistance (R1).

Table 4.1 displays estimated component parameters and values of the equivalent circuit. P1 and n1 are parameters of the constant-phase element, representing the pre-exponential factor and exponent, respectively. The fitted value of n1 dictates the capacitive behaviour of CPE1 as shown in Table 4.1 [168]. The evaluation error was <2.8% for the equivalent circuit parameters. $r^2_{amplitude}$ indicates the deviation of the experimentally observed value from the optimal solution.

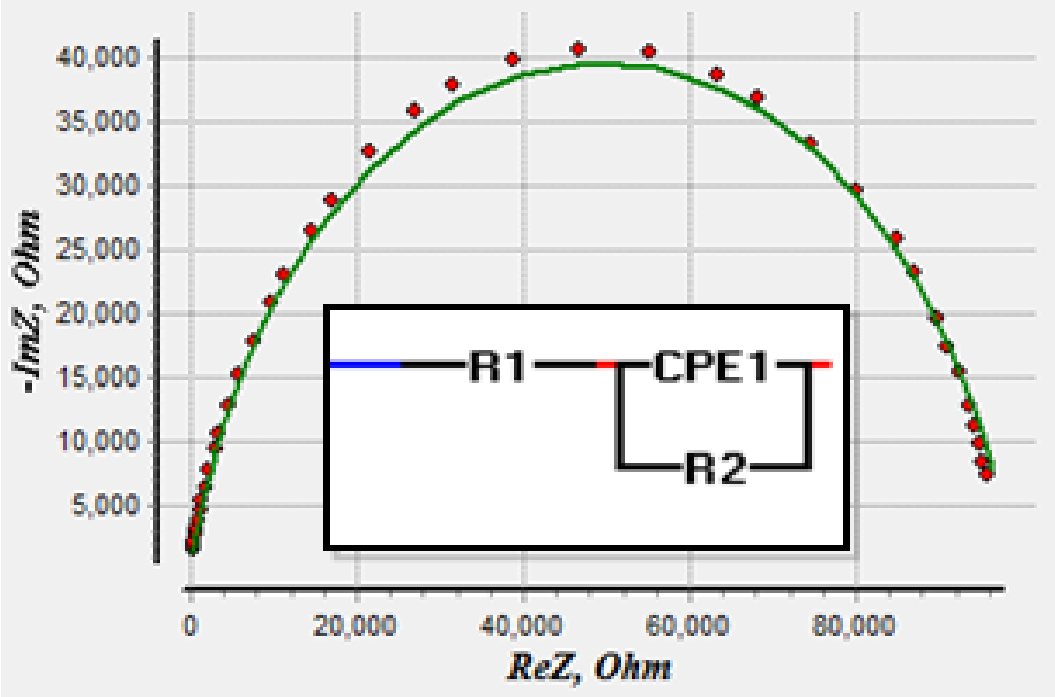

Figure 4.7 Proposed equivalent circuit by CNLS with a parallel combination of a constant-phase element (CPE1) and a charge-transfer resistance (R2) in series with the solution resistance (R1).

Table 4.2 Equivalent Circuit Parameters.

Component parameters	0.147 ng/ml	0.437 ng/ml	0.798 ng/ml	1.693 ng/ml
R1 (Ω)	1.790E-14	1.686E-14	1.657E-14	1.660E-12
R2 (Ω)	1.153E05	1.347E05	1.480E05	1.596E05
P1	1.535E-08	1.588E-08	1.036E-08	6.464E-09
n1	0.7944	0.7944	0.8345	0.8823
$r_{amplitude}{}^2$	0.0133	0.0100	0.0161	0.0246

4.3.3 Multivariate Chemometric Analysis

The results of impedance-spectroscopy measurements were subjected to multivariate data evaluation. Principal Component Analysis (PCA) was used to identify possible outliers and to discover the multidimensional patterns of the individual parameters, namely Real part of impedance R (Ohm), reactance X (Ohm) and Phase shift (Degrees). Results of PCA showed that the highest variation related to the concentration change of CTx-I occurs in the lower frequency range in the case of all the three measured parameters. Therefore, the frequency range between 42 and 5917 Hz was used for the further chemometric evaluation. PCA models were calculated using the truncated frequency range for all the three individual parameters. The first two principal components (PC1 and PC2) described more than 98% of the whole variation in all the three models. Furthermore, PC1 and PC2 presented a good separation of the groups of the different concentration CTx-I samples.

PCA results of the X (reactance) parameter are shown in Figure 4.8 (a) and (b). PCA score plots (PC1 and PC2) of reactance (X) were calculated based on the frequency range between 42 to 5917 Hz. Figure 4.8 (a) demonstrates a tendency to separation of the different concentration CTx-I samples based on their increasing concentration. The loadings of the PCA model in Figure 4.9 (b) imply the importance of the frequency range between 42 and about 2000 Hz in this separation.

Following the PCA calculations, regression models were built with Partial Least-Square Regression using the three individual parameters (Rs, X and Phase angle), separately and using the frequency range between 42 and 5917 Hz to regress on the CTx-I concentration.

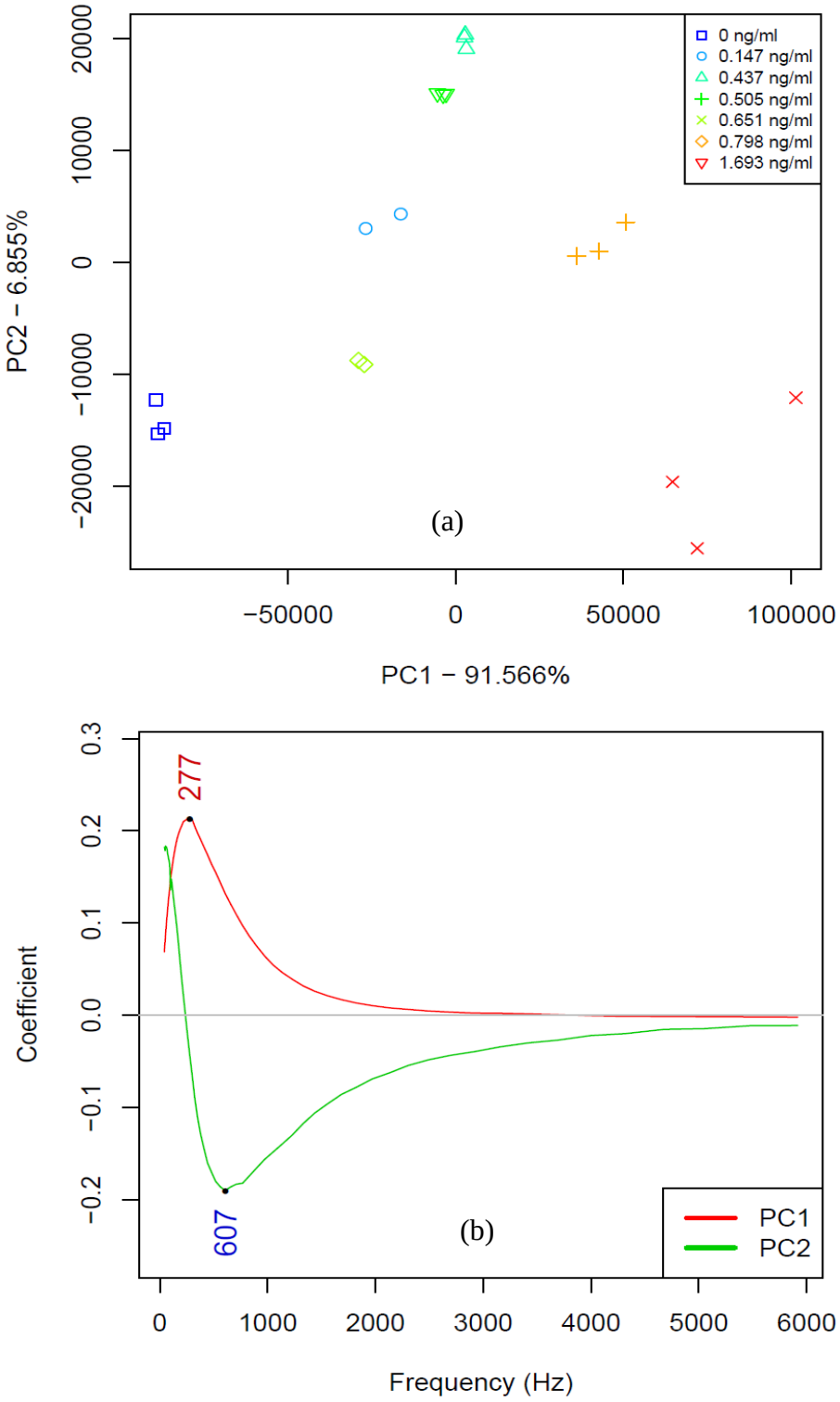

Figure 4.8 (a) Principal Component Analysis score plot (PC1-PC2); (b) Principal Component Analysis loadings plot (PC1-PC2).

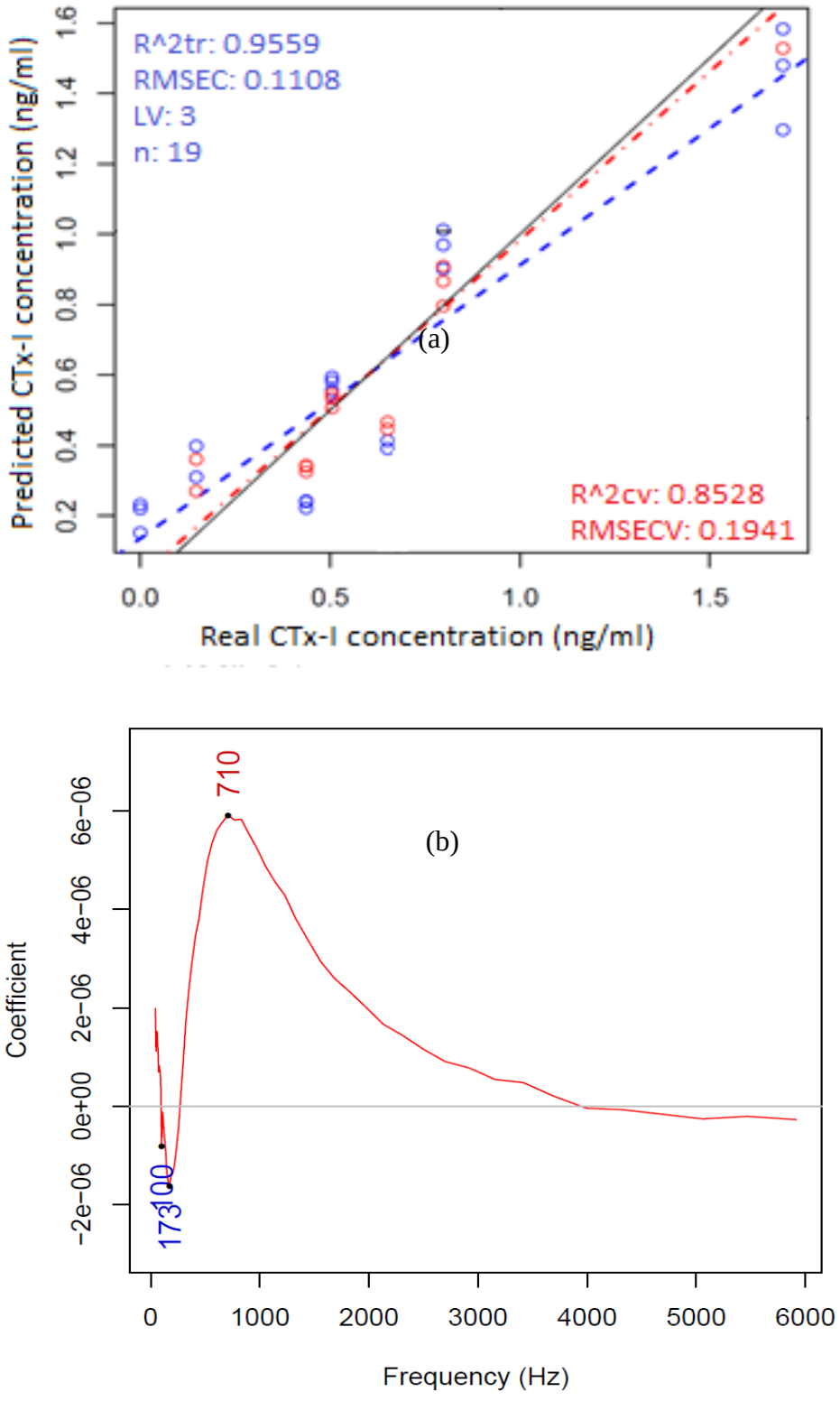

Figure 4.9 (a) Partial Least-Square Regression model to regress on CTx-I concentration (red colour is for calibration and the blue colour is for the cross-validation model), (b) regression vector of Partial Least-Square Regression model showing 710 Hz as the most discriminating frequency.

The best regression model was found for the reactance (X) data as shown in Figure 4.9 (a), (b). The PLSR model of the reactance (X) parameter provided relatively close correlation and a low prediction error. Results of cross-validation showed the concentration of CTx-I samples could be predicted based on reactance (X) with an error of 0.1941 ng/ml in the concentration range between 0 and 1.693 ng/ml using the frequency range between 42 and 5917 Hz. The regression vector of the PLSR model (Figure 4.9 (b)) emphasises the high importance of 710 Hz for the regression of the CTx-I concentration.

4.3.4 CTx-I Measurement in Unknown Samples using the Ag-Ab-based Biosensor

Based on the results from multivariate analyses the sensitivity of the sensor was calculated at a frequency of 710 Hz from the reactance (X) data using the following equation:

$$Sensitivity\ (\%) = \frac{\mathrm{X}\,(Control) - \mathrm{X}\,(Sample)}{\mathrm{X}\,(Control)} \times 100 \qquad \textbf{(4.1)}$$

A reference curve was obtained by plotting the sensitivity against the concentration, and is shown in Figure 4.10. This curve could be used to measure the concentration of CTx-I in any unknown sample with the CTx-I concentration ranging between 0 ng/ml to 1.693 ng/ml.

Once the reference curve was plotted, further experiments were performed in order to evaluate the CTx-I concentration for the two unknown samples of sheep blood that were evaluated using ELISA in order to validate the EIS system performance. The calculated concentration of CTx-I in the first unknown CTx-I concentration sheep blood sample was evaluated to be 0.6229 ng/ml, whereas the calculated concentration of CTx-I was 0.5280 ng/ml in the second sample. The results obtained were validated using ELISA. The error for the first sample was 4.3% and for the second one was 4.6%. The results of the real sample measurement using both methods are given in Table 4.2.

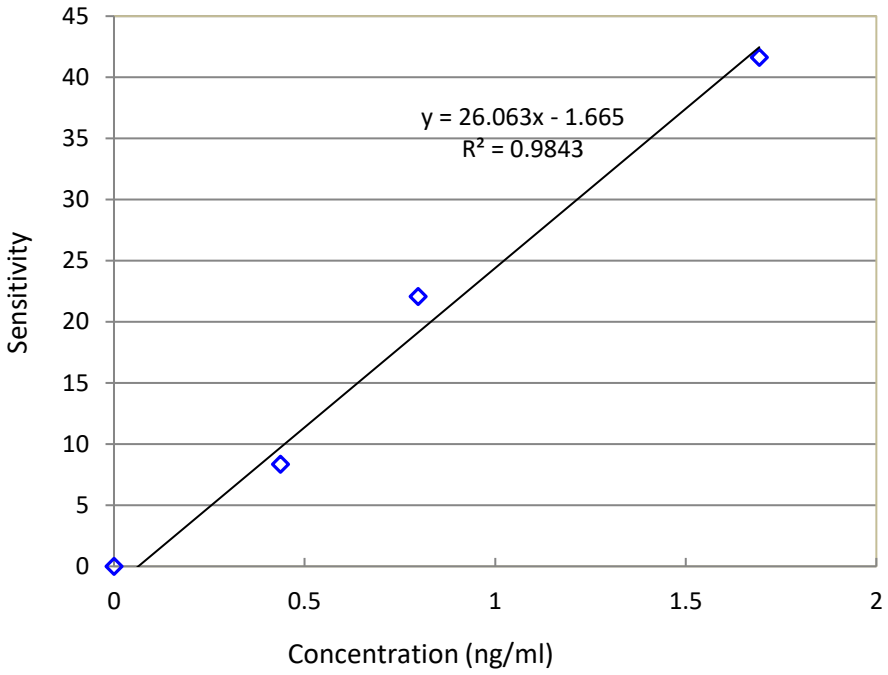

Figure 4.10 The reference calibration curve for the sensitivity of the sensor vs. concentration evaluated at 710 Hz.

Table 4.3 Unknown sample measurement and validation with standard ELISA method.

Sample	CTx-I level (ppb)		Error (%)
	Ag-Ab-based proposed method	Reference method ELISA	
1	0.6229	0.6514	4.3
2	0.5280	0.5049	4.6

4.4 Chapter Summary

A non-invasive, real-time and label-free sensing technique towards early detection of bone loss has been reported. The proposed system incorporates Ag-Ab based functionalisation by employing Streptavidin Agarose as a cross-linker for binding CTx-I peptide. A silicon substrate-based planar sensor, patterned with gold interdigital electrodes, has been used in conjunction with EIS to measure the electrochemical impedance of the

samples. The equivalent circuit has been deduced by applying the complex non-linear least-square curve-fitting technique. Multivariate chemometric analyses have been performed to determine the single optimal frequency that could provide the highest sensitivity to the sensing system. Calibration experiments have been conducted with various known CTx-I concentrations in a buffer solution to obtain a reference curve that was used to quantify the concentration of an analyte in the unknown serum sample. Two unknown samples, obtained from sheep blood, have been tested by the developed sensing system and the results were validated using ELISA. All the experiments were performed 5 times to ensure the repeatability and accuracy of the proposed sensing device.

However, there are some limitations in using the developed system. It is time-consuming, requires several steps to prepare the antigen-antibody solution and requires a laboratory-based environment to carry out the experiments. Moreover, natural antibodies are very expensive, sensitive to harsh environmental conditions and have limited stability. The next chapter describes the development of artificial antibodies for CTx-I molecules, in order to overcome the mentioned limitations.

5

MIP-based Sensor for CTx-I Detection

Publication pertaining to this chapter:

- ***N. Afsarimanesh***, S.C. Mukhopadhyay and M. Kruger. "Molecularly Imprinted Polymer-Based Electrochemical Biosensor for Bone Loss Detection". **IEEE Transactions on Biomedical Engineering, 2017,** vol. 65, no. 6, pp. 1264-1271, June **2018**..
- ***N. Afsarimanesh,*** S.C. Mukhopadhyay and M. Kruger. "Performance Assessment of Interdigital Sensor for Varied Coating Thicknesses to Detect CTX-I**", IEEE Sensors Journal**, vol. 18, no. 10, pp. 3924-3931, May **2018**.

5.1 Introduction

As mentioned in the last chapter, there are some limitations in using natural antibodies: the antibody immobilisation procedure is complicated, biological antibodies are expensive and have limited stability. Moreover, sample preparation is a complex and time-consuming process. The use of artificial antibodies can be very helpful to overcome these problems. Molecular imprinting technology is a rapid and inexpensive technique to synthesise polymers that have selectivity and sensitivity to a predetermined molecule, called Molecular Imprinted Polymers (MIPs). MIP technology has been utilised for a range of different template molecules [169-172] and has been successfully employed in different applications as solid-phase extraction materials [173], binding assays [174, 175] and enzyme-mimic catalysts [176-178], and they are progressively being used in imprinted layers to develop chemical sensors [179, 180].

The use of MIPs has been reported for the development of electrochemical sensors depending on different transduction models such as conductometric [181], potentiometric [182], voltametric [183] and capacitive sensors [184].

The aim of this research is to design a smart biosensing system for early detection of bone loss that is easy to use, inexpensive, and quick and can be used as a Point-of-Care (PoC) device outside the laboratories. Therefore, the development of a sensing system that combines the advantages of MIP-based artificial antibodies with a fast and inexpensive electrochemical sensor seems to be a very promising approach towards our goal.

To our knowledge, so far, no MIP-based interdigital sensor has been introduced for CTx-I detection. This chapter explains the development of an impedometric CTx-I biosensor, combining MIP technology and the EIS technique for a sensitive and rapid measurement of serum CTx-I.

5.2 General Principle of Molecular Imprinting Technology

Molecular imprinting is an inexpensive and relatively straightforward technique for the preparation of polymers having selective adsorption binding sites for a given molecule to replace natural receptors [185-188]. The molecular imprinted polymer is formed by mixing functional monomers, template molecules, a cross-linker and the initiator in a proper solvent. Subsequently, this mixture is subjected to heat in order to start polymerisation. The

complexes formed between the functional monomers and the template molecules are fixed within a highly cross-linked polymer. After that, the template molecules will be extracted out of the polymer; 3D cavities will be left in the polymer matrix, which are complementary in shape, size and chemical functionality to the template. The high degree of cross-linking causes the cavities to keep their shape after removing the template and enables their rebinding and recognising the template molecule [189]. Figure 5.1 illustrates the general procedure of MIP.

The major advantages of using MIP include ease of preparation, low production cost, storage stability, high mechanical strength, durability to pressure and heat, suitability in the harsh chemical environment and repeating the operation without losing the activity [175]. Molecular imprinting has become increasingly attractive in different fields of biology and chemistry, as a technique for the creation of artificial recognition sites with a memory of a predetermined target molecule. Some of the most promising areas of MIP applications are for sensors [136, 190-192], assays [193], artificial antibodies [194, 195] and chromatographic stationary phases [196, 197].

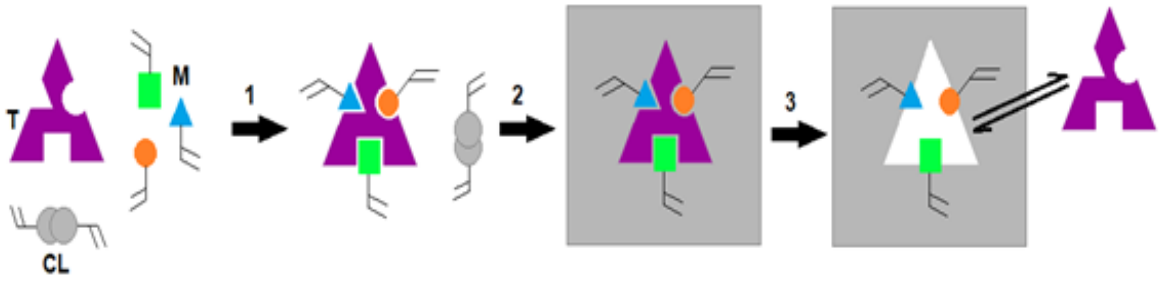

Figure 5.1 General principle of molecular imprinting technology. A template molecule (*T*) is mixed with functional monomers (*M*) and a cross-linker (*CL*) forming a self-assembled complex (*1*). The polymerisation of the resulting system produces a highly cross-linked structure including imprinted sites (*2*). Finally comes the extraction of the template living cavities that can selectively recognise and bind the target molecule (*3*)

5.2.1 MIP Categories

Based on the covalent or non-covalent bonds between the template and functional monomers, two types of molecular imprinting strategies have been established. The non-covalent approach has been used extensively due to its many advantages such as easy preparation, easy removal of the template molecule, and faster rebinding [198-201].

Covalent imprinting

In the covalent approach, the template molecule is covalently coupled to the functional monomer by utilising reversible covalent bonds. After the polymerisation, the imprint template is chemically cleaved from the polymer matrix. The covalent bond will be formed again while reintroducing the template into the polymer matrix. The covalent approach has been used for different types of template molecules like sugars [202] and glyceric acid [203]. The requirements for covalent imprinting differ from the requirement for a non-covalent approach, especially based on the ratio of the template, monomer, and cross-linker.

The main advantage of this approach is that a homogenous distribution of recognition sites will be formed in the polymer matrix [186, 204]. However, this technique requires an acid hydrolysis procedure to cleave the imprinted molecule from the polymer matrix [186].

Non-covalent imprinting

Non-covalent imprinting is the most commonly used technique to prepare the MIP due to its simplicity. In the non-covalent imprinting method, the template-monomer complex is formed by non-covalent weak interactions (ionic, hydrophobic and hydrogen bonding) between the template molecule and the monomer [205-207]. Different functional monomers can be used in the non-covalent method, but methacrylic acid (MAA) has been used extensively as a functional monomer due to its ability to interact with different functional groups [186].

Amino acids are usually used in the non-covalent method due to their strong interaction with MAA [208]. However, the formation of bonds between the template and monomers can be easily disrupted in polar environments.

5.2.2 Effects of Monomers, Cross-linker, Porogenic Solvents and Initiator in MIP

Monomers

Monomers play a very important role in the synthesis of MIP, to provide complementary interactions with the template molecule and substrates. In the covalent imprinting method, no effect can be observed in varying the ratio of the template to functional monomers because the template itself determines the number of functional monomers that should be attached covalently. However, in the non-covalent approach, the optimal ratio of template to monomer is achieved experimentally by trying different template/monomer ratios [209].

It is very important that the functionality of the monomer be matched with the functionality of the template in a complementary fashion in order to maximise the imprinting effect. Figure 5.2 shows the common functional monomers used in the non-covalent molecular imprinting method.

Cross-linkers

The amount and type of cross-linker in the preparation of the MIP can greatly influence the selectivity. The cross-linker plays three major roles in the synthesis of the MIP: controlling the morphology of the MIP, stabilizing the imprinted recognition sites, and giving mechanical stability to the polymer matrix. The chemical structure of some common cross-linkers used in non-covalent molecular imprinting is given in Figure 5.3.

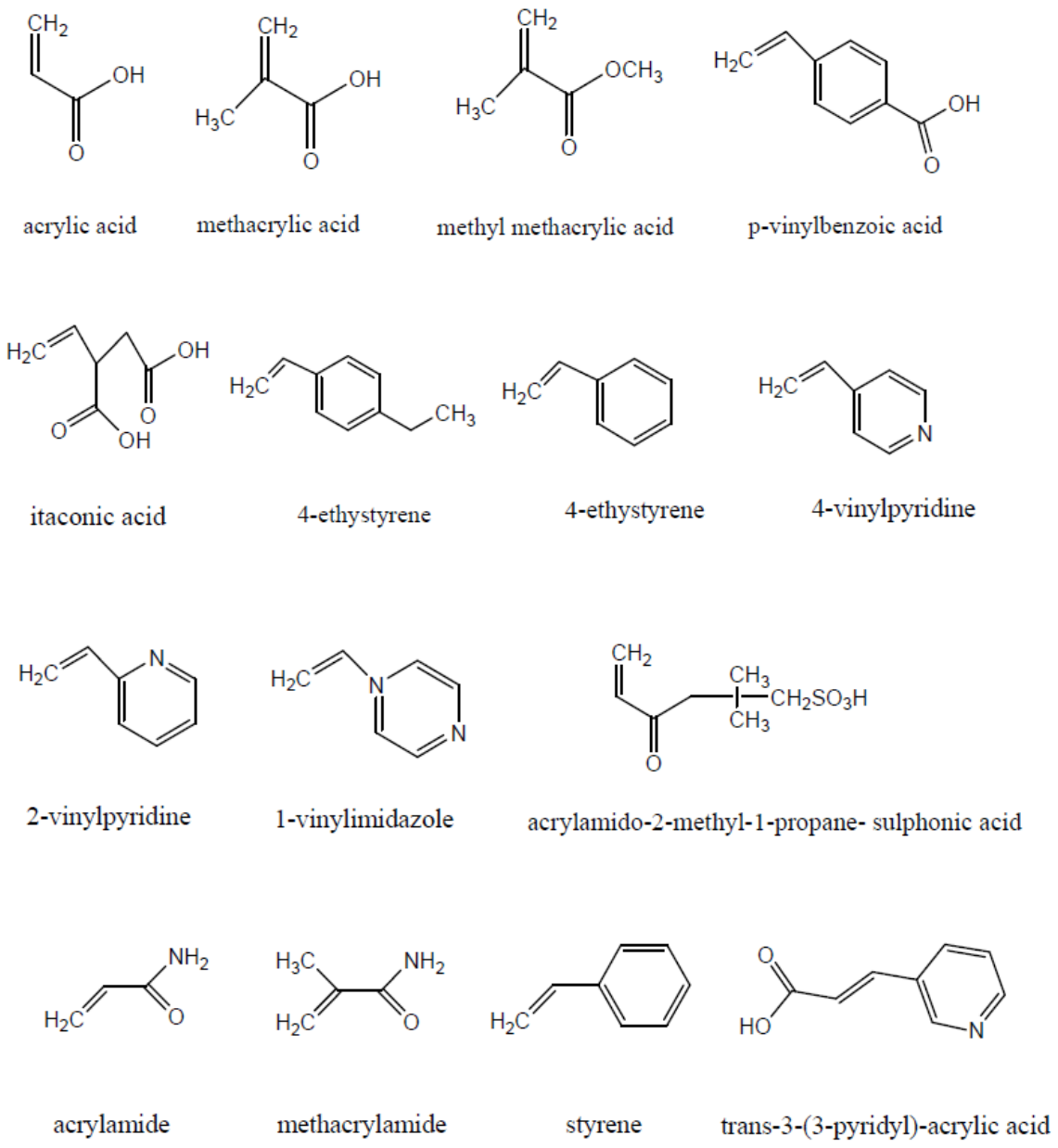

Figure 5.2 Chemical structure of common functional monomers used in non-covalent molecular imprinting [186].

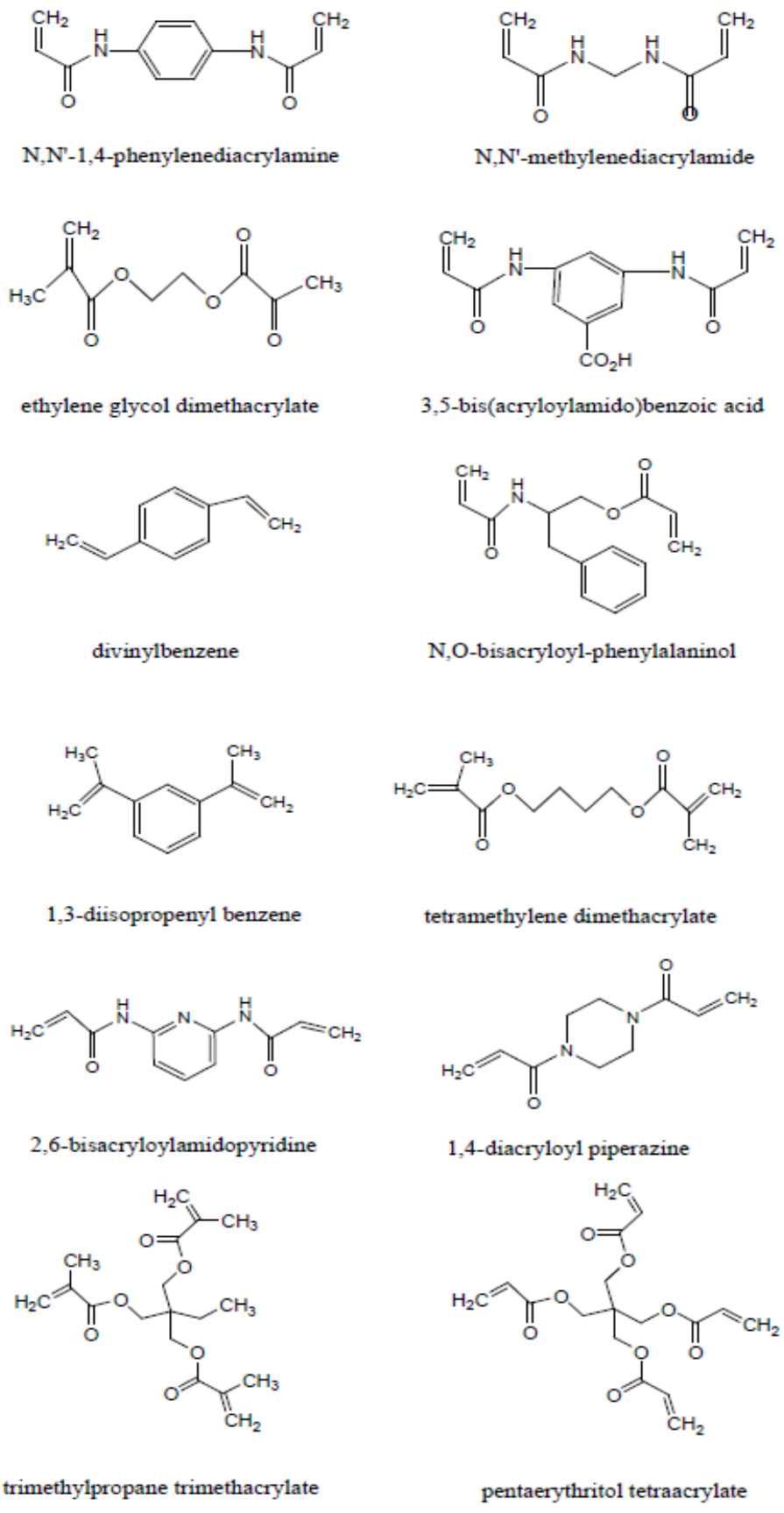

Figure 5.3 Common cross-linkers used in non-covalent molecular imprinting [186].

Progenic solvent

Progenic solvents play an important role to determine the strength of non-covalent bonds and affect polymer morphology which directly influences the performance of MIP. Progenic solvents can influence the formation of the porous structure of the polymer matrix [210]. Template, monomer, cross-linker and initiator should be soluble in the porogenic solvents. Moreover, the porogenic solvents should form large pores to make sure of the proper flow-through properties of the polymer. In addition, the progenic solvent should have relatively low polarity to reduce interference during the template/ monomer complex formation, which is very important to obtain high selectivity [186].

Initiators

Several initiators with different chemical structures and properties can be used to initiate the polymerisation. Figure 5.4 shows the chemical structure of some initiators used in non-covalent MIP.

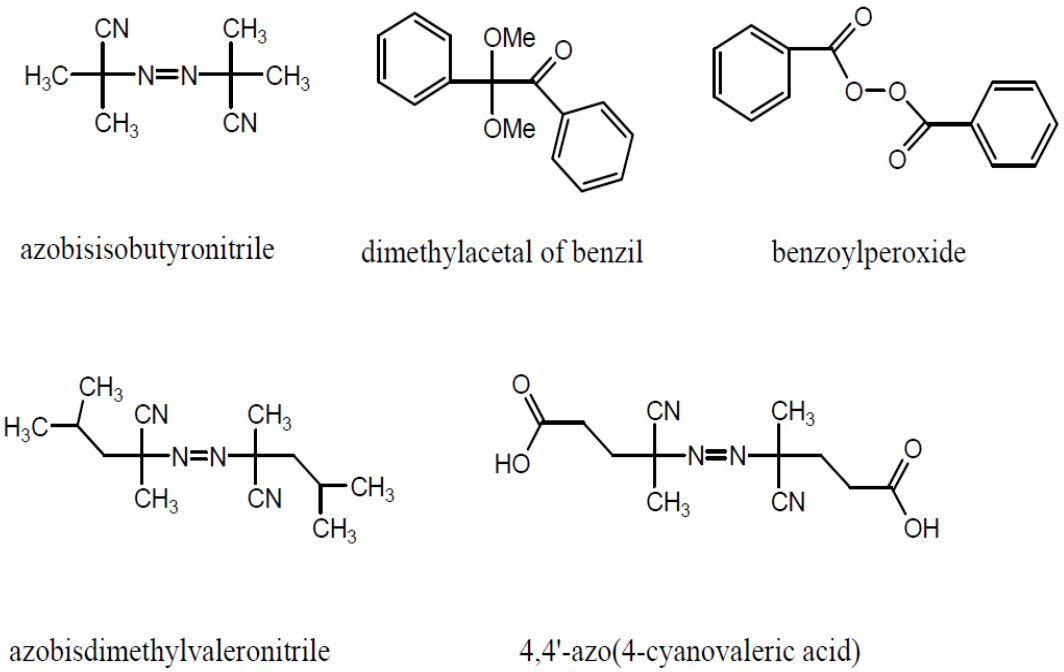

Figure 5.4 Chemical structure of some initiators used in non-covalent MIP [186].

5.2.3 Preparation Methods of MIP

MIPs can be prepared in different configurations, like polymer monoliths, microspheres and nanospheres, for different applications. For a long time, bulk polymerisation was extensively used to synthesise MIPs in the form of a hard monolith which had to be crushed, ground and sieved to obtain the desired particle size. These steps are time-consuming and also, during the crushing and grounding of the MIP, some recognition sites will be damaged. Moreover, the shape of the particles is not regular which is not ideal for their applications [211]. Later on, several novel preparation methods have been reported such as precipitation [212, 213], suspension [200, 214] and emulsion polymerisation [215, 216]. Precipitation polymerisation is unique within this group because the rest of the above mentioned methods all need additives such as stabilisers which can adversely influence the imprinting process. By using precipitation polymerisation microspheres with a uniform size can be obtained; they offer a higher active surface so it can contain more recognition sites than the MIP prepared by bulk polymerisation. In this method, the size and porosity can be easily tuned by changing the polymerization conditions. A summary of the advantages and disadvantages of different preparation methods of MIP is given in Table 5.1.

5.3 Materials and Methods

5.3.1 Materials and Apparatus

CTx-I peptide was synthesised by LifeTein (USA). Methacrylic acid (MAA), 2,2-azoisobutronitrile (AIBN), ethylene glycol methacrylate (EGDMA), acetonitrile (ACN), methanol (MeOH), acetic acid (AcOH), and acrylic resin were purchased from Sigma-aldrich (USA).

A high-precision 3536 LCR meter (Hioki, Japan) was employed to conduct EIS experiments. SIGMA 6-165 centrifuge instrument was used during the preparation of MIP. The DIONEX Ultimate 3000 HPLC device provided with the Luna 5µ C18 100A column and the Serum CrossLaps® ELISA kit (IDS company-UK) were employed for data validation. JEOL 6480LA SEM was utilised to take SEM images and a PTL-MM01 dip coater was employed to immobilise the coating material on the sensing area.

Table 5.1 Summary of different preparation methods of MIP.

MIP method	Advantages	Disadvantages
Bulk polymerisation	• Simplicity and universality. • No need for complicated instrumentation.	• Extra procedure of grinding and sieving. • Non-uniform size and shape. • Low performance.
Suspension polymerisation	• Spherical particles. • Highly reproducible. • Large scale possible.	• Phase partitioning. • Water is incompatible with many imprinted products.
Multi-step swelling polymerisation	• Excellent for HPLC. • The diameter of the monodisperse beads are controllable.	• Complex procedure. • Require aqueous emulsions.
Precipitation polymerisation	• Imprinted microspheres. • Uniform size.	• Large volume of template. • High dilution factor.
Surface polymerisation	• Monodispersed polymers. • Thin imprinted layers.	• Sophisticated system. • Time-consuming.
In-situ polymerisation	• One-step preparation. • In-situ. • Cost-efficient.	• Each new template system need extra optimisation.

5.3.2 Preparation of Artificial Antibodies using Molecular Imprinting Technology

A selective polymer for CTx-I was synthesised by precipitation polymerisation using MAA as the functional monomer, CTx-I peptide as the template, AIBN as the initiator and EGDMA as the cross-linker.

A mixture was prepared by dissolving 450 mg of the template molecule (CTx-I) in 50 ml acetonitrile in a 150 ml round-bottom flask, and then adding 260 µl of the functional monomer MAA, 3 ml of the cross-linker EGDMA, and 120 mg of the initiator. The N_2 gas was blown through for 10 minutes to evacuate air completely from the solution, since the presence of oxygen hampers the polymerisation process [217, 218]. The sealed flask was

then kept in a 60˚C water bath for 20 hours to complete the polymerisation process. The microspheres were collected by centrifugation for 10 minutes at 5000 rpm and then washed with acetonitrile to eliminate any excess peptides and chemicals. The extraction of the template was done using the Soxhlet extraction method with a mix of methanol/acetic acid 50/50 (v/v) for 24 hours. The non-imprinted polymer (NIP) was also prepared using the same method but in the absence of the template molecule. The NIP and MIP were air dried at room temperature and used for the experiments.

5.3.3 Preparation of the Functionalised Biosensing Surface

The MIP coating material was immobilised on the biosensing area of the interdigital sensor using a self-assembled monolayer (SAM) of the acrylic resin. 1g of MIP powder, 200 µl of the acrylic resin and 1.5 ml of acetone were mixed together to prepare the coating suspension. The sensor was immersed into the coating material at a speed of 200 mm/min and pulled out at the same speed to create a uniform layer. Figure 5.5 is an illustrative representation of the biosensing surface preparation. It also depicts the detection procedure of the target molecule using the developed biosensor.

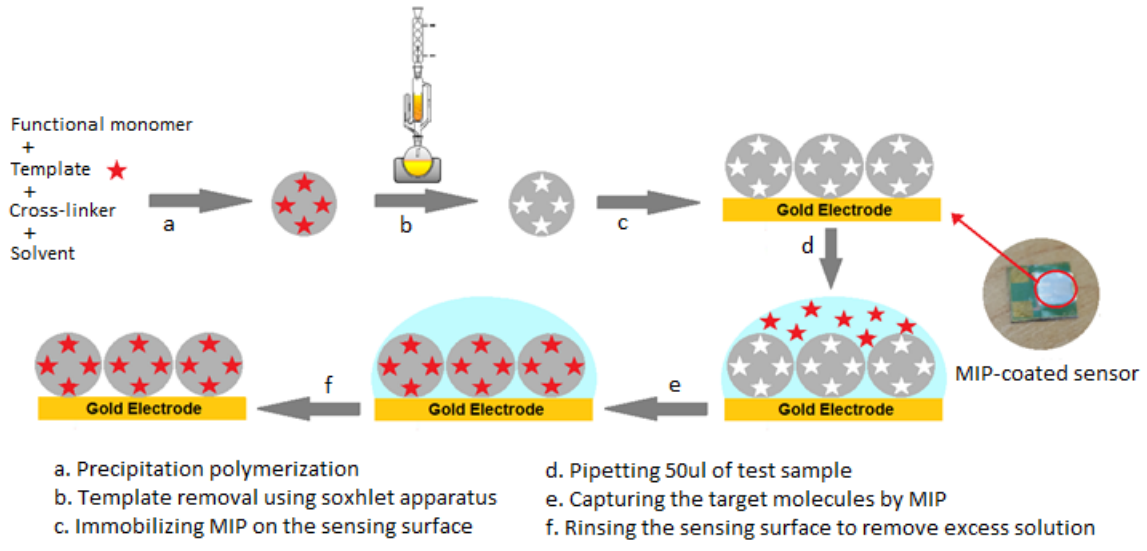

Figure 5.5 Schematic diagram of the biosensing surface preparation for CTx-I recognition.

5.3.4 Preparation of the CTx-I Samples

A stock solution of 60 ppm CTx-I was prepared by mixing 60 mg of CTx-I in one litre deionised water and it was kept in a refrigerator for further use. The serial dilution technique was utilised to prepare samples with lower concentrations. Distilled water with a zero level of CTx-I was treated as the control.

5.3.5 Experimental Measurements

The EIS technique was used to investigate the dielectric properties of the test samples at different concentrations. Although this measurement technique is very powerful and popular, it is very sensitive to humidity and temperature. Therefore, all the experiments were conducted in a controlled laboratory under the same humidity and temperature levels. The coated sensor was connected to the LCR meter using gold pin connectors and a 10 Hz-100 kHz signal with 1V amplitude was applied to the electrodes. After pipetting the test sample (50 µl) on the MIP-coated area, the sensor was kept on a shaking plate for 30 seconds to ensure uniform dispersion of the sample. Then, a seven minutes' delay was given for capturing CTx-I molecules by MIP. The extra solution was then washed out using deionised water. Finally, the EIS measurement was done after five minutes, when the coating surface was dried.

5.4 Results and Discussions

CTx-I imprinted polymer was synthesised through the precipitation polymerisation method, chosen for its advantages such as high selectivity, robustness and physiochemical stability. In the pre-polymerisation process, the template molecule interacted with the functional monomers through the non-covalent binding, and during the polymerisation procedure, they were properly imprinted in the polymer matrix. The non-covalent method is more popular because it involves less effort to take the template out from the polymer matrix, while covalent bonding needs more energy to extract the template from the polymer. Furthermore, the prepared MIP can be used immediately after template extraction, whereas MIPs synthesised through bulk polymerisation need to be crushed and ground before use.

5.4.1 SEM Characterisation

After preparing the imprinted polymer in the form of microbeads and immobilising the resultant polymer on the sensing area, SEM images were provided to study the polymer morphological structure as shown in Figure 5.6(a).

It was observed that the size of the particles was variable from 0.5 µm to 1 µm. Moreover, an MIP coating with an average thickness of 16 µm could be achieved on the biosensing surface, as can be seen in Figure 5.6(b).

5.4.2 Sorption Studies of CTx-I to MIP and NIP

The adsorption characteristics of the synthesized microbeads were determined by HPLC analysis. A DIONIX HPLC device equipped with a Luna C18 column was used to determine the amount of CTx-I molecules entrapped by the polymer.

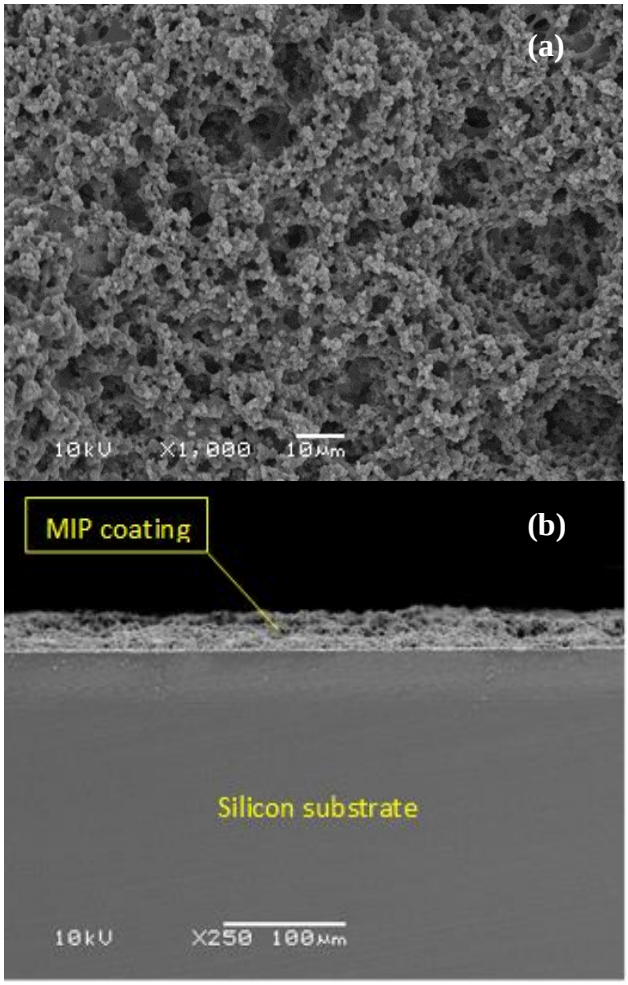

Figure 5.6 (a) SEM image of MIP-coated biosensing surface and (b) SEM image of the MIP-coated sensor to show the thickness of the coating layer.

Two different solutions were prepared for the mobile phase. Solution 'A' contained 0.1% trifluoroacetic acid in acetonitrile, and solution 'B' was prepared by mixing 0.1% trifluoroacetic acid in water. Isocratic elution was performed for 25 min with a mobile phase configuration of 26% A and 74% B. The flow rate was kept at 1 ml/min.

The injection volume was set at 100 µl and the detection was done at λ=220 nm. The static adsorption capacity of the polymer was calculated using

$$Q = \frac{V(C_i - C_f)}{m} \tag{5.1}$$

where Q (mg g^{-1}) is the mass of CTx-I adsorbed per gram of polymer, *V* (l) is the total volume of the adsorption solution. C_i (mg.l^{-1}) and C_f (mg.l^{-1}) are the initial and final concentrations of CTx-I, respectively and *m* (g) is the mass of the polymer.

The kinetic studies were useful to estimate the time required by the polymer to entrap the CTx-I molecules present in the sample. This study was carried out by mixing 10 mg of MIP in 10 ml of CTx-I sample with the concentration of 30 mg.l^{-1}.

Figure 5.7(a) represents the results for the adsorption kinetics of CTx-I to MIP and NIP. The results indicate that the MIP had a rapid response and binding equilibrium was observed in 7 minutes. Figure 5.7(b) depicts a static absorption study of the target molecule to NIP as well as MIP in a range of 1-60 mg.l^{-1}. The graph indicates the amount of CTx-I captured by the polymer, which increased along with the increase in the level of CTx-I below 30 mg.l^{-1}. The adsorption capacity graph became parallel to the concentration axis and saturated at high concentration. However, the amount of CTx-I bound to NIP reached saturation at only 20 mg.l^{-1}.

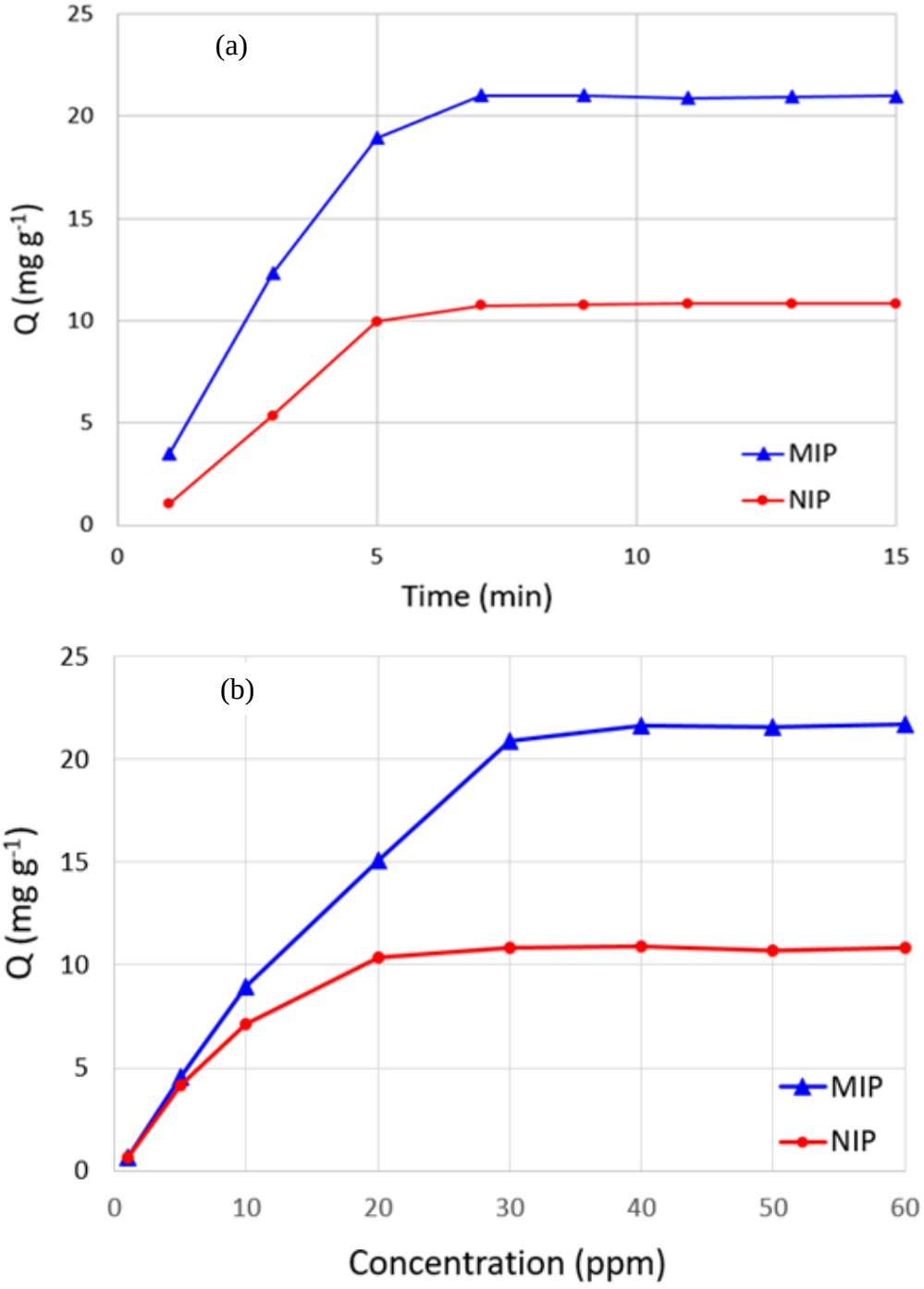

Figure 5.7(a) Uptake kinetics of CTx-I to MIP and NIP, and (b) Isotherms for static adsorption capacity of CTx-I to MIP and NIP.

5.4.3 EIS Measurement and Analytical Measurement

The detection of CTx-I binding to the synthesised recognition sites was determined using the EIS technique. Six sample solutions with different levels of CTx-1 (0.1, 0.5, 1, 1.5, 2 and 2.5 ppb) were tested using the MIP-coated sensor and the LCR meter. The results are represented in Figure 5.8 in the form of a Nyquist plot. It was observed that the diameter of the Nyquist plot decreased as the CTx-1 concentration increased. Figure 5.9 depicts the reactance in a frequency range of 10 Hz-100 kHz for six standard solutions with different concentrations of CTx-1, and the real part of the impedance (resistance) is shown in Figure 5.10. As depicted in Figure 5.9, the imaginary part of the impedance (reactance) showed distinct variations with variations in the CTx-1 level, that is ascribed to the dielectric properties of the test solution. These variations are more evident in a frequency range of 50-600 Hz, shown in Figure 5.9 as "*sensitive area*". On the other hand, changes in the real part occurred within a small frequency range (1-160 Hz), where it is shown as "sensitive area" in the figure. Therefore, the reactance part of the impedance was used for further analysis and investigation.

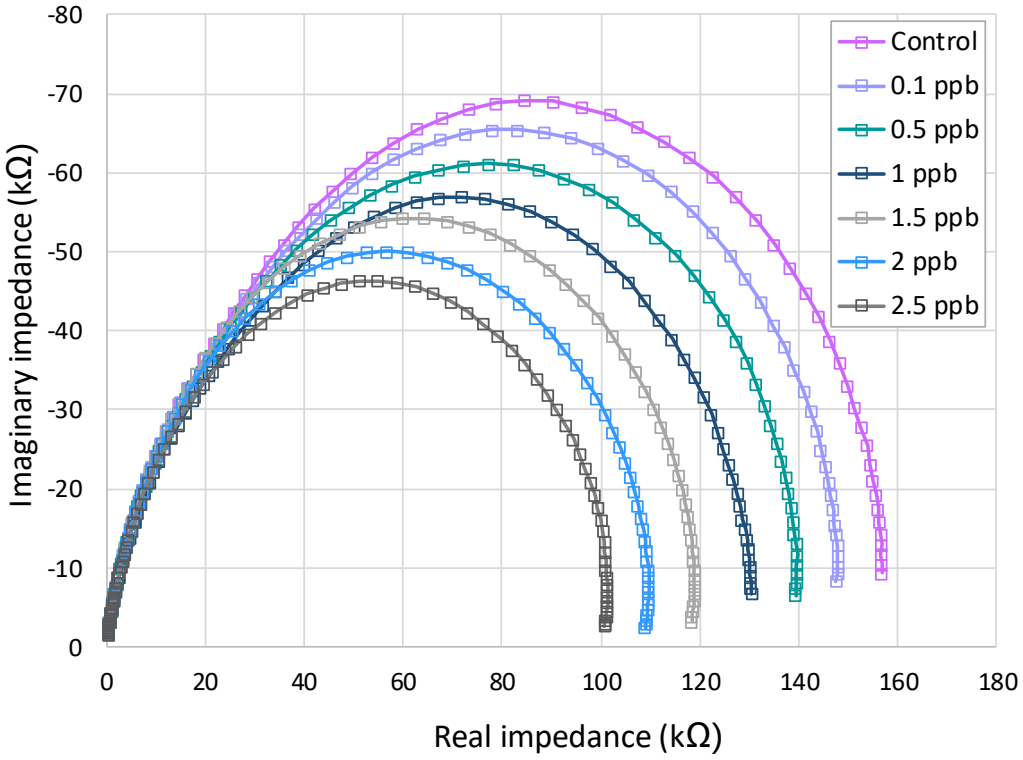

Figure 5.8 Nyquist plot for various concentrations of CTx-1 molecules.

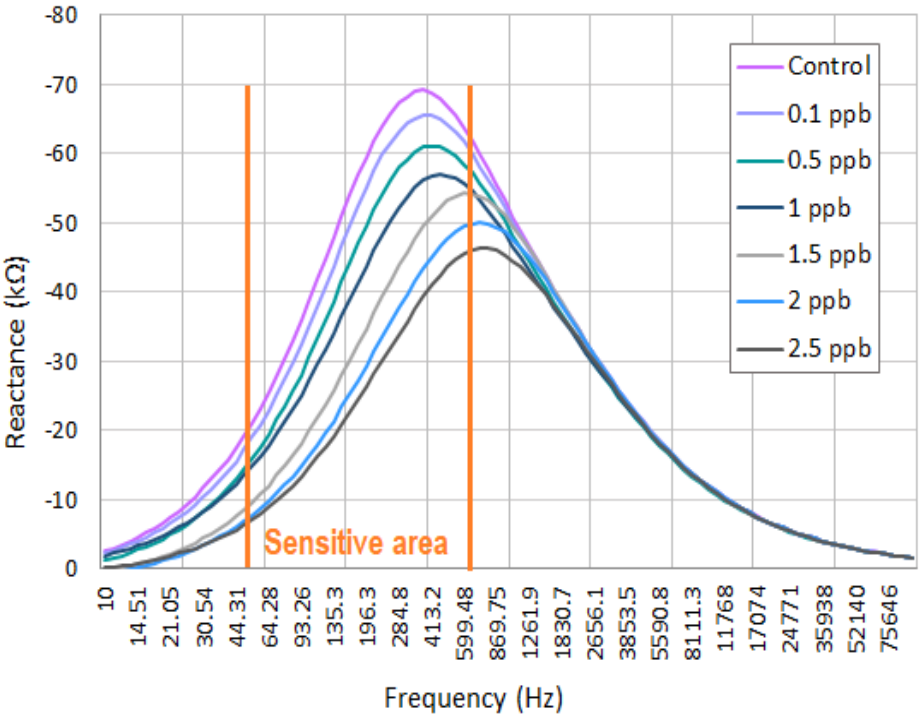

Figure 5.9 Imaginary part of impedance (Reactance) vs. frequency for various concentrations of CTx-1 molecules.

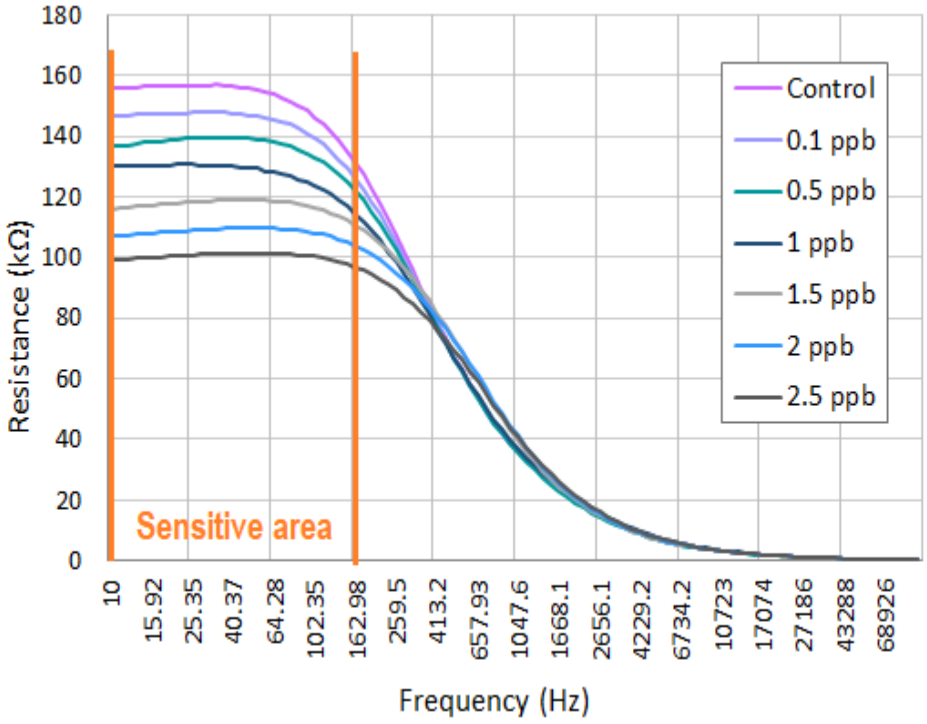

Figure 5.10 Real part of impedance (Resistance) vs frequency for various concentrations of CTx-1 molecules.

In order to assure the reliability of the sensor, each measurement was done three times in the identical conditions, and the mean value was considered as the data. Figure 5.11 shows the reactance values for each reading and the mean value of the reactance for different concentrations. The maximum deviation observed from the mean value was 0.5%, which demonstrates the consistency of the proposed biosensor.

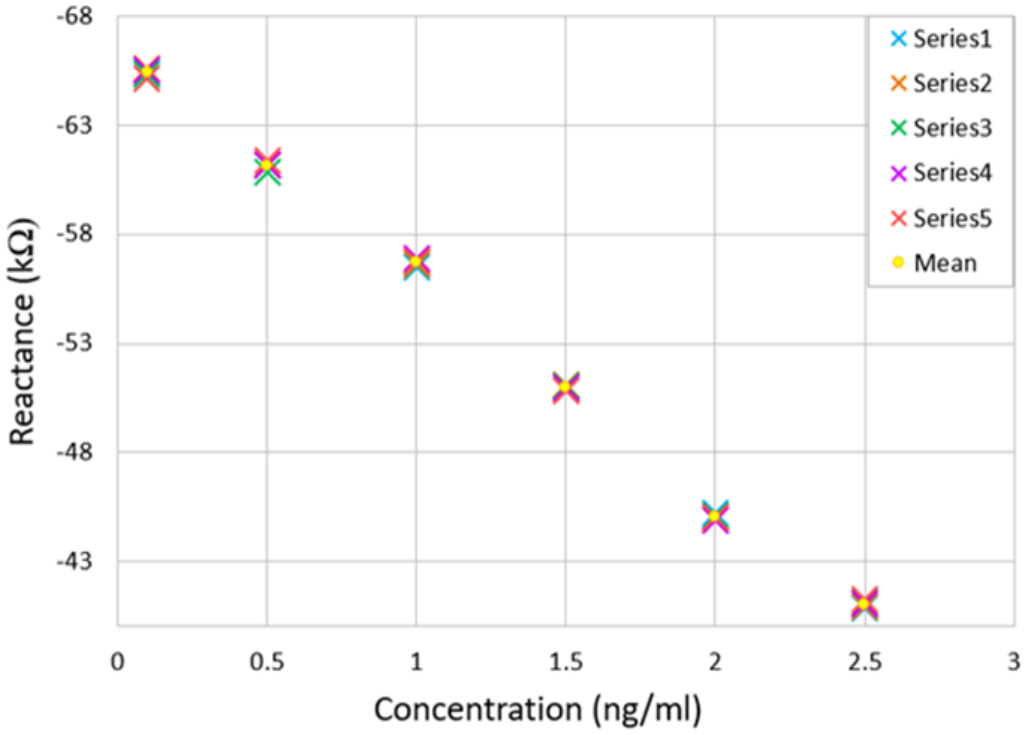

Figure 5.11 Reactance value for five times reading to show the consistency of the biosensor.

5.4.4 CNLS–based Biosensor Response

Figure 5.12 shows the Nyquist plot and its corresponding Randle's circuit estimated by using the CNLS technique [219]. The red markers on the graph illustrate the obtained results by experiment and the green line indicates the CNLS-fitted curve. The observed semicircle of the Nyquist plot is modelled using a parallel sketch of R_{ct} and a constant-phase element (CPE). The solution resistance is represented by R_s.

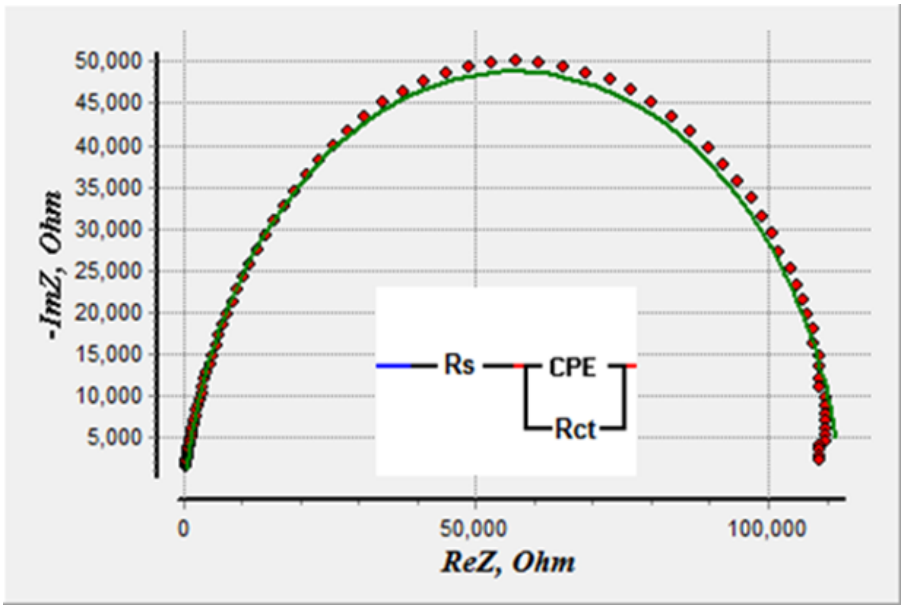

Figure 5.12 The Nyquist plot and its corresponding Randle's model estimated by CNLS analysis.

The equivalent circuit parameters for different concentrations of analyte are provided in Table 5.2, where $r^2{}_{amplitude}$ represents the variation of the experimentally obtained values from the optimum value.

From Table 5.2, it is seen that the charge transfer resistance, $R_{ct,}$ has a very clear relationship with the concentration of CTx-I. Therefore, the CNLS-based calibration curve can be plotted with the R_{ct} obtained from CNLS analysis and the following equation can be used to compute the change in R_{ct}:

Table 5.2 Equivalent circuit parameters for different CTx-I concentrations.

Component parameters	Control	0.1 ng/ml	0.5 ng/ml	1 ng/ml	1.5 ng/ml	2 ng/ml	2.5 ng/ml
R_s (Ω)	349.05	342.58	279.88	316.74	307.99	276.46	294.75
R_{ct} (kΩ)	163.3	154.4	144.6	135.3	121.9	112.3	104.2
CPE1(E-09)	6.356	6.463	6.750	5.986	4.181	3.998	4.324
$r^2{}_{amplitude}$	0.0029	0.0029	0.0024	0.0026	0.0016	0.0015	0.0015

From Table 5.2, it is seen that the charge transfer resistance, $R_{ct,}$ has a very clear relationship with the concentration of CTx-I. Therefore, the CNLS-based calibration curve can be plotted with the R_{ct} obtained from CNLS analysis and the following equation can be used to compute the change in R_{ct}:

$$\frac{\Delta R_{ct}}{R_{ct0}}(\%) = \frac{R_{ct}\,(control) - R_{ct}\,(sample)}{R_{ct}\,(control)} \times 100 \qquad (5.2)$$

Figure 5.13 presents the CNLS-based calibration curve generated for 0.1, 0.5, 1, 1.5, 2 and 2.5 ng/ml of CTx-I. A linear correlation between R_{ct} and the level of CTx-I was observed (R^2= 0.9953).

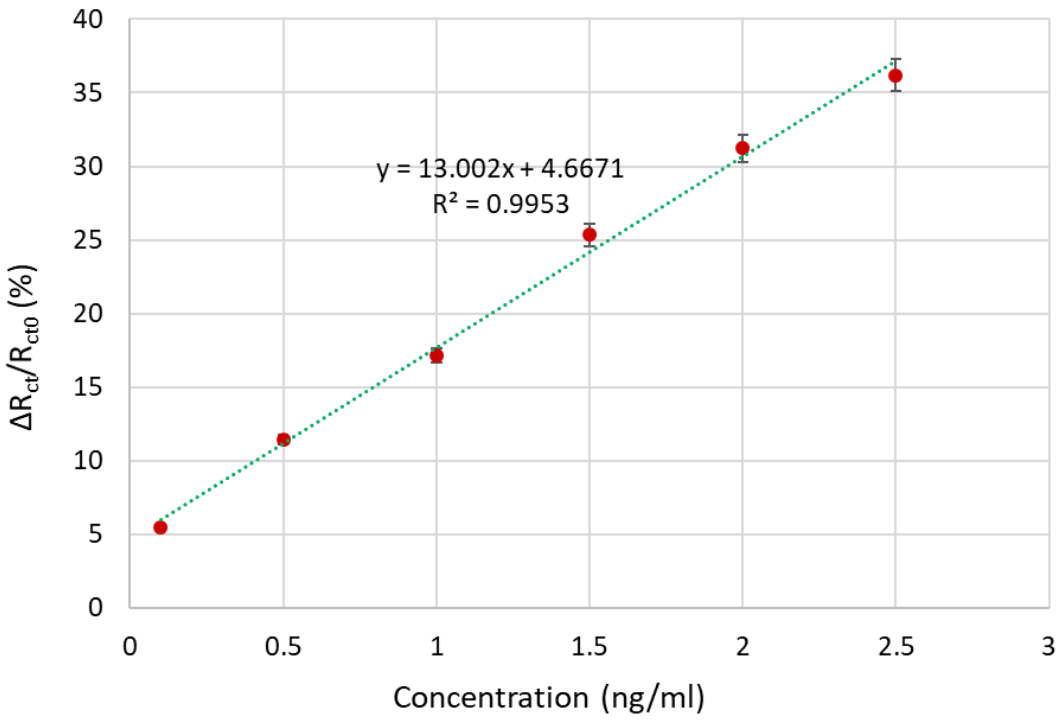

Figure 5.13 CNLS-based calibration curve, representing changes in R_{ct} for various concentrations of CTx-I.

5.4.5 Measurement of CTx-I in Real Serum Samples using the CNLS–based calibration Curve

Sheep serum samples were tested using the developed biosensor as well as the ELISA kit for the validation of the proposed technique. CTx-I quantification in the real samples was done using the CNLS-based calibration curve (shown in Figure 7(a)). The accuracy of the CTx-I quantification was examined by comparing the results achieved by the developed system with those achieved from the ELISA kit. All the results are given in Table 5.3. The results achieved from the two methods were in good agreement.

Table 5.3 Determination of CTx-I concentration in real serum samples using the CNLS-based calibration curve.

Sample	CTx-I level (ng/ml)		Error (%)
	Proposed sensor	Reference method ELISA	
S1	1.416	1.465	3.3
S2	0.184	0.187	1.6
S3	0.098	0.100	2.0
S4	0.453	0.450	0.6

5.4.6 Single-frequency Reactance–based Biosensor Response

The proposed biosensor has a great potential to be used as a PoC device for prognosis of bone turnover. Narrowing the frequency range to a single frequency makes data analysis more straightforward and efficient. It also reduces the total experimentation time. Therefore, the frequency of 319 Hz was determined as the optimum frequency according to the Nyquist analysis and changes in the reactance values. The percent change in reactance was then calculated at 319 Hz using

$$\frac{\Delta X}{X_0}(\%) = \frac{X\,(control) - X\,(sample)}{X\,(control)} \times 100 \tag{5.3}$$

The single-frequency reactance-based biosensor response is displayed in Figure 5.14. It depicts the change in reactance for various concentrations of CTx-I (0.1-2.5 ng/ml) at 319 Hz. There was a linear relationship between the reactance and the level of CTx-I, with a 0.9977 correlation coefficient.

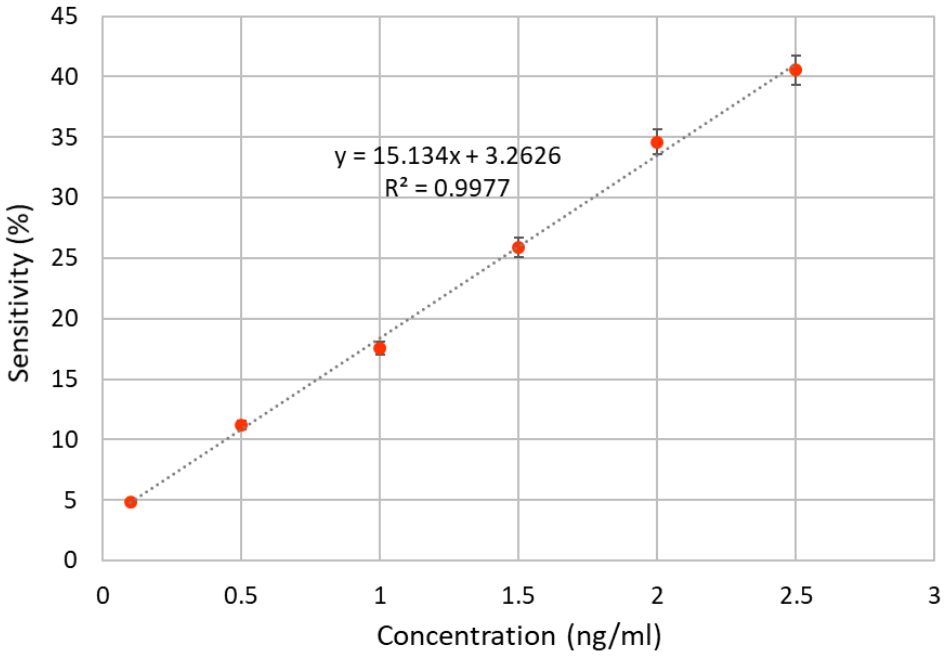

Figure 5.14 Single-frequency reactance-based calibration curve, representing changes in reactance X to various concentrations of CTx-I measured at 319 Hz.

5.4.7 Measurement of CTx-I in Real Serum Samples using Single-frequency-based Calibration Curve

After developing the single-frequency calibration curve (Figure 5.14), the CTx-I quantification in sheep serum samples was performed using the developed calibration curve. The accuracy of the biosensor response was then compared with the ELISA response and the result of the comparison was presented as the percentage error in Table 5.4.

Table 5.4 Determination of CTx-I concentration in real serum samples using the **single-frequency calibration curve.**

Sample	CTx-I level (ng/ml)		Error (%)
	Proposed sensor	Reference method ELISA	
S1	1.412	1.465	3.6
S2	0.182	0.187	2.1
S3	0.097	0.100	3.0
S4	0.447	0.450	0.6

5.4.8 Comparison Between the CNLS-based Measurement and Single-frequency Measurement

By comparing the results provided in Tables 5.3 and 5.4, it can be observed that the CNLS-based testing can give more accurate results, as the measurement would be done in a wide range of frequencies. Moreover, the R_{ct} parameter is obtained from the theoretical fits and CNLS analysis. However, there are some significant advantages in implementing the single-frequency measurement, which are very useful in developing a portable PoC device. The main advantage of using the single-frequency based measurement is that CNLS analysis is not required to derive the R_{ct} value. This would considerably minimise the actual measurement time for the biosensor and simplify the testing procedure. Therefore, the single-frequency measurement would be highly preferred as a sensing system, as it can offer a straightforward measurement approach and reduce the response time, which are predominant features in developing a quick and simple POC device.

5.5 Performance Assessment of Interdigital Sensor for Varied Coating Thicknesses

Reducing the influences of chemical and environmental contaminants on surfaces has been an objective of researchers for many years. The surface coating is one of the most effective methods that have been used to control the chemical and environmental impacts. Various coating studies have been done to improve corrosion resistance [220, 221], to detect environmental contamination [222] and to protect biological interfaces [223-225].

Moreover, a coating membrane not only can protect a sensing surface from environmental and chemical reactions, but also it can be effectively used as a selective layer. The selective coating layer increases the selectivity of the sensor to detect a particular molecule. A selective coating layer has been reported to detect a variety of molecules such as tyrosine in milk [226], cholesterol [227], phthalate in beverages [156] and an ovarian cancer marker [228].

In this investigation, the dip-coating method was used to create the coating layer on the sensing surface. Among the simple and conventional coating techniques such as spin coating [229, 230] and spray coating [231, 232], dip coating is very popular due to the low cost, reproducibility and simplicity of operation. In this process, the substrate is inserted

into a bath of the coating solution and then removed with a controlled speed. The solution innately and uniformly covers the surface. After evaporation, a solid coating layer will be formed on the surface [223, 233-235]. The solution viscosity, withdrawal speed and evaporation conditions are very significant parameters to control the coating characteristics [220, 233, 236]. Figure 5.15 schematically represents the dip coating technique. In this study, the effect of withdrawal speed and dipping time during the dip coating process has been studied.

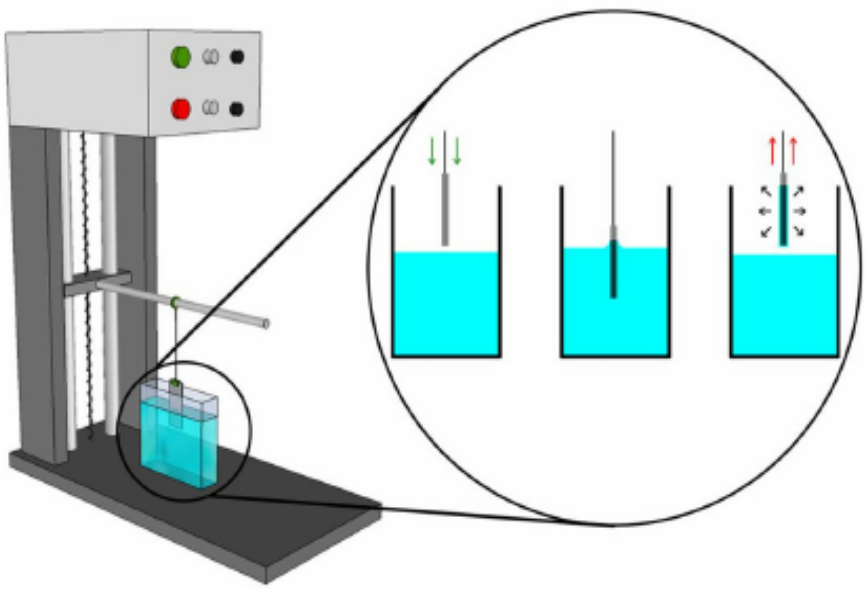

Figure 5.15 Graphical illustration of dip-coating technique [220].

The sensitivity of the interdigital sensor is highly dependent on the thickness of the coating layer. Therefore, in this study we have investigated the role of coating thickness on the performance of the planar interdigital sensor for CTx-I measurement. The performance of an acrylic coat as well as the selective coating layer was evaluated to estimate the sensitivity of the sensor.

5.5.1 Coating the Sensing Surface with Acrylic

In this research, the acrylic resin was employed as the coating material for the planar interdigital sensor. Firstly, the sensing surface was washed using acetone. Then, the acrylic coater was immobilised on the sensing area as a protective coating layer. The coating process was done using the PTL-MM01 dip coater in order to get a uniform coating layer

and the sensor was dried for 30 minutes at room temperature. Figure 5.16 shows an SEM image of the acrylic-coated interdigital sensor. The effect of some coating parameters such as speed and time on the coating thickness was investigated. Moreover, a sensor with a different coating thickness was prepared to study the effect of coating thickness on the sensitivity and performance of the sensor.

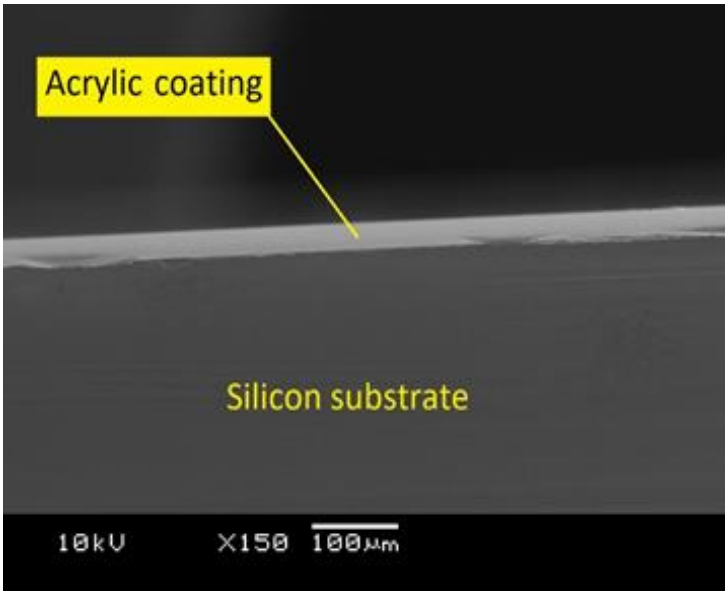

Figure 5.16 SEM image of acrylic-coated sensor to show the coating layer.

5.5.2 Coating the Sensing Area with Selective Material

Since the acrylic-coated sensor is not selective to the target molecule, it cannot measure the CTx-I levels in real samples (urine or serum) as different types of particles are available in real samples. Therefore, the sensing surface should be functionalized using a selective material to introduce the selectivity of the target molecule. The selective coating material was prepared using the Molecular Imprinted Polymer (MIP) technique, which is a very popular and useful method to create artificial recognition sites for a target molecule [237-239]. The detailed procedure of MIP preparation has been reported in section 5.3.2. Methacrylic acid, 2, 2-azoisobutronitrile, ethylene glycol methacrylate and CTx-I peptide were the main reagents to prepare the MIP. A SEM image of the MIP-coated sensor is given in Figure 5.17.

Initially the sensor was washed with acetone to remove any impurities. Then, a coating material was prepared by mixing MIP, acrylic lacquer and acetone in a beaker. A PTL-MM01 dip coater was employed to perform the coating task, as illustrated in Figure 5.18.

After that, the sensor was withdrawn slowly to get a uniform coating layer. Finally, the sensor was dried at room temperature for 1 hour.

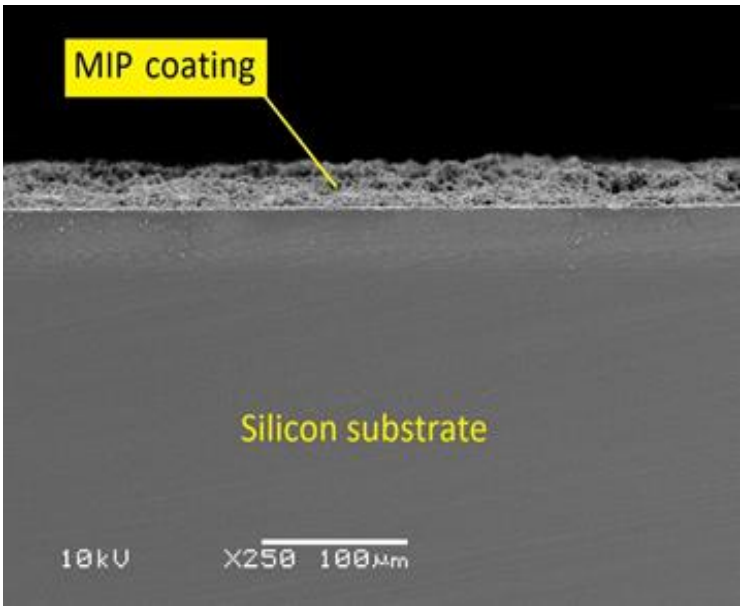

Figure 5.17 SEM image of MIP-coated sensor to show the coating layer.

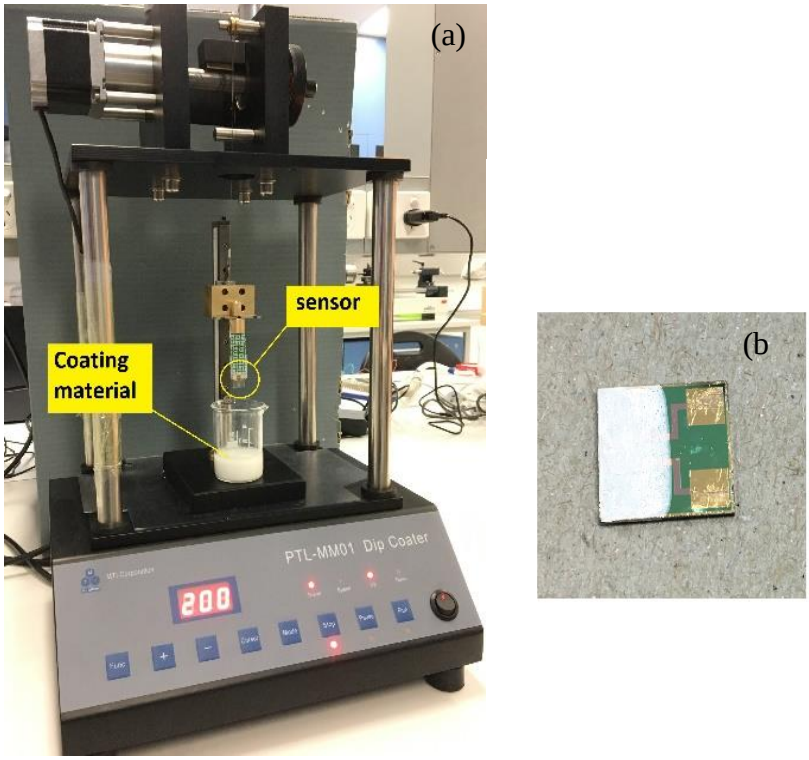

Figure 5.18 (a) Selective layer development and (b) Coated sensor.

5.5.3 CTX-I Measurement using the Coated Interdigital Sensor

CTx-I sample solutions with different concentrations (0.5 ppm, 2.5 ppm, 5 ppm and 7.5 ppm) were prepared by dissolving CTx-I peptide in distilled water. Initially, the measurement of CTx-I was done with an acrylic-coated sensor that was prepared with various coating thicknesses (30, 65, 100 and 145 µm). The different coating layer thicknesses were achieved by repeating the coating procedure. Initially, the uncoated sensor was EIS characterised using the LCR meter to determine the sensitive frequency range. After coating the sensor, it was characterised in air to compare the profiles of different coating thicknesses. There were significant changes in the size of the semicircular diameter for different thicknesses and it was relatively saturated at 145 µm, which could be due to a higher coating thickness than the penetration depth of the fringing electric field. After coating the sensor with acrylic and profiling it in air, the coated sensor was tested with the sample solutions of different CTx-I levels. The same experiments were carried out with coating thicknesses of 30, 65, 100 and 145 µm.

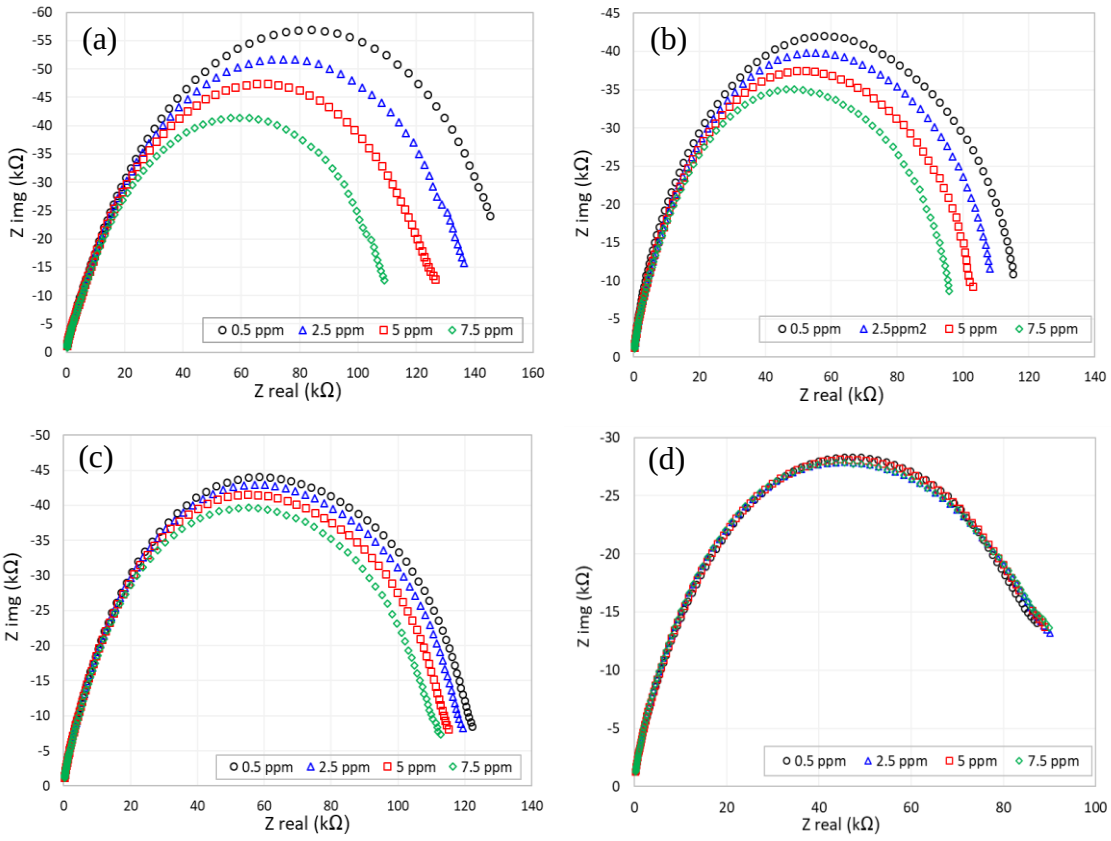

Figure 5.19 Measurement of CTx-I samples by acrylic-coated sensor with various coating thicknesses: (a) 30 µm, (b) 65 µm, (c) 100 µm, and (d) 145 µm

Figure 5.19 shows the results of the experiments in the form of Nyquist plots. It is seen that symmetric changes occurred for the real and imaginary parts of the impedance for thicknesses between 30 µm to 145 µm. As the thickness of the coating layer decreased, the difference shown in each Nyquist plot for different concentrations were more prominent. However, the acrylic-coated sensor with the thickness of 145 µm could not show any changes for different levels of CTx-I.

In the next step, the MIP-coated sensor was employed to test the CTx-I samples. Different thicknesses of the MIP-coating layer (40, 75, 130 and 165 µm) were obtained by repeated dip coating and a similar procedure was followed to perform experiments using the MIP-coated sensor. Four samples with different CTx-I levels were tested using the MIP-coated sensor. Figure 5.20 represents the Nyquist plot for the MIP-coated sensor with different coating thicknesses (40, 75, 130 and 165 µm). For the coating thicknesses ranging between 40 µm and 165 µm, a decrease in the diameter of the semicircle shows an increase in the concentration of CTx-I in the solution. Nevertheless, the sensor was saturated at 165 µm and could not show any reaction to different concentrations.

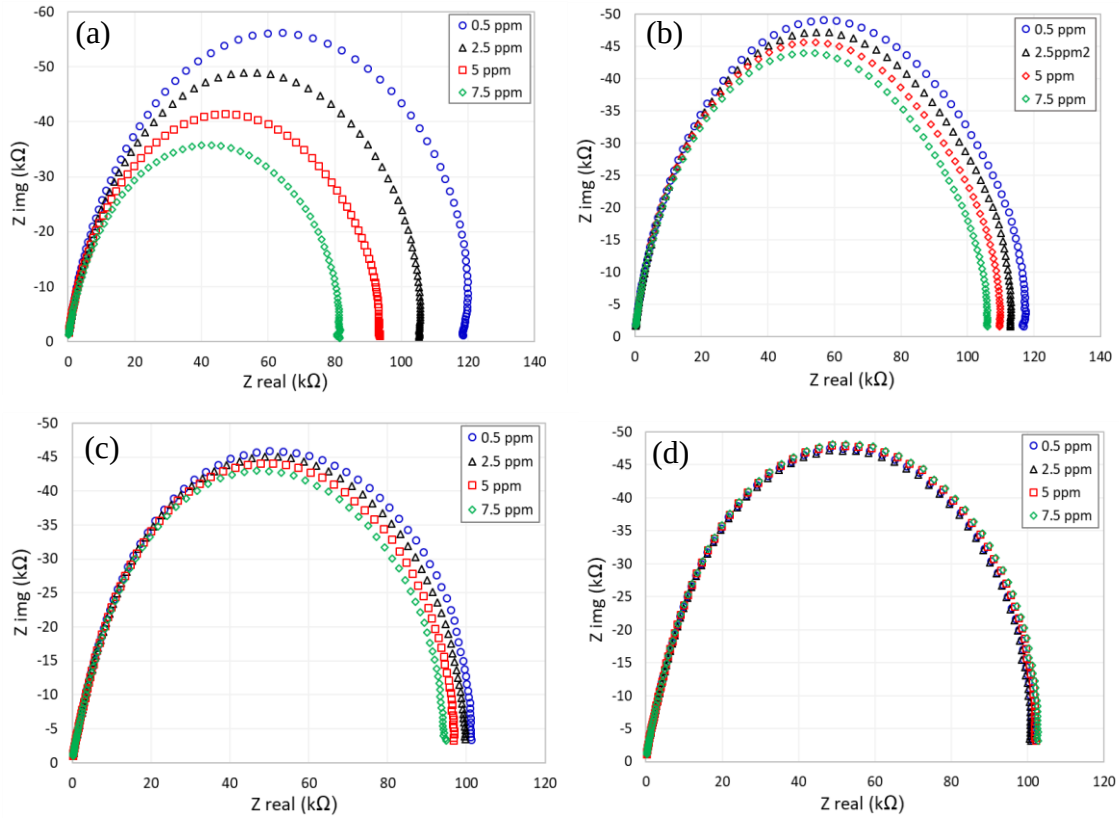

Figure 5.20 Measurement of CTx-I samples by MIP-coated sensor with various coating thicknesses: (a) 40 µm, (b) 75 µm, (c) 130 µm, and (d) 165 µm.

5.5.4 Sensitivity of the Coated Sensor and the Saturation Level

In order to investigate the sensitivity of the sensor, a calibration curve was developed for the coated sensor of different coating thicknesses. The calibration curves were developed by plotting the reactance against CTx-I concentration at 710 Hz, as the maximum changes in the imaginary part of the impedance (reactance) could be observed at 710 Hz. Figure 5.21 shows the calibration curves for the acrylic- coated sensor with three different coating thicknesses.

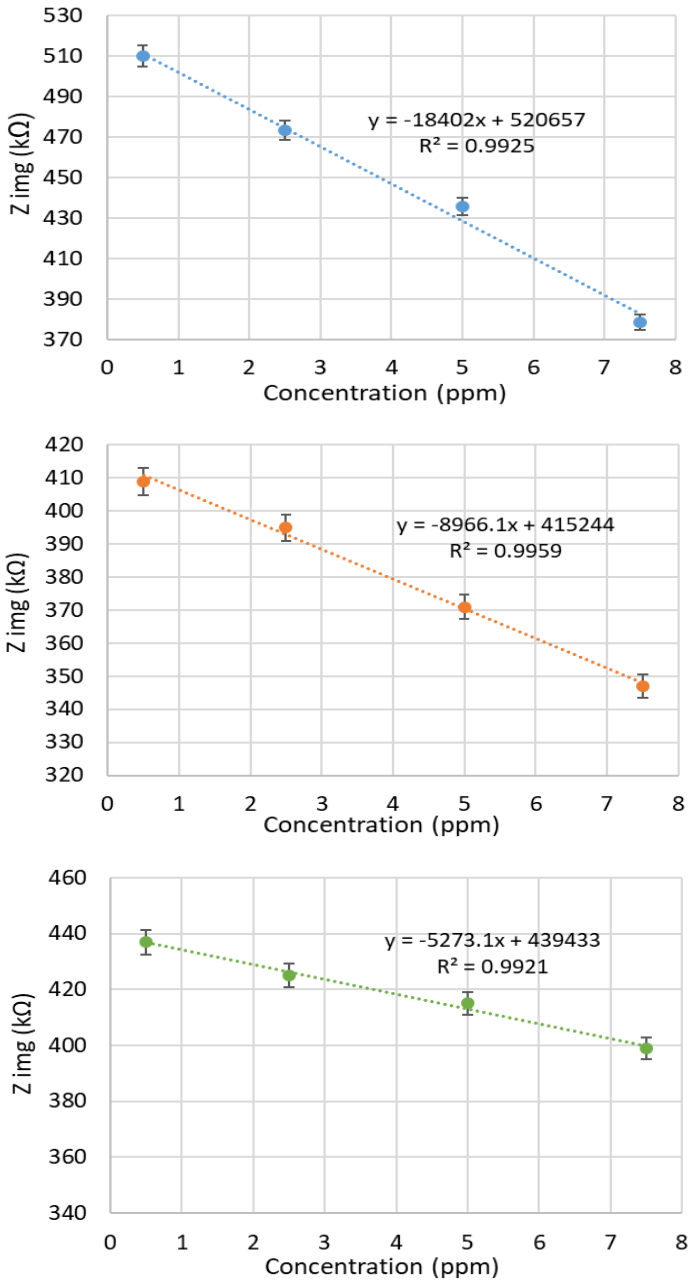

Figure 5.21 Calibration curves for the acrylic-coated sensor with different coating thicknesses: (a) 30 µm, (b) 65 µm and (c) 100 µm.

The developed calibration curves for the MIP-coated sensor are depicted in Figure 5.22. The slope of the calibration curves indicates the sensitivity of the sensor. It can be observed that the slope of the curves decreases as the thickness of the coating layer increases. In other words, the thinner the coating layer, the higher the sensitivity that can be achieved.

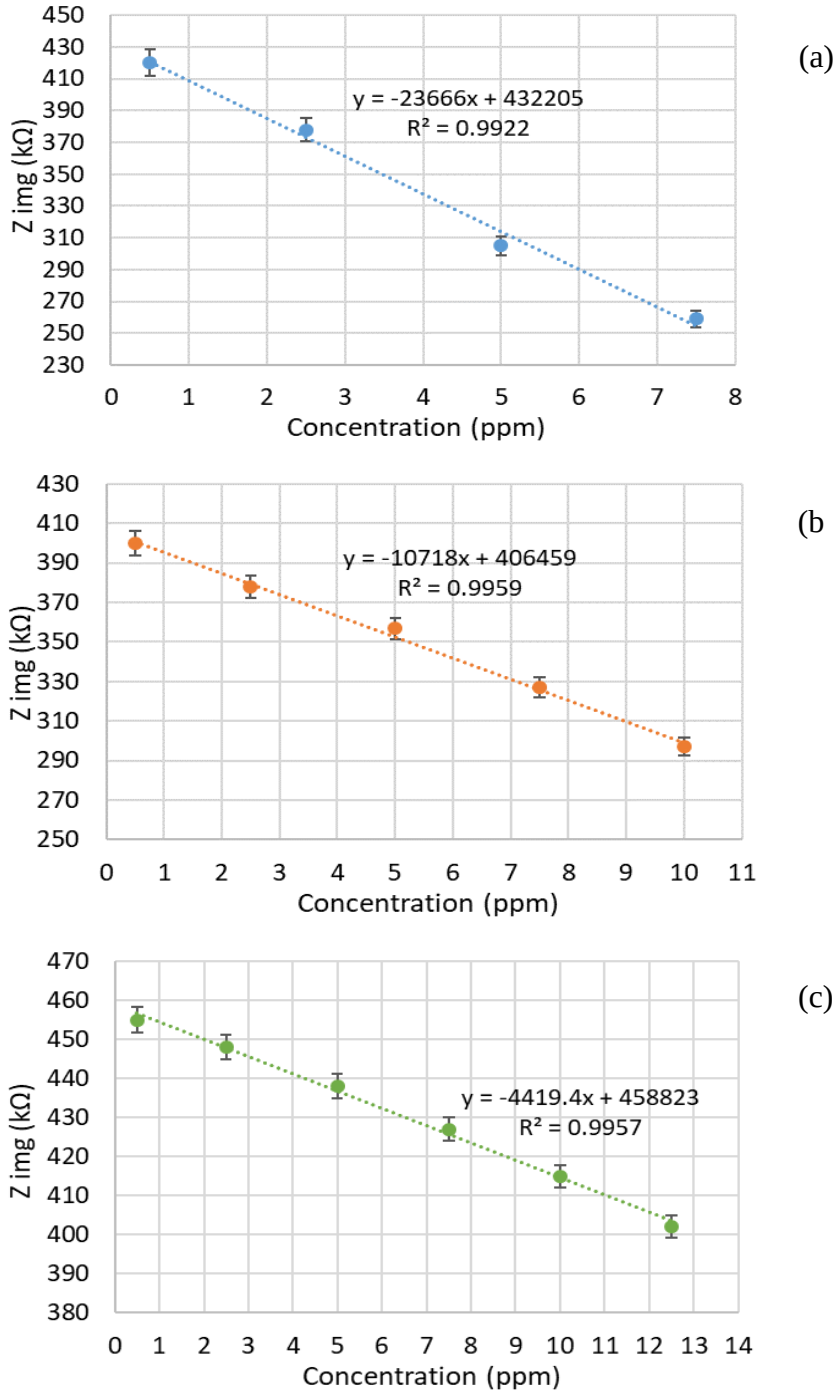

Figure 5.22 Calibration curves for the MIP-coated sensor with different coating thicknesses: (a) 40 µm, (b) 85 µm and (c) 130 µm.

Figure 5.23 shows the sensitivity of the acrylic-coated sensor as well as the MIP-coated sensor at different coating thicknesses. In both the coating materials, the sensitivity is decreased non-linearly by increasing the coating thickness. It can be seen the MIP-coated sensor showed more sensitivity to CTx-I molecules than the acrylic-coated sensor.

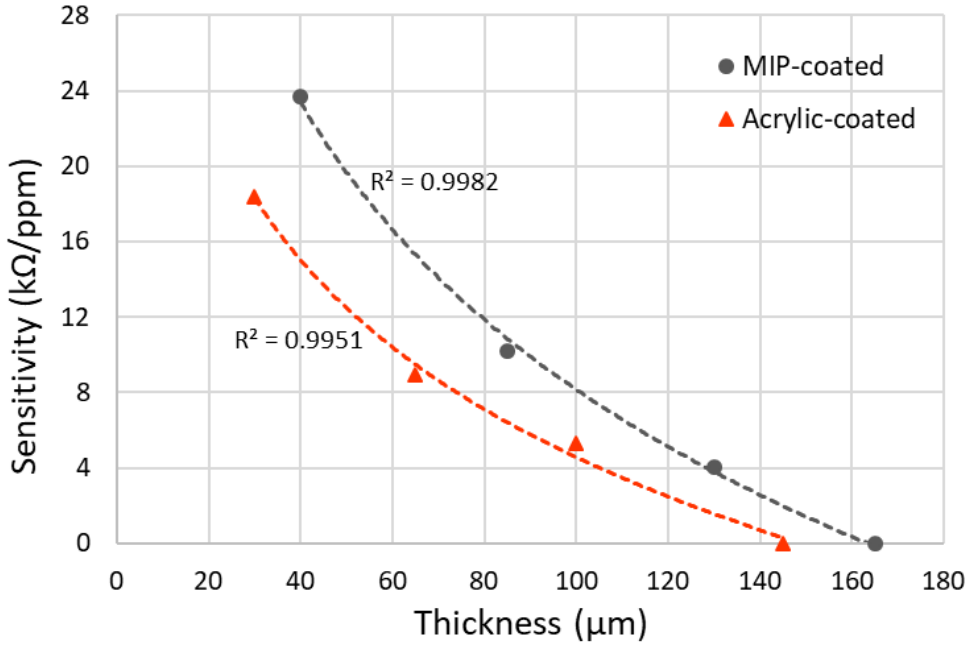

Figure 5.23 Sensitivity of the MIP-coated sensor and the acrylic-coated sensor.

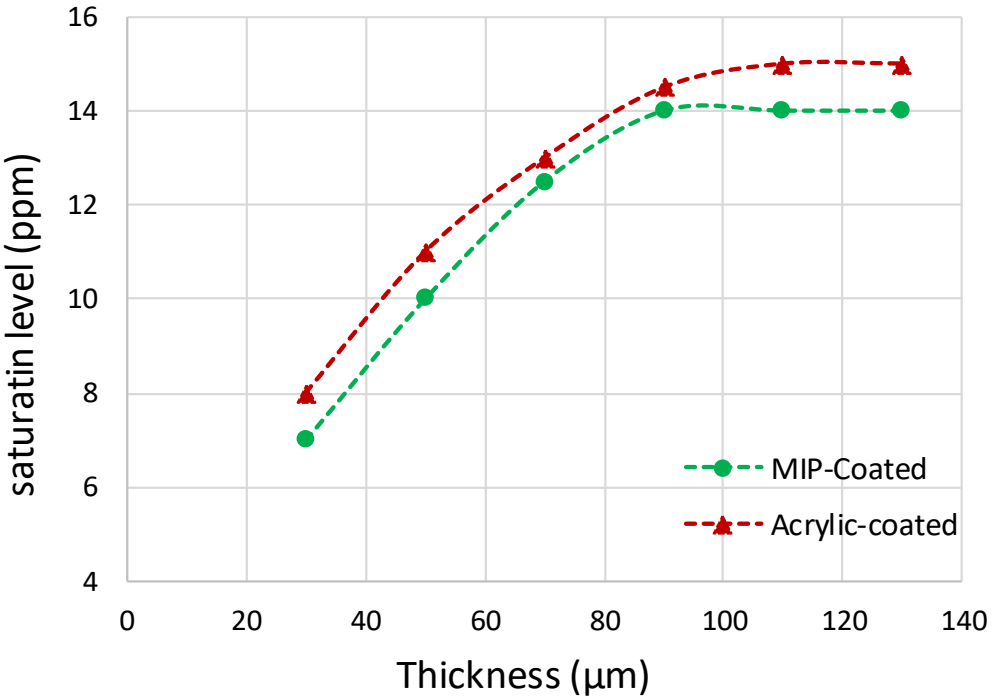

Figure 5.24 Saturation level of the coated sensor.

CTx-I samples with various concentrations have been tested using the coated sensor, in order to verify the saturation level of the sensor. The results are illustrated in Figure 5.24. It was observed that increasing the thickness of the coating layer, enhances the saturation level. Therefore, a compromise should be reached between the sensitivity and the saturation level, when the coating thickness is being decided.

5.5.5 Dependence of Coating Thickness on Withdrawal Speed and Dipping Time

During the dip coating process, the thickness of the coating layer was studied by analysing the withdrawal speed and dipping time. The investigation was done on the acrylic coater as well as the MIP coater. To study the influence of the withdrawal speed on the coating thickness, the dipping time was set for 10 seconds and the speed was varied from 10 mm/s to 200 mm/s. Figure 5.25 depicts the dependence of the coating thickness on the withdrawal speed. The thickness of the coating layer increased from 21 µm to 35 µm for the acrylic coater and from 30 µm to 42 µm for the selective coater and the maximum thickness was obtained at 150 mm/s.

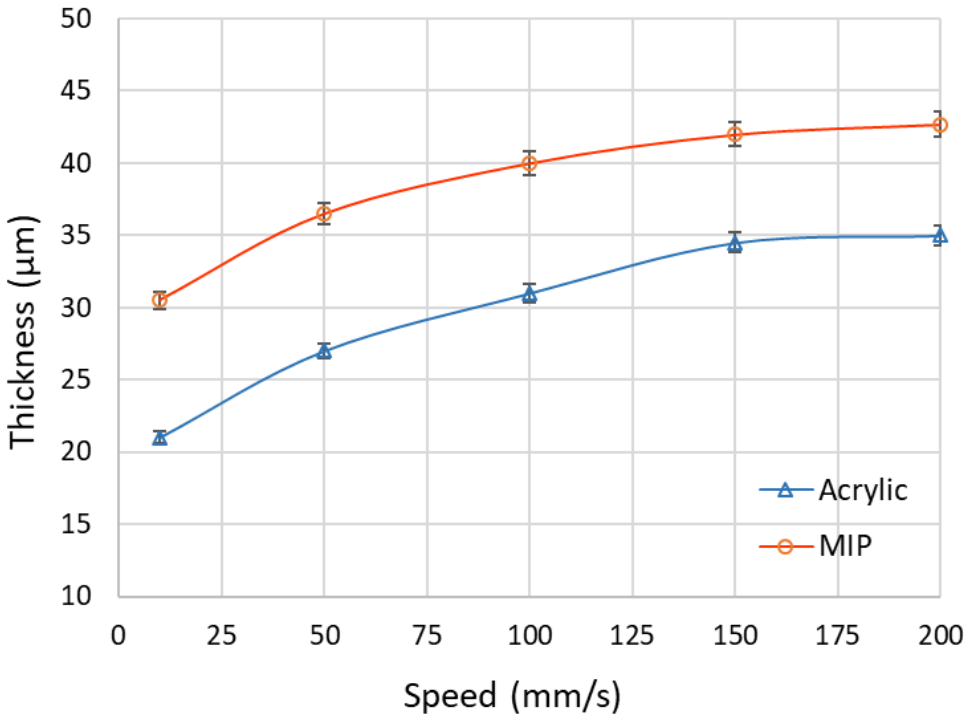

Figure 5.25 Speed-dependent thickness of the coated sensor.

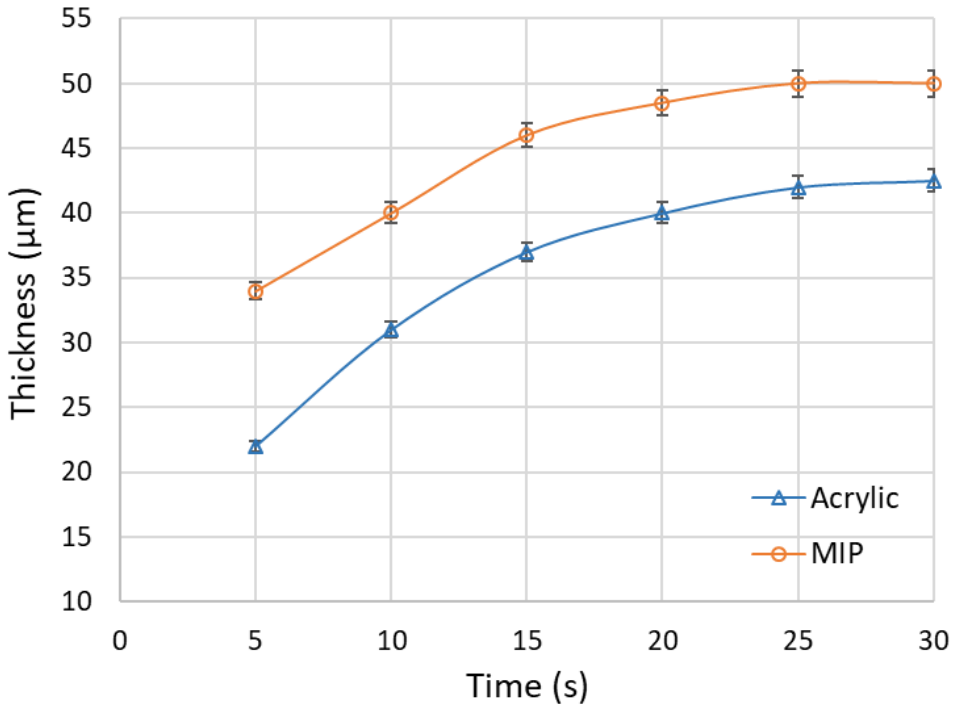

Figure 5.26 Time-dependent thickness of the coated sensor.

In order to investigate the time-dependent coating thickness, the withdrawal speed was kept at 100 mm/s and the dipping time was changed from 5 s to 30 s. The result of the coating layer thickness as a function of dipping time is illustrated in Figure 5.26. It is seen that the coating thickness quickly increased in 10 seconds and the maximum thickness was achieved after 25 seconds for both the coating materials.

5.6 Chapter Summary

A novel sensing technique for the recognition of CTx-I by combining electrochemical impedance spectroscopy and MIP technology was explained in this chapter. The experiments were conducted on real serum samples. The proposed biosensor exhibited good selectivity and quick rebinding capacity towards the target molecule. 0.09 ng/ml was the lowest level that could be detected by the developed biosensor. The limit of detection (LOD) obtained using the standard technique ELISA is 0.02 ng/ml, which is indeed less than the LOD obtained from the developed biosensor. However, at this stage, it should be noted that the proposed biosensing method represents a much simpler, quicker and more cost effective CTx-I detection technique. Moreover, the use of artificial antibodies highly

improved the stability of the system. Therefore, the results demonstrate the potential of the developed biosensing system to be employed as a Point-of-Care (PoC) device for prognostic applications, and can be utilised for a user-friendly and regular assessment of bone loss.

Moreover, in this chapter, the role of the coating thickness on the sensitivity of the planar interdigital sensors has been investigated, as selectivity and sensitivity are the two most important features of a sensor. The sensor had been coated with two different types of materials: acrylic lacquer as a protective layer and Molecular Imprinted Polymer (MIP) as a selective layer. The performance of the coated sensor was studied by estimating the sensitivity of the sensor with various coating thicknesses. CTx-I samples with different concentrations were used for this study. It was concluded that the MIP-coated sensor exhibited more sensitivity than the acrylic-coated one for CTx-I measurement. The dip-coating method was employed to coat the sensor. The effect of two important parameters, withdrawal speed and immersion time, on the thickness of the coating layer was studied. This investigation concluded that the faster the withdrawal, the thicker the coating layer. Furthermore, the thickness of the coating layer was increased by increasing the dipping time. However, the results show that increasing the thickness enhances the saturated level. Depending on the application, you need to have a trade-off between the saturation level and the sensitivity obtained by varying the coating thickness.

6

IoT-enabled Microcontroller-based System

Publication pertaining to this chapter:

- ***N. Afsarimanesh,*** M. E. E. Alahi, S. C. Mukhopadhyay and M. Kruger. "Development of IoT-Based Impedometric Biosensor for Point-of-Care Monitoring of Bone Loss", **IEEE Journal on Emerging and Selected Topics in Circuits and Systems, 2018**.

6.1 Introduction

Point-of-Care (PoC) testing is near-patient testing and is useful in prognostic monitoring of various diseases by measuring specific biomarkers [240-242]. The main aim of PoC testing is to produce results rapidly, so that treatment can start immediately. In this way, patient care can be improved with reduced cost. Small, rapid, portable, low-cost and user-friendly devices are most suitable for PoC testing, especially for household use [242-244].

As explained in Chapter 2, during the last few years, some investigations on the development of low-cost ELISA-based sensing systems have been reported for the measurement of CTx-1 levels [115, 119, 146], where biological antibodies have been used to capture the target molecule, CTx-1. Using natural antibodies increases the total cost and reduces the stability of the system in harsh environments. They also require a complicated sample preparation, which increases the time of the procedure. Creating artificial antibodies using molecular imprinting technique can be useful to overcome the limitations of natural antibodies.

Electrochemical biosensors are widely used for the development of portable and lab-on-a-chip devices. They have played an important role in the transition from costly and sophisticated laboratory devices towards easy-testing home-use devices [245-248]. Electrochemical biosensors have been extensively used in different applications, especially in clinical diagnostic and environmental monitoring, due to their low cost, ease of use, portability and reliability [155, 249-253]. An Internet of Things (IoT) enabled sensing system assists to transfer the measured sensing data directly to the cloud server. IoT is a concept, which refers to the connected objects that surround us being on the internet in one form or another. IoT-connected devices provide wide applications such as smart home, smart hospital, waste management, smart industry, and smart city. One of the most attractive application areas of IoT would be medical and health-care applications such as health monitoring, early detection and elderly care to provide a healthy life. IoT-enabled smart devices and health services reduce medical costs, increase the quality of life, and provide early information to the house physician, which could reduce the life threat [254]. It can also help to provide important health information without any mobility of the patient.

The purpose of this research is to design a portable IoT-based biosensing system for monitoring the level of CTx-1 biomarker in serum. The objective is to achieve a PoC testing device, which can quantify the level of CTx-1 and transfer the data to an IoT-based cloud

server. The transferred data will be stored and provided to the health-care contributor for further analysis and investigation. As reported in the earlier chapters, an MIP-based electrochemical biosensor was developed for bone-loss monitoring, where a high-precision impedance analyser was used to estimate the dielectric properties of the sample solution using the EIS technique. In spite of the high sensitivity and reliability, impedance-analyser instruments are expensive, bulky and not suitable for household applications. In the present work, we have replaced the bulky and costly impedance-analyser instrument with a low-cost (~ 100 USD) handheld device that connects to an IoT-based cloud server using an integrated WiFi connection.

6.2 Electrochemical Impedance Monitoring using the Microcontroller-based System

6.2.1 Block Diagram of the Point-of-Care System

This work is based on the electrochemical impedance measurements using an interdigital sensor and then developing a PoC system for taking data. Figure 6.1 shows the block diagram of the proposed PoC system. The system is a low-power-microcontroller-based system. An impedance analyser is used to collect the impedance information, generated by varying CTx-1 concentrations. The microcontroller did a conversion of impedance data to actual CTx-1 concentrations, and other necessary calculations. The power was supplied from a battery to the microcontroller. Finally, the calculated CTx-1 concentration was transferred to an IoT-based cloud server to allow assessment of the data by a house physician or responsible person.

The microcontroller board has integrated WiFi, which helps to connect the PoC device with any gateway to transfer the data to the remote server. Thingspeak [255] is a free IoT-based cloud server which was used to store the data. This cloud server is accessible from any location, which helps a health care provider to monitor the real-time data for early detection of bone loss. The Arduino Ciao [256] library was used to transfer the measured data to the designated private channel in Thingspeak. Ciao is the library, which uses the HTTP POST protocol to send the measured concentration to the Thingspeak cloud server.

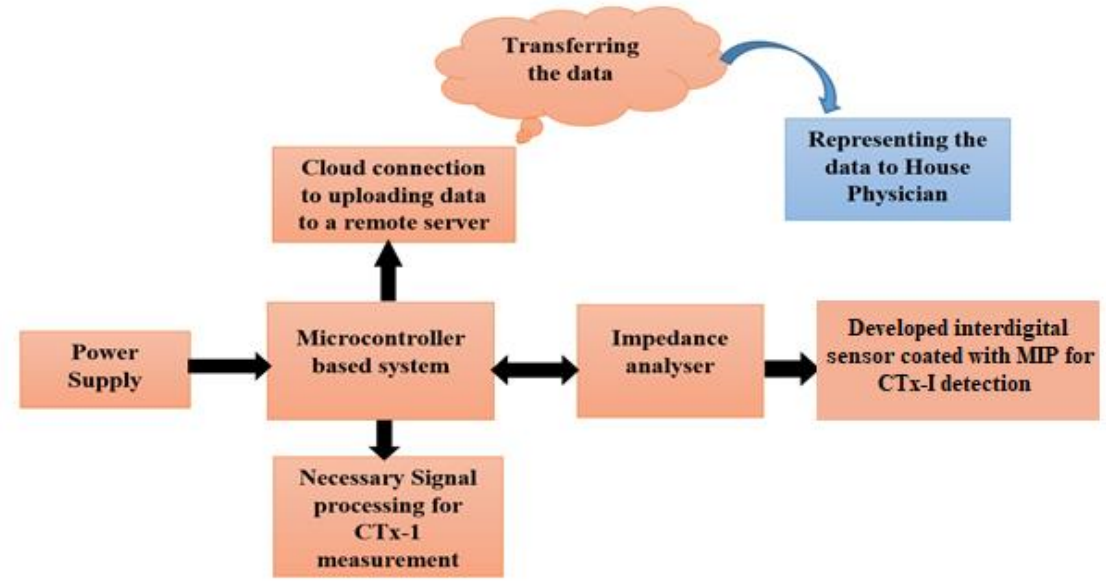

Figure 6.1 Complete Block diagram of the point-of-care system.

6.2.2 Circuit Diagram of the Proposed System

Figure 6.2 shows the circuit diagram of the proposed system. It contains the Arduino Uno Wifi [257] as a master microcontroller, an AD5933 [258] as an impedance analyser to calculate the impedance of the coated sensor and an ADG849[259] as a 2:1 multiplexer during calibration of the impedance analyser. The impedance analyser provides the AC (Alternating Current) voltage of 1.98 V p-p (peak to peak) to the excitation electrode of the coated sensor. The DC (Direct Current) bias voltage was 1.48 V. The direct digital synthesis (DDS) [260] technique was used to generate the AC excitation signal with a specific operating frequency, in this case, 320 Hz. The I2C protocol [261] was used to collect the impedance data from the coated sensor. 2.1 kΩ resistance was used to calibrate the impedance analyser to calculate the gain, which is necessary to calculate the impedance of the coated sensor. A supply voltage (3.3 V) is provided from Arduino Uno WiFi to the AD5933 and ADG849. The ADG849 is used as a switch to calibrate the system before every measurement. The main microcontroller is powered from a rechargeable battery.

The microcontroller collects the impedance data from the impedance analyser and uses the standard calibration graph to calculate the CTx-1 concentration. It is also required to do some error correction to get the actual concentration of CTx-1.

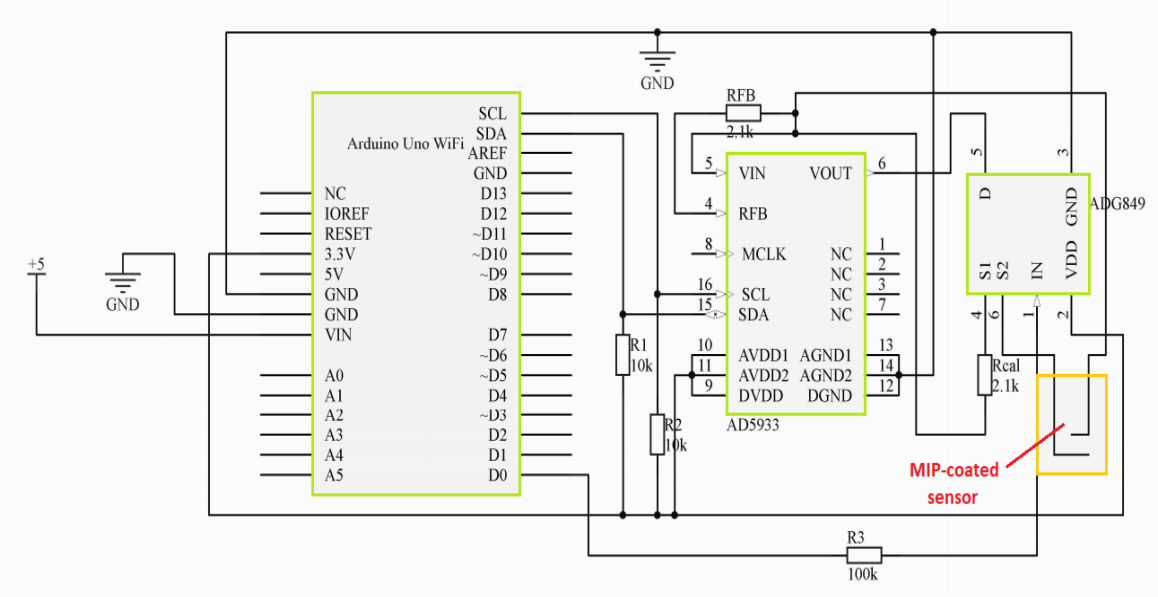

Figure 6.2 Circuit diagram of the proposed point-of-care device.

6.2.3 Software Process Flow of the PoC Device

Figure 6.3 shows the complete software process flow of the developed PoC device. The Arduino IDE (Integrated Development Environment) was used to write all the sketches; it contains a text editor for writing code, a text console, a message area and a toolbar with buttons for common functions [262]. It is seen from Figure 6.3 that the PoC device will initialise the rest connector, the server address and the microcontroller after powering on the device. The developed function is also used to calculate the CTx-1 concentration. The impedance analyser is also initialised to its operating frequency to calculate the gain and phase for the coated sensor. If the initialisation is unsuccessful, it repeats the steps till the completion of the process. The phase is required to calculate the imaginary impedance, which was used to identify the corresponding CTx-1 concentration from the calibration standard. Fitting is done by the developed system if it is required. The calculated concentration was fitted to the standard calibration curve, which was developed from LCR measurements. Finally, the data is transferred to the IoT-based cloud server. If the PoC device is unable to send the calculated data to the cloud server, it will start from the beginning as shown in Figure 6.3.

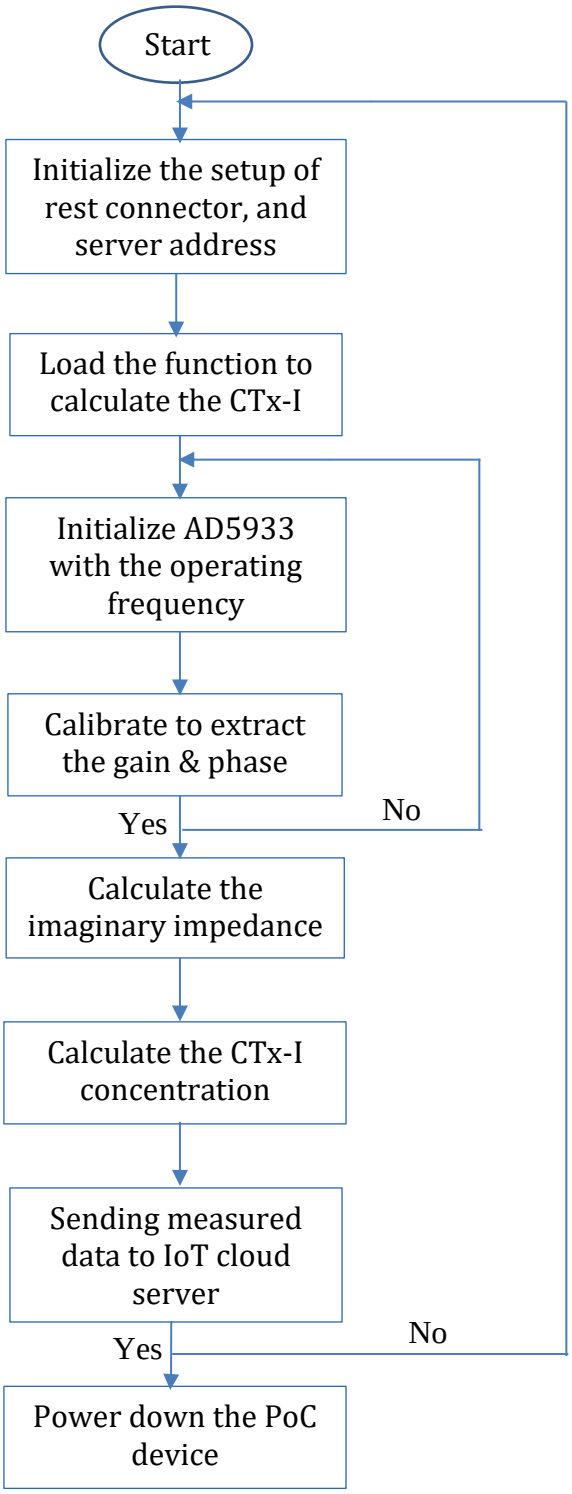

Figure 6.3 Software flow of the point-of-care device for CTx-1 calculation and transfer to the IoT cloud server

Figure 6.4 represents the first prototype, with dimensions of 15 cm × 10 cm, which was used as a PoC device.

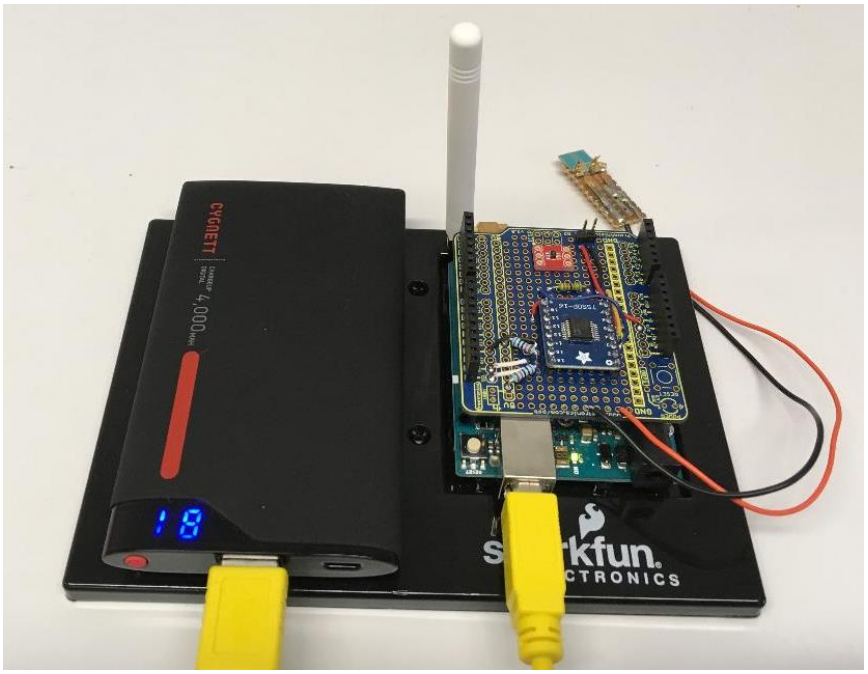

Figure 6.4 First prototype of the point-of-care system**.**

The microcontroller was connected with any local gateway and the secured Application Process Interface (API) key was provided in the code for secure transmission. After transmitting the data, the device turns off automatically. The final collected data can be seen immediately in the Thingspeak cloud for the house physician or any other person who is interested to monitor the CTx-1 concentration.The developed PoC device requires an SSID (Service Set Identifier) and password to get access to a Wi-Fi network. A WPA2 (Wi-Fi Protected Access 2) key has been used which is a standard for wireless security. It is an alphanumeric password which is used to get the access from a PoC device.

6.3 Results and Discussion

6.3.1 Calibration Curve Development from the Proposed System

The PoC device was calibrated to measure the unknown samples. The calibration experiments were performed using the six standard solutions (0.1, 0.5, 1, 1.5, 2 and 2.5 ppb). 320 Hz was taken as the optimum frequency as was suggested by measurements with the LCR meter. Finally, the calibration curve was developed by plotting the concentration on the x-axis and the reactance on the y-axis (Figure 6.5). It is seen that the concentration

of CTx-1 has a good correlation (R^2= 0.99) which is similar to the earlier one. The sensitivity of the calibration standard is 745.09 Ω/ppb, which is smaller than the calibration standard developed by the LCR meter. It can be seen the reactance decreases with an increase in the CTx-1 concentration. The following equation was deduced from the linear-regression analysis:

$$C = \frac{X + 53373}{745.09} \qquad (6.1)$$

where C (ppb) is the CTx-1 concentration and X (Ω) is the reactance. The PoC device employed (6.1) to measure the CTx-1 concentration in the unknown samples.

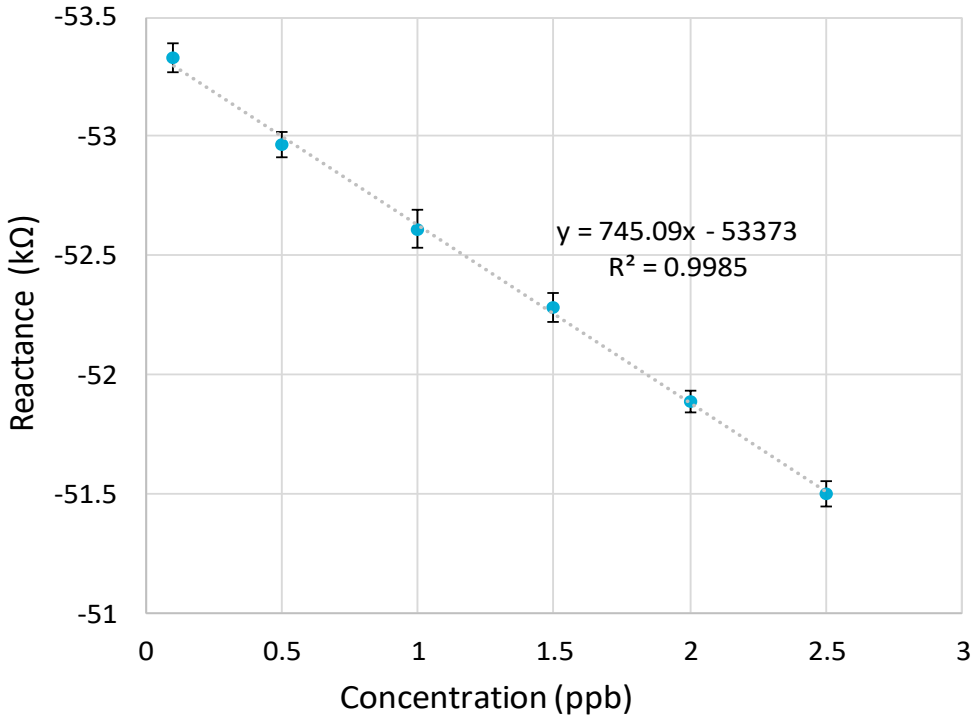

Figure 6.5 Calibration standard of the PoC device.

6.3.2 Unknown Sample Measurement

Sheep blood samples were collected (approval number 14/103, Massey University Animal Ethics Committee) between 8am and 10am in fasting animals due to the circadian

rhythm of CTx-1. The samples were kept on ice until being centrifuged. The samples were centrifuged at 4 ˚C within an hour, and then aliquoted into cryovials. The samples were stored at -80 ˚C until further assays were done. They were thawed in the refrigerator, 30 min before starting the experiments.

Four different samples collected from sheep blood were tested using the PoC device to measure the level of CTx-1. All the experiments were performed five times and the mean value was used as the result to ensure the repeatability and accuracy of the proposed device. The results validation was done using a commercial serum CrossLaps® ELISA kit. The results of both the methods are summarised in Table 6.1 and the comparison is illustrated in Figure 6.6. Correlation analysis between the proposed PoC device and a standard ELISA for CTx-I measurement is shown in Figure 6.7. It is seen that the measured data from the PoC device are very close to those from the standard method and the error is ≤ 3%. It is also noticed that the error is more in greater at concentrations.

Table 6.1 Unknown sample measurement and validation with standard ELISA method.

Sample	CTx-I level (ppb)		Difference (%)
	Proposed method PoC	Reference method ELISA	
1	0.4532	0.4497	0.8
2	1.4233	1.3999	1.7
3	1.5027	1.4651	2.6
4	0.3688	0.3722	0.9

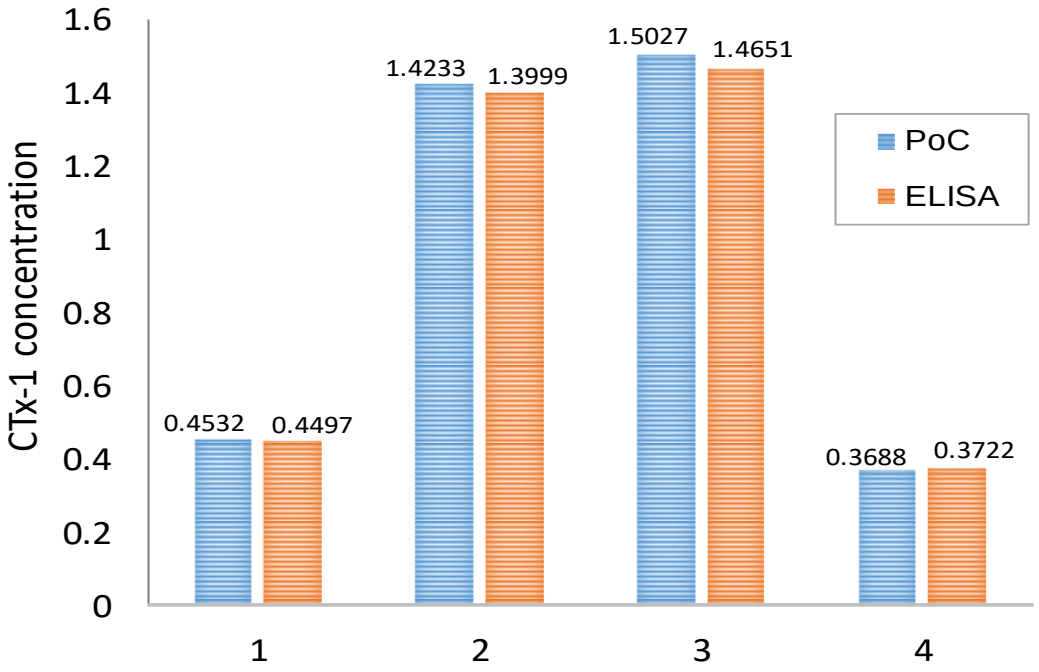

Figure 6.6 Comparison between the PoC results and the ELISA results.

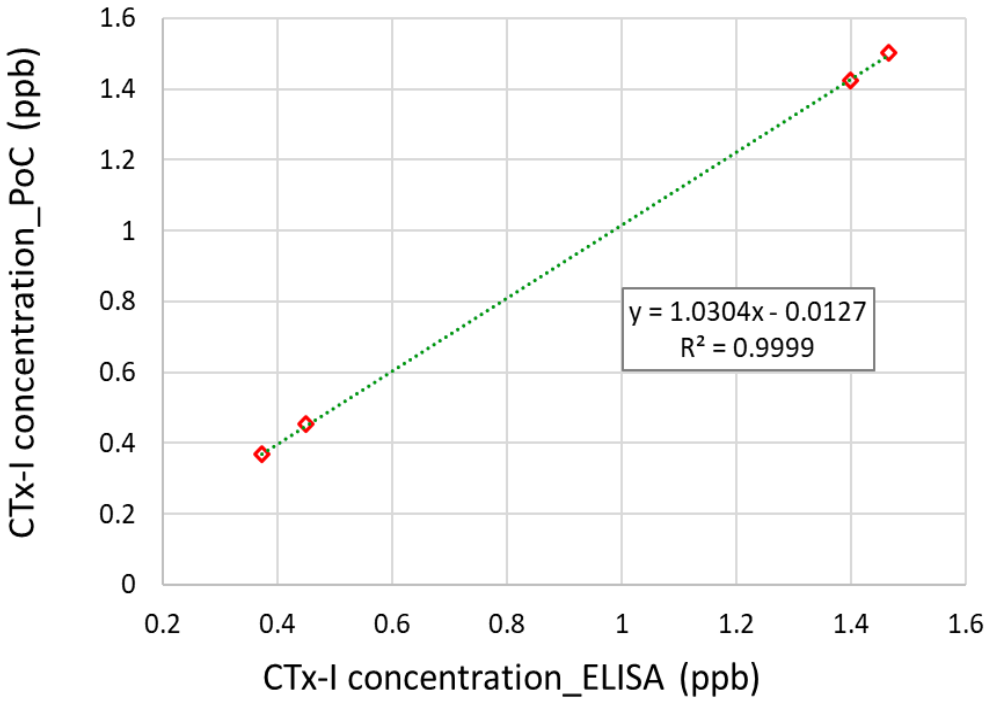

Figure 6.7 Correlation analysis between the proposed PoC device and a standard ELISA kit for CTx-I measurement.

6.3.3 IoT Data from the Point-of-care Device

Figure 6.8 shows the real-time data of CTx-1. The measured concentration was 0.45 ppb and the system was used for three hours continuously to see the performance. The secured server is accessible from any location and the physician can easily monitor the CTx-1 level and alert the patient if required. The device is portable, light, and easy to use.

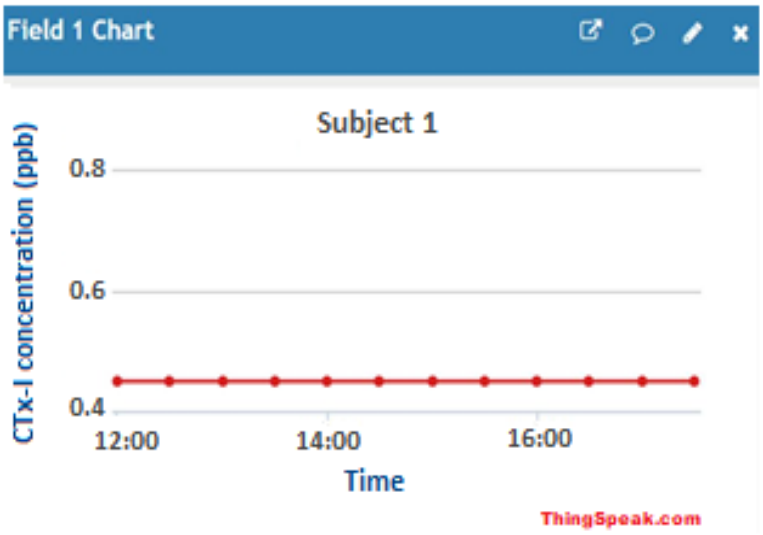

Figure 6.8 Real-time data from developed point-of-care device.

6.4 Chapter Summary

In summary, an IoT-based biosensor was developed for PoC monitoring of bone loss by detection and measurement of the CTx-1 biomarker in serum. The developed biosensing system is able to detect CTx-1 molecules in concentrations as low as 0.9 ppb. Initially an LCR meter was used to test the behaviour of the biosensor using the EIS technique. After that, a microcontroller-based system was developed to perform the CTx-1 measurement and transfer the data to an IoT-based cloud server. Four unknown serum samples obtained from sheep blood were tested and result validation was done by using ELISA. The results were in good agreement, with an error of $\leq 3\%$.

The proposed IoT-based biosensor provides a fast, simple, low-priced and portable device for direct measurement of CTx-1 in serum. ELISA requires at least 3 h to complete the assay, whereas using the developed PoC device each measurement can be performed

within 15 minutes. The developed PoC device can be used by anyone with minimum training, which is ideal for a regular evaluation of bone loss.

There are certain limitations, which will be part of the future work. The sensitivity of the PoC device needs to be improved to increase the accuracy of the measurements. It is also required to include security, as the PoC device is dealing with personal information. The data latencies, transmission time and data security can be studied in future, which can improve the PoC device's acceptability.

7

Conclusion and Future Work

Publication pertaining to this chapter:

- ***N. Afsarimanesh***, M. E. E. Alahi, S. C. Mukhopadhyay, and M. Kruger, "Smart Sensing System for Early Detection of Bone Loss: Current Status and Future Possibilities," **MDPI Journal of Sensor and Actuator Networks**, vol. 7, 10, pp. 1-11, **2018**.

7.1 Conclusion

Osteoporosis is still a serious concern in most countries and it is increasing with the aging population. Early detection of bone loss is important to successfully manage the disease. Monitoring the bone turnover markers can be helpful in early detection, diagnosis and monitoring bone disorders and deciding on medication and treatment. Bone loss can be detected and monitored by regular measurement of serum or urine C-terminal telopeptide of type 1 collagen (CTx-1). Rapid, portable and low-cost point-of-care devices are highly desirable.

In this research, we have developed an IoT-based selective, sensitive, quick and inexpensive device for the detection and quantification of CTx-1 levels in serum. A capacitive interdigital sensor was coated with artificial antibodies, prepared by molecular imprinting technology. Artificial antibodies were used to improve the stability of the system and reduce the total cost. Electrochemical impedance spectroscopy was used to evaluate the resistive and capacitive properties of the sample solutions. A microcontroller-based system was developed for the measurement of the level of CTx-1 in serum and for data transmission to an Internet of Things (IoT)-based cloud server. The data can be provided to the medical practitioner and a detailed investigation can start for early detection and treatment. The developed sensing system responded linearly in a range of 0.1 ppb to 2.5 ppb, which covers the normal reference range of CTx-1 in serum, with a LOD of 0.09 ppb. The results demonstrated that the proposed portable biosensing system could provide a rapid, simple and selective approach for CTx-1 measurement in serum. Sheep serum samples were tested using the proposed system and the validation of the results was done using an ELISA kit.

7.2 Future Possibilities

The developed system uses the blood serum as the test sample. In spite of the excellent performance of the proposed PoC device, use of blood sampling is being extremely unpopular for continuous monitoring, as blood sampling is not possible and acceptable for most people who are going to use this device at home. Therefore, development of a PoC device which can use urine as the test sample would be highly desirable. A smart toilet can

be developed by attaching a PoC urine testing device to toilet. The bone-loss monitoring can be done automatically and without human interaction. The data collected from each measurement would be transmitted wirelessly to the health care center for further actions.

Urinary CTx-I is considered as a normalized ratio to urinary creatinine in order to adjust the variations in urine flowrate. Therefore, CTx-I and creatinine should be measured from the same aliquot. Once the concentration of creatinine is determined in the urine sample, the concentration of CTx-I should be corrected with the creatinine level, using the following equation [263]:

$$Corrected\ CTx-I\ value\ (ng/mmol) = \frac{1000 \times CTx-I\ level\ (\mu g/L)}{Creatinine\ level\ (mmol/L)} \quad (7.1)$$

Special memory sites for creatinine can be synthesized using molecular imprinting technology [264, 265]. Creatinine is a polar molecule, so improved interaction could be expected with MIPs synthesized from highly hydrophobic monomers like methacrylic acid (MAA). Therefore, in order to prepare the creatinine-selective MIP, MAA can be used as the monomer, EGDMA as the cross-linker and creatinine as the template molecule. Precipitation polymerization method can be used to make the imprinted polymer in the form of microspheres. The synthesized MIP will be immobilized on the sensing surface using a self-assembled monolayer such as acrylic resin.

However, recent literatures claimed that single biomarker measurement is not enough for detection of bone loss or monitoring a treatment procedure, advising that simultaneous measurement of multiple bone turnover markers could be beneficial [266]. Recently, multiplex PoC devices have been developed for the diagnosis of different diseases [267-269]. Urinary calcium (Ca^{2+}) is another marker of bone resorption. A simultaneous measurement of CTx-I, creatinine and calcium in urine can give an accurate and reliable information about the rate of bone-loss.

Calcium-imprinted polymers can be prepared using ion imprinted polymers (IIPs) by solidification of polymers in the presence of calcium ions as the template. IIPs have been increasingly developed during the last 20 years, on the principle of MIPs. Ion imprinting technology is a useful approach to synthesize artificial materials as biomimetic antibodies that can recognize any target ions [270]. A Ca^{2+} selective polymer can be synthesized by precipitation polymerization using calcium ions as the template, itaconic acid (ITA) as the functional monomer, EGDMA as the cross-linker and 2,2-azoisobutronitrile (AIBN) as the

initiator. Figure 7.1 represents the schematic of the method of Ca^{2+}- IIP and the related recognition mechanism [271].

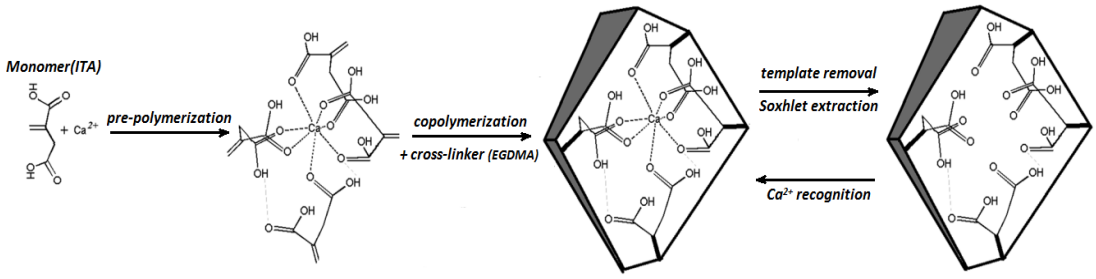

Figure 7.1 Schematic representation of Ca^{+2}- IIP method.

A multiplex assay can be developed by designing a sensor array for better and quicker measurement of calcium, CTx-I and creatinine biomarkers. The developed device could be attached to toilet for automatic sampling of urine. The simultaneous measurement of calcium, CTx-I and creatinine could be done and the measured values would be transferred to the medical practitioner for further investigation. A schematic diagram of the proposed sensor array for simultaneous measurement of CTx-I, creatinine and calcium in urine is shown in Figure 7.2.

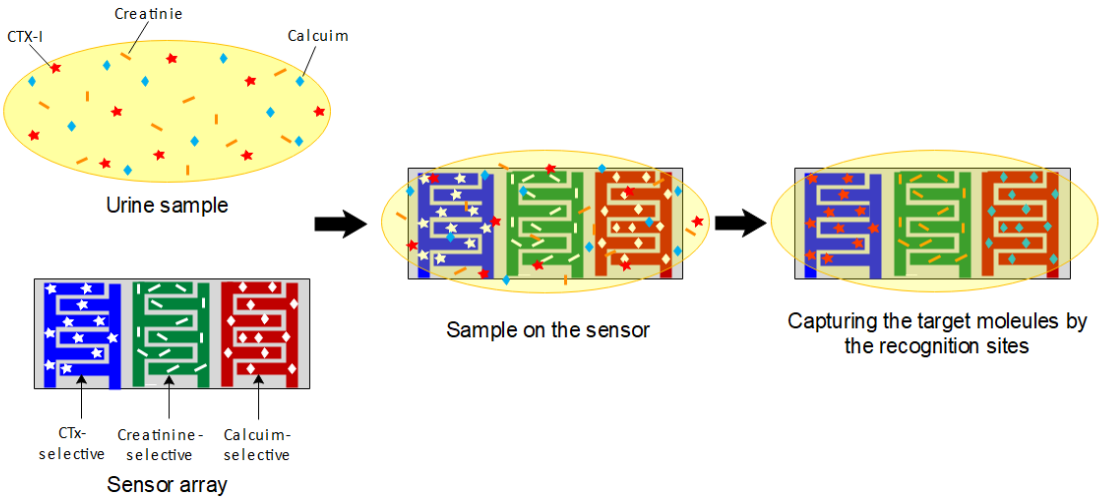

Figure 7.2 Schematic diagram of the proposed sensor array for simultaneous measurement of CTx-I, creatinine and calcium in urine.

The smart toilet provides the regular real-time monitoring of different biochemical markers in urine without human interaction. This device can indicate the early stages of osteoporosis so that the treatment can be started earlier when it is most effective, without waiting for a long time, identified by a DXA scan. DXA scan can be used for extra precautionary measurement. Figure 7.3 shows a schematic diagram of the possible smart toilet for continuous monitoring of bone-loss.

There are many challenges to make this idea feasible for real life application. One of the problem is the effect of toxic materials (such as urine or chemical for wash) on the life and performance of the sensor.

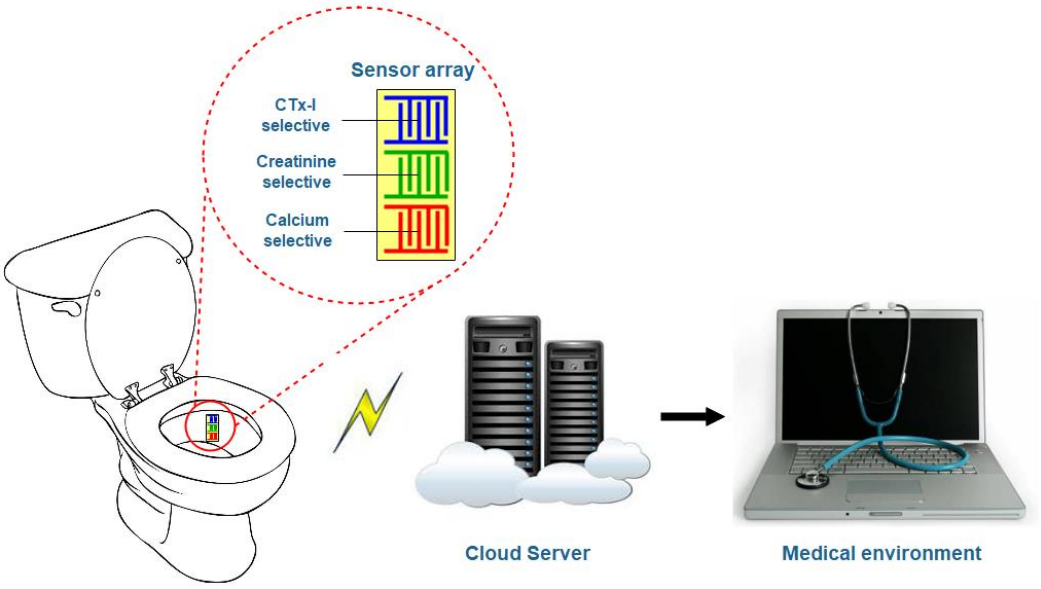

Figure 7.3 Schematic diagram of the possible smart toilet for continuous monitoring of bone-loss.

An IoT-enabled portable sensing device based on the developed MIP coated interdigital sensor for measuring the serum CTx-I molecule was developed. The artificial antibodies prepared by molecular imprinting technology were used to introduce selectivity of CTx-I to a planar interdigital sensor. The developed PoC device is able to measure the concentration of CTx-I in serum and transfer the measured data to an IoT-based cloud server. The transferred data will be delivered to a medical practitioner for further analysis and investigation. The After developing the calibration curve using known-concentration samples, four unknown-concentration sheep serum samples were tested using the proposed device, which are then compared with ELISA-based measurement. The proposed PoC

device exhibited a linear behavior in the range of 0.1 ng/ml to 2.5 ng/ml, which is good enough for bone-loss detection. The results obtained from the developed device are in good agreement with ELISA results. However, design and development of a smart toilet could be more beneficial as a PoC device. The initial investigations and the results are based on laboratory data and serum has been available for test sample. The sensor can be also used for the detection of CTx-I from blood. However, that may not be too attractive so, urine is considered as the future possibility. In this case, portable system is extremely important to be installed at the toilet, and data can be uploaded in cloud for remote monitoring.

References

[1] *Osteoporosis in RA*. Available: https://www.nras.org.uk/osteoporosis-in-ra

[2] (14/01/2018). *10 facts on ageing and health*. Available: http://www.who.int/features/factfiles/ageing/en/

[3] A. Odén, E. V. McCloskey, J. A. Kanis, N. C. Harvey, and H. Johansson, "Burden of high fracture probability worldwide: secular increases 2010–2040," *Osteoporosis International*, vol. 26, pp. 2243-2248, September 01 2015.

[4] *What is osteoporosis?* Available: https://jeanhailes.org.au/health-a-z/bone-health/what-is-osteoporosis

[5] *Health-care expenditure on arthritis and other musculoskeletal conditions 2008–09*. Available: https://www.aihw.gov.au/reports/health-welfare-expenditure/health-care-expenditure-2008-09/contents/table-of-contents

[6] J. J. Watts, J. Abimanyi-Ochom, and K. M. Sanders, "Osteoporosis costing all Australian: a new burden of disease analysis-2012 to 2022," 2013.

[7] J. E. Adams, "Dual-energy X-ray absorptiometry," in *Osteoporosis and Bone Densitometry Measurements*, ed: Springer, 2013, pp. 101-122.

[8] N. B. Watts, "Fundamentals and pitfalls of bone densitometry using dual-energy X-ray absorptiometry (DXA)," *Osteoporosis international*, vol. 15, pp. 847-854, 2004.

[9] R. I. Gafni and J. Baron, "Overdiagnosis of osteoporosis in children due to misinterpretation of dual-energy x-ray absorptiometry (DEXA)," *The Journal of pediatrics*, vol. 144, pp. 253-257, 2004.

[10] G. M. Blake and I. Fogelman, "Technical principles of dual energy x-ray absorptiometry," in *Seminars in nuclear medicine*, 1997, pp. 210-228.

[11] *Bone Mineral Density Scan*. Available: http://www.medbroadcast.com/procedure/getprocedure/bone-mineral-density-scan

[12] R. H. Christenson, "Biochemical markers of bone metabolism: an overview," *Clinical biochemistry*, vol. 30, pp. 573-593, 1997.

[13] S. P. Chubb, "Measurement of C-terminal telopeptide of type I collagen (CTX) in serum," *Clinical biochemistry*, vol. 45, pp. 928-935, 2012.

[14] R. Eastell, P. Garnero, C. Audebert, and D. L. Cahall, "Reference intervals of bone turnover markers in healthy premenopausal women: results from a cross-sectional European study," *Bone*, vol. 50, pp. 1141-1147, 2012.

[15]

WHO. scientific group on the prevention and management of osteoporosis. Prevention and management of osteoporosis: report of a WHO scientific group (2008). Available: http://apps.who.int/iris/bitstream/handle/10665/42841/WHO_TRS_921.pdf;jsessionid=B8944EEBA8D30C36A771A5762C195451?sequence=1

[16] K. Singh, K.-S. Lee, D. Lee, Y. K. Kim, and K. C. Kim, "Spectroscopic techniques as a diagnostic tool for early detection of osteoporosis," *Journal of mechanical science and technology,* vol. 24, pp. 1661-1668, 2010.

[17] K. Singh, S. H. Lee, and K. C. Kim, "Osteoporosis: new biomedical engineering aspects," *Journal of mechanical science and technology,* vol. 20, pp. 2265-2283, 2006.

[18] D. J. Hadjidakis and I. I. Androulakis, "Bone remodeling," *Annals of the New York Academy of Sciences,* vol. 1092, pp. 385-396, 2006.

[19] L. J. Raggatt and N. C. Partridge, "Cellular and molecular mechanisms of bone remodeling," *Journal of Biological Chemistry,* vol. 285, pp. 25103-25108, 2010.

[20] A. Schindeler, M. M. McDonald, P. Bokko, and D. G. Little, "Bone remodeling during fracture repair: The cellular picture," in *Seminars in cell & developmental biology*, 2008, pp. 459-466.

[21] M. J. Seibel, "Biochemical markers of bone turnover part I: biochemistry and variability," *The Clinical biochemist. Reviews/Australian Association of Clinical Biochemists.,* vol. 26, p. 97, 2005.

[22] P. Marie, "Strontium ranelate: a physiological approach for optimizing bone formation and resorption," *Bone,* vol. 38, pp. 10-14, 2006.

[23] D. B. Burr, "Bone Biomechanics and Bone Quality: Effects of Pharmaceutical Agents Used to Treat Osteoporosis," *Clinical Reviews in Bone and Mineral Metabolism,* vol. 14, pp. 197-217, September 01 2016.

[24] C. Hernandez and T. Keaveny, "A biomechanical perspective on bone quality," *Bone,* vol. 39, pp. 1173-1181, 2006.

[25] F. Pagani, C. Francucci, and L. Moro, "Markers of bone turnover: biochemical and clinical perspectives," *Journal of endocrinological investigation,* vol. 28, pp. 8-13, 2005.

[26] S. Schuit, M. Van der Klift, A. Weel, C. De Laet, H. Burger, E. Seeman, *et al.*, "Fracture incidence and association with bone mineral density in elderly men and women: the Rotterdam Study," *Bone,* vol. 34, pp. 195-202, 2004.

[27] T. T. Hlaing and J. E. Compston, "Biochemical markers of bone turnover–uses and limitations," *Annals of clinical biochemistry*, vol. 51, pp. 189-202, 2014.

[28] K. I. Mac Pherson, "Osteoporosis and menopause: a feminist analysis of the social construction of a syndrome," *Advances in Nursing Science*, vol. 7, pp. 11-22, 1985.

[29] S. C. Marks and P. R. Odgren, "Structure and development of the skeleton," in *Principles of Bone Biology (Second Edition)*, ed: Elsevier, 2002, pp. 3-15.

[30] A. Ferreira, I. Alho, S. Casimiro, and L. Costa, "Bone remodeling markers and bone metastases: from cancer research to clinical implications," *BoneKEy reports*, vol. 4, 2015.

[31] S. Vasikaran, R. Eastell, O. Bruyère, A. Foldes, P. Garnero, A. Griesmacher, *et al.*, "Markers of bone turnover for the prediction of fracture risk and monitoring of osteoporosis treatment: a need for international reference standards," *Osteoporosis International*, vol. 22, pp. 391-420, 2011.

[32] S. M. Hart and R. Eastell, "Biochemical markers of bone turnover," *Current opinion in nephrology and hypertension*, vol. 8, pp. 421-427, 1999.

[33] P. Magnusson, L. Larsson, M. Magnusson, M. W. Davie, and C. A. Sharp, "Isoforms of bone alkaline phosphatase: characterization and origin in human trabecular and cortical bone," *Journal of Bone and Mineral Research*, vol. 14, pp. 1926-1933, 1999.

[34] R. B. McComb, G. N. Bowers Jr, and S. Posen, *Alkaline phosphatase*: Springer Science & Business Media, 2013.

[35] C. Drechsler, M. Verduijn, S. Pilz, R. T. Krediet, F. W. Dekker, C. Wanner, *et al.*, "Bone alkaline phosphatase and mortality in dialysis patients," *Clinical Journal of the American Society of Nephrology*, vol. 6, pp. 1752-1759, 2011.

[36] K. Kalantar-Zadeh, A. Shah, U. Duong, R. C. Hechter, R. Dukkipati, and C. P. Kovesdy, "Kidney bone disease and mortality in CKD: revisiting the role of vitamin D, calcimimetics, alkaline phosphatase, and minerals," *Kidney International*, vol. 78, pp. S10-S21, 2010.

[37] L. Gorman and B. E. Statland, "Clinical usefulness of alkaline phosphatase isoenzyme determinations," *Clinical biochemistry*, vol. 10, pp. 171-174, 1977.

[38] J. Farley, C. Chesnut, and D. Baylink, "Improved method for quantitative determination in serum of alkaline phosphatase of skeletal origin," *Clinical chemistry*, vol. 27, pp. 2002-2007, 1981.

[39] M. Abramowitz, P. Muntner, M. Coco, W. Southern, I. Lotwin, T. H. Hostetter, *et al.*, "Serum alkaline phosphatase and phosphate and risk of mortality and hospitalization," *Clinical Journal of the American Society of Nephrology*, p. CJN. 08621209, 2010.

[40] C. Gundberg, A. Looker, S. Nieman, and M. Calvo, "Patterns of osteocalcin and bone specific alkaline phosphatase by age, gender, and race or ethnicity," *Bone,* vol. 31, pp. 703-708, 2002.

[41] A. Khan, J. Bilezikian, A. Kung, S. Dubois, T. Standish, and Z. Syed, "Alendronate therapy in men with primary hyperparathyroidism," *Endocrine Practice,* vol. 15, pp. 705-713, 2009.

[42] S. L. Greenspan, R. D. Emkey, H. G. Bone, S. R. Weiss, N. H. Bell, R. W. Downs, *et al.*, "Significant Differential Effects of Alendronate, Estrogen, or Combination Therapy on the Rate of Bone Loss after Discontinuation of Treatment of Postmenopausal OsteoporosisA Randomized, Double-Blind, Placebo-Controlled Trial," *Annals of internal medicine,* vol. 137, pp. 875-883, 2002.

[43] P. J. Meunier, C. Roux, E. Seeman, S. Ortolani, J. E. Badurski, T. D. Spector, *et al.*, "The effects of strontium ranelate on the risk of vertebral fracture in women with postmenopausal osteoporosis," *New England Journal of Medicine,* vol. 350, pp. 459-468, 2004.

[44] Q. Q. Hoang, F. Sicheri, A. J. Howard, and D. S. Yang, "Bone recognition mechanism of porcine osteocalcin from crystal structure," *Nature,* vol. 425, p. 977, 2003.

[45] C. P. Price and P. W. Thompson, "The role of biochemical tests in the screening and monitoring of osteoporosis," *Annals of clinical biochemistry,* vol. 32, pp. 244-260, 1995.

[46] M. S. Calvo, D. R. Eyre, and C. M. Gundberg, "Molecular basis and clinical application of biological markers of bone turnover," *Endocrine Reviews,* vol. 17, pp. 333-368, 1996.

[47] R. T. Ingram, Y.-K. Park, B. L. Clarke, and L. A. Fitzpatrick, "Age-and gender-related changes in the distribution of osteocalcin in the extracellular matrix of normal male and female bone. Possible involvement of osteocalcin in bone remodeling," *Journal of Clinical Investigation,* vol. 93, p. 989, 1994.

[48] J. Brown, L. Malaval, M. Chapuy, P. Delmas, C. Edouard, and P. Meunier, "Serum bone Gla-protein: a specific marker for bone formation in postmenopausal osteoporosis," *The Lancet,* vol. 323, pp. 1091-1093, 1984.

[49] K. K. Ivaska, S.-M. Käkönen, P. Gerdhem, K. J. Obrant, K. Pettersson, and H. K. Väänänen, "Urinary osteocalcin as a marker of bone metabolism," *Clinical chemistry,* vol. 51, pp. 618-628, 2005.

[50] K. K. Ivaska, T. A. Hentunen, J. Vääräniemi, H. Ylipahkala, K. Pettersson, and H. K. Väänänen, "Release of intact and fragmented osteocalcin molecules from bone matrix during bone resorption in vitro," *Journal of Biological Chemistry,* vol. 279, pp. 18361-18369, 2004.

[51] M. Knapen, L. Schurgers, and C. Vermeer, "Vitamin K2 supplementation improves hip bone geometry and bone strength indices in postmenopausal women," *Osteoporosis International,* vol. 18, pp. 963-972, 2007.

[52] J. P. Brown, C. Albert, B. A. Nassar, J. D. Adachi, D. Cole, K. S. Davison, *et al.*, "Bone turnover markers in the management of postmenopausal osteoporosis," *Clinical biochemistry,* vol. 42, pp. 929-942, 2009.

[53] R. Swaminathan, "Biochemical markers of bone turnover," *Clinica chimica acta,* vol. 313, pp. 95-105, 2001.

[54] A. Tromp, M. Ooms, C. Popp-Snijders, J. Roos, and P. Lips, "Predictors of fractures in elderly women," *Osteoporosis international,* vol. 11, pp. 134-140, 2000.

[55] V. R. Jagtap and J. V. Ganu, "Effect of antiresorptive therapy on urinary hydroxyproline in postmenopausal osteoporosis," *Indian Journal of Clinical Biochemistry,* vol. 27, pp. 90-93, 2012.

[56] V. Indumati and V. Patil, "Biochemical markers of bone remodeling in osteoporosis-current concepts," *Journal of Clinical and Diagnostic research,* vol. 4, pp. 2089-97, 2010.

[57] L. Yang and V. Grey, "Pediatric reference intervals for bone markers," *Clinical biochemistry,* vol. 39, pp. 561-568, 2006.

[58] U. Naidoo, D. Goff, and A. Klibanski, "Hyperprolactinemia and bone mineral density: the potential impact of antipsychotic agents," *Psychoneuroendocrinology,* vol. 28, pp. 97-108, 2003.

[59] M. Plebani, D. Bernardi, M. F. Meneghetti, F. Ujka, and M. Zaninotto, "Biological variability in assessing the clinical value of biochemical markers of bone turnover," *Clinica chimica acta,* vol. 299, pp. 77-86, 2000.

[60] M. J. Seibel, S. P. Robins, and J. P. Bilezikian, *Dynamics of bone and cartilage metabolism: principles and clinical applications*: Academic Press, 2006.

[61] J. M. Lane, "Dynamics of Bone and Cartilage Metabolism," *JBJS*, vol. 83, p. 639, 2001.

[62] C. A. Burtis and D. E. Bruns, *Tietz Fundamentals of Clinical Chemistry and Molecular Diagnostics-E-Book*: Elsevier Health Sciences, 2014.

[63] S. Viguet-Carrin, P. Garnero, and P. Delmas, "The role of collagen in bone strength," *Osteoporosis international,* vol. 17, pp. 319-336, 2006.

[64] N. Afsarimanesh, S. C. Mukhopadhyay, and K. Marlena, "- Biosensors For the Measurement of C-Terminal Telopeptide of Type I Collagen (CTX-I)," *Journal of Osteoporosis and Physical Activity,* vol. 5, 2017.

[65] M. Baumann, R. Eastell, N. Hoyle, and L. Wieczorek, *Bone markers: biochemical and clinical perspectives*: Taylor & Francis, 2001.

[66] M. Herrmann and M. Seibel, "The amino-and carboxyterminal cross-linked telopeptides of collagen type I, NTX-I and CTX-I: a comparative review," *Clinica Chimica Acta,* vol. 393, pp. 57-75, 2008.

[67] P. Kyd, K. De Vooght, F. Kerkhoff, E. Thomas, and A. Fairney, "Clinical usefulness of biochemical resorption markers in osteoporosis," *Annals of clinical biochemistry,* vol. 36, pp. 483-491, 1999.

[68] Y. Nishizawa, T. Nakamura, H. Ohta, K. Kushida, I. Gorai, M. Shiraki, *et al.*, "Guidelines for the use of biochemical markers of bone turnover in osteoporosis (2004)," *Journal of bone and mineral metabolism,* vol. 23, pp. 97-104, 2005.

[69] J.-H. ZHANG, J. Wang, J. Tang, B. Barnett, J. Dickson, N. Hahsimoto, *et al.*, "Bone sialoprotein promotes bone metastasis of a non-bone-seeking clone of human breast cancer cells," *Anticancer research,* vol. 24, pp. 1361-1368, 2004.

[70] B. Ganss, R. H. Kim, and J. Sodek, "Bone sialoprotein," *Critical Reviews in Oral Biology & Medicine,* vol. 10, pp. 79-98, 1999.

[71] G. Carlinfante, D. Vassiliou, O. Svensson, M. Wendel, D. Heinegård, and G. Andersson, "Differential expression of osteopontin and bone sialoprotein in bone metastasis of breast and prostate carcinoma," *Clinical and Experimental Metastasis,* vol. 20, pp. 437-444, 2003.

[72] J. M. Halleen, S. L. Tiitinen, H. Ylipahkala, K. M. Fagerlund, and H. K. Vaananen, "Tartrate-resistant acid phosphatase 5b (TRACP 5b) as a marker of bone resorption," *Clinical laboratory,* vol. 52, pp. 499-510, 2006.

[73] P. Delmas, "Committee of Scientific Advisers of the International Osteoporosis Foundation. The use of biochemical markers of bone turnover in osteoporosis," *Osteoporosis Int,* vol. 11, pp. S2-S17, 2000.

[74] A. Nenonen, S. Cheng, K. K. Ivaska, S. L. Alatalo, T. Lehtimäki, H. Schmidt-Gayk, *et al.*, "Serum TRACP 5b is a useful marker for monitoring alendronate treatment: comparison with other markers of bone turnover," *Journal of Bone and Mineral Research,* vol. 20, pp. 1804-1812, 2005.

[75] J. M. Halleen, S. L. Alatalo, H. Suominen, S. Cheng, A. J. Janckila, and H. K. Väänänen, "Tartrate-resistant acid phosphatase 5b: a novel serum marker of bone resorption," *Journal of Bone and Mineral Research,* vol. 15, pp. 1337-1345, 2000.

[76] P. Leung, M. Pickarski, Y. Zhuo, P. Masarachia, and L. Duong, "The effects of the cathepsin K inhibitor odanacatib on osteoclastic bone resorption and vesicular trafficking," *Bone,* vol. 49, pp. 623-635, 2011.

[77] Z. Li, Y. Yasuda, W. Li, M. Bogyo, N. Katz, R. E. Gordon, *et al.*, "Regulation of collagenase activities of human cathepsins by glycosaminoglycans," *Journal of Biological Chemistry,* vol. 279, pp. 5470-5479, 2004.

[78] J. L. Pérez-Castrillón, F. Pinacho, D. De Luis, M. Lopez-Menendez, and A. Dueñas Laita, "Odanacatib, a new drug for the treatment of osteoporosis: review of the results in postmenopausal women," *Journal of osteoporosis,* vol. 2010, 2010.

[79] G. Holzer, H. Noske, T. Lang, L. Holzer, and U. Willinger, "Soluble cathepsin K: a novel marker for the prediction of nontraumatic fractures?," *Journal of Laboratory and Clinical Medicine,* vol. 146, pp. 13-17, 2005.

[80] M. Skoumal, G. Haberhauer, G. Kolarz, G. Hawa, W. Woloszczuk, and A. Klingler, "Serum cathepsin K levels of patients with longstanding rheumatoid arthritis: correlation with radiological destruction," *Arthritis Res Ther,* vol. 7, p. R65, 2004.

[81] S. Aydin, "A short history, principles, and types of ELISA, and our laboratory experience with peptide/protein analyses using ELISA," *Peptides,* vol. 72, pp. 4-15, 2015.

[82] R. M. Lequin, "Enzyme immunoassay (EIA)/enzyme-linked immunosorbent assay (ELISA)," *Clinical chemistry,* vol. 51, pp. 2415-2418, 2005.

[83] E. Engvall, "The ELISA, enzyme-linked immunosorbent assay," *Clinical Chemistry,* vol. 56, pp. 319-320, 2010.

[84] S. D. Gan and K. R. Patel, "Enzyme immunoassay and enzyme-linked immunosorbent assay," *J. Invest. Dermatol,* vol. 133, p. e12, 2013.

[85] J. A. Owen, J. Punt, and S. A. Stranford, *Kuby immunology*: WH Freeman New York, 2013.

[86] R. P. Revoltella, L. L. Robbio, and B. Liedberg, "Comparison of conventional immunoassays (RIA, ELISA) with surface plasmon resonance for pesticide detection and monitoring," *Biotherapy,* vol. 11, pp. 135-145, 1998.

[87] L. H. Graham, J. Bolling, G. Miller, N. Pratt-Hawkes, and S. Joseph, "Enzyme-immunoassay for the measurement of luteinizing hormone in the serum of African elephants (Loxodonta africana)," *Zoo Biology,* vol. 21, pp. 403-408, 2002.

[88] V. Bansal, "High performance liquid chromatography: a short review," *Journal of Global Pharma Technology,* vol. 2, 2010.

[89] B. L. Reuhs, "High-performance liquid chromatography," in *Food analysis*, ed: Springer, 2017, pp. 213-226.

[90] P. Khashayar, G. Amoabediny, B. Larijani, and J. Vanfleteren, "Bone biosensors: knowing the present and predicting the future," *Journal of Micromechanics and Microengineering,* vol. 26, p. 023002, 2016.

[91] L. Liu and T. J. Webster, "In situ sensor advancements for osteoporosis prevention, diagnosis, and treatment," *Current osteoporosis reports*, vol. 14, pp. 386-395, 2016.

[92] Y. M. Chung and Y. C. Liu, "Biosensor and method for bone mineral density measurement," ed: Google Patents, 2009.

[93] P. D. Miller, C. Zapalowski, C. A. Kulak, and J. P. Bilezikian, "Bone densitometry: the best way to detect osteoporosis and to monitor therapy," *The Journal of Clinical Endocrinology & Metabolism,* vol. 84, pp. 1867-1871, 1999.

[94] J. Kuball, J. Schüz, H. Gamm, and M. Weber, "Bone marrow punctures and pain," *Acute Pain,* vol. 6, pp. 9-14, 2004.

[95] B. J. Parmar, W. Longsine, E. P. Sabonghy, A. Han, E. Tasciotti, B. K. Weiner, *et al.*, "Characterization of controlled bone defects using 2D and 3D ultrasound imaging techniques," *Physics in medicine and biology,* vol. 55, p. 4839, 2010.

[96] F. Burny, M. Donkerwolcke, F. Moulart, R. Bourgois, R. Puers, K. Van Schuylenbergh, *et al.*, "Concept, design and fabrication of smart orthopedic implants," *Medical engineering & physics,* vol. 22, pp. 469-479, 2000.

[97] Y.-H. Wen, G. Y. Yang, V. J. Bailey, G. Lin, W. C. Tang, and J. H. Keyak, "Mechanically robust micro-fabricated strain gauges for use on bones," in *Microtechnology in Medicine and Biology, 2005. 3rd IEEE/EMBS Special Topic Conference on,* 2005, pp. 302-304.

[98] C. Pang, G.-Y. Lee, T.-i. Kim, S. M. Kim, H. N. Kim, S.-H. Ahn, *et al.*, "A flexible and highly sensitive strain-gauge sensor using reversible interlocking of nanofibres," *Nature materials*, vol. 11, pp. 795-801, 2012.

[99] M. Hsieh, Y.-K. Fang, M. Ju, J.-J. Ho, and S. Ting, "Development of a new contact-type piezoresistive micro-shear-stress sensor," in *Symposium on Design, Test, Integration, and Packaging of MEMS/MOEMS 2002*, 2002, pp. 285-295.

[100] S. Sirivisoot, C. Yao, X. Xiao, B. W. Sheldon, and T. J. Webster, "Developing biosensors for monitoring orthopedic tissue growth," in *MATERIALS RESEARCH SOCIETY SYMPOSIUM PROCEEDINGS*, 2007, p. 81.

[101] F. Umbrecht, P. Wägli, S. Dechand, F. Gattiker, J. Neuenschwander, U. Sennhauser, *et al.*, "Wireless implantable passive strain sensor: design, fabrication and characterization," *Journal of Micromechanics and Microengineering*, vol. 20, p. 085005, 2010.

[102] S. Bhalla and S. Bajaj, "Bone characterization using piezotransducers as biomedical sensors," *Strain*, vol. 44, pp. 475-478, 2008.

[103] E. L. Tan, B. D. Pereles, B. Horton, R. Shao, M. Zourob, and K. G. Ong, "Implantable biosensors for real-time strain and pressure monitoring," *Sensors*, vol. 8, pp. 6396-6406, 2008.

[104] N. Hu, H. Fukunaga, S. Atobe, Y. Liu, and J. Li, "Piezoresistive strain sensors made from carbon nanotubes based polymer nanocomposites," *Sensors*, vol. 11, pp. 10691-10723, 2011.

[105] T. Fresvig, P. Ludvigsen, H. Steen, and O. Reikerås, "Fibre optic Bragg grating sensors: an alternative method to strain gauges for measuring deformation in bone," *Medical engineering & physics*, vol. 30, pp. 104-108, 2008.

[106] P. Dharap, Z. Li, S. Nagarajaiah, and E. Barrera, "Nanotube film based on single-wall carbon nanotubes for strain sensing," *Nanotechnology*, vol. 15, p. 379, 2004.

[107] M. Liebshner, "OsteoSonicT M, Noninvasive bone and joint damage detection device," *NASA Tech Briefs*, 2004.

[108] F. Nogata, A. Shimamoto, and T. Habu, "Estimation of in vivo bone strength using ultrasound signals," *International Journal of Modern Physics B*, vol. 17, pp. 1381-1387, 2003.

[109] F. Alfaro, L. Weiss, P. Campbell, M. Miller, and G. K. Fedder, "Design of a multi-axis implantable MEMS sensor for intraosseous bone stress monitoring," *Journal of Micromechanics and Microengineering*, vol. 19, p. 085016, 2009.

[110] J. F. Alfaro, L. E. Weiss, P. G. Campbell, M. C. Miller, C. Heyward, J. S. Doctor, *et al.*, "Bioimplantable bone stress sensor," in *Engineering in Medicine and Biology Society, 2005. IEEE-EMBS 2005. 27th Annual International Conference of the*, 2006, pp. 518-521.

[111] P. Roriz, O. Frazão, A. B. Lobo-Ribeiro, J. L. Santos, and J. A. Simões, "Review of fiber-optic pressure sensors for biomedical and biomechanical applications," *Journal of biomedical optics*, vol. 18, pp. 050903-050903, 2013.

[112] V. Mishra, N. Singh, D. Rai, U. Tiwari, G. Poddar, S. Jain, *et al.*, "Fiber Bragg grating sensor for monitoring bone decalcification," *Orthopaedics & Traumatology: Surgery & Research*, vol. 96, pp. 646-651, 2010.

[113] P. Singh and A. Shrivastava, "Optical biosensor based on microbendings technique: an optimized mean to measure the bone strength," *Advances in Optical Technologies*, vol. 2014, 2014.

[114] R. K. McCormick, "Osteoporosis: integrating biomarkers and other diagnostic correlates into the management of bone fragility," *Alternative Medicine Review*, vol. 12, p. 113, 2007.

[115] Y.-H. Yun, A. Bhattacharya, N. B. Watts, and M. J. Schulz, "A label-free electronic biosensor for detection of bone turnover markers," *Sensors*, vol. 9, pp. 7957-7969, 2009.

[116] P. Caglar, S. Tuncel, N. Malcik, J. Landers, and J. Ferrance, "A microchip sensor for calcium determination," *Analytical and bioanalytical chemistry*, vol. 386, pp. 1303-1312, 2006.

[117] N. Afsarimanesh, S. C. Mukhopadhyay, and M. Kruger, "Molecularly Imprinted Polymer-Based Electrochemical Biosensor for Bone Loss Detection," *IEEE Transactions on Biomedical Engineering*, 2017.

[118] N. Afsarimanesh, A. Zia, S. Mukhopadhyay, M. Kruger, P.-L. Yu, J. Kosel, *et al.*, "Smart Sensing System for the Prognostic Monitoring of Bone Health," *Sensors*, vol. 16, p. 976, 2016.

[119] M. Ramanathan, M. Patil, R. Epur, Y. Yun, V. Shanov, M. Schulz, *et al.*, "Gold-coated carbon nanotube electrode arrays: Immunosensors for impedimetric detection of bone biomarkers," *Biosensors and Bioelectronics*, vol. 77, pp. 580-588, 2016.

[120] P. Khashayar, G. Amoabediny, M. Hosseini, R. Verplancke, F. Razi, J. Vanfleteren, *et al.*, "An electrochemical biosensor based on AuNP-modified gold electrodes for selective determination of serum levels of osteocalcin," *IEEE Sensors Journal*, vol. 17, pp. 3367-3374, 2017.

[121] L. Zhang, L. Liu, and N. Xia, "Electrochemical sensing of alkaline phosphatase activity based on difference of surface charge of electrode," *Int J Electrochem Sci,* vol. 8, pp. 8311-9, 2013.

[122] F. Lung, H.-Y. Chen, and H.-T. Lin, "Monitoring bone loss using ELISA and surface plasmon resonance (SPR) technology," *Protein and peptide letters,* vol. 10, pp. 313-319, 2003.

[123] M. Seibel, H. Woitge, I. Farahmand, H. Oberwittler, and R. Ziegler, "Automated and manual assays for urinary crosslinks of collagen: which assay to use?," *Experimental and clinical endocrinology & diabetes,* vol. 106, pp. 143-148, 1998.

[124] A. Claudon, P. Vergnaud, C. Valverde, A. Mayr, U. Klause, and P. Garnero, "New automated multiplex assay for bone turnover markers in osteoporosis," *Clinical chemistry,* vol. 54, pp. 1554-1563, 2008.

[125] P. Khashayar, G. Amoabediny, B. Larijani, M. Hosseini, R. Verplancke, D. Schaubroeck*, et al.*, "A Multiplexed Microfluidic Platform for Bone Marker Measurement: A Proof-of-Concept," *Micromachines,* vol. 8, p. 133, 2017.

[126] A. S. Abu-Abed and R. G. Lindquist, "Capacitive interdigital sensor with inhomogeneous nematic liquid crystal film," *Progress In Electromagnetics Research B,* vol. 7, pp. 75-87, 2008.

[127] A. V. Mamishev, K. Sundara-Rajan, F. Yang, Y. Du, and M. Zahn, "Interdigital sensors and transducers," *Proceedings of the IEEE,* vol. 92, pp. 808-845, 2004.

[128] Y. Chen, C. Zhu, M. Cao, and T. Wang, "Photoresponse of SnO2 nanobelts grown in situ on interdigital electrodes," *Nanotechnology,* vol. 18, p. 285502, 2007.

[129] M. S. A. Rahman, S. C. Mukhopadhyay, and P.-L. Yu, "Novel planar interdigital sensors," in *Novel Sensors for Food Inspection: Modelling, Fabrication and Experimentation*, ed: Springer, 2014, pp. 11-35.

[130] A. M. Syaifudin, K. Jayasundera, and S. Mukhopadhyay, "A low cost novel sensing system for detection of dangerous marine biotoxins in seafood," *Sensors and Actuators B: Chemical,* vol. 137, pp. 67-75, 2009.

[131] A. M. Syaifudin, S. Mukhopadhyay, and P. Yu, "Electromagnetic field computation using COMSOL Multiphysics to evaluate the performance of novel interdigital sensors," in *Applied Electromagnetics Conference (AEMC), 2009*, 2009, pp. 1-4.

[132] M. Yunus, S. Mukhopadhyay, and K. Jayasundera, "A novel planar interdigital sensor for environmental monitoring," in *Sensors, 2009 IEEE*, 2009, pp. 105-110.

[133] H. Arwin, "Application of ellipsometry techniques to biological materials," *Thin Solid Films,* vol. 519, pp. 2589-2592, 2011.

[134] Y. Yang, G. Chiesura, G. Luyckx, T. Vervust, F. Bossuyt, J. Vanfleteren, *et al.*, "In situ on-line cure monitoring of composites by embedded interdigital sensor," in *16th European conference on Composite Materials (ECCM-16)*, 2014.

[135] A. I. Zia, A. M. Syaifudin, S. Mukhopadhyay, P. Yu, I. Al-Bahadly, C. P. Gooneratne, *et al.*, "Electrochemical impedance spectroscopy based MEMS sensors for phthalates detection in water and juices," in *Journal of Physics: Conference Series*, 2013, p. 012026.

[136] A. I. Zia, S. C. Mukhopadhyay, P.-L. Yu, I. Al-Bahadly, C. P. Gooneratne, and J. Kosel, "Rapid and molecular selective electrochemical sensing of phthalates in aqueous solution," *Biosensors and Bioelectronics,* vol. 67, pp. 342-349, 2015.

[137] A. Zia, S. Mukhopadhyay, I. Al-Bahadly, P. Yu, C. P. Gooneratne, and J. Kosel, "Introducing molecular selectivity in rapid impedimetric sensing of phthalates," in *Instrumentation and Measurement Technology Conference (I2MTC) Proceedings, 2014 IEEE International*, 2014, pp. 838-843.

[138] A. Syaifudin, K. Jayasundera, and S. Mukhopadhyay, "A novel planar interdigital sensor based sensing and instrumentation for detection of dangerous contaminated chemical in seafood," in *Instrumentation and Measurement Technology Conference, 2009. I2MTC'09. IEEE*, 2009, pp. 701-706.

[139] J. Fischer, H. Dejmkova, and J. Barek, "Electrochemistry of pesticides and its analytical applications," *Current Organic Chemistry,* vol. 15, pp. 2923-2935, 2011.

[140] M. Khafaji, S. Shahrokhian, and M. Ghalkhani, "Electrochemistry of Levo-Thyroxin on Edge-Plane Pyrolytic Graphite Electrode: Application to Sensitive Analytical Determinations," *Electroanalysis,* vol. 23, pp. 1875-1880, 2011.

[141] L. Li, F. Yang, J. Yu, X. Wang, L. Zhang, Y. Chen, *et al.*, "In situ growth of ZnO nanowires on Zn comb-shaped interdigitating electrodes and their photosensitive and gas-sensing characteristics," *Materials Research Bulletin,* vol. 47, pp. 3971-3975, 2012.

[142] M. Dhull and A. Arora, "Design of MEMS Based Microheater for Enhanced Efficiency of Gas Sensors," *Journal of Thermal Engineering and Applications,* vol. 2, pp. 16-21, 2015.

[143] D. Grieshaber, R. MacKenzie, J. Voeroes, and E. Reimhult, "Electrochemical biosensors-sensor principles and architectures," *Sensors,* vol. 8, pp. 1400-1458, 2008.

[144] F. Lisdat and D. Schäfer, "The use of electrochemical impedance spectroscopy for biosensing," *Analytical and bioanalytical chemistry*, vol. 391, p. 1555, 2008.

[145] D. Ribeiro and J. Abrantes, "Application of electrochemical impedance spectroscopy (EIS) to monitor the corrosion of reinforced concrete: a new approach," *Construction and Building Materials*, vol. 111, pp. 98-104, 2016.

[146] N. Afsarimanesh, A. I. Zia, S. C. Mukhopadhyay, M. Kruger, P.-L. Yu, J. Kosel, *et al.*, "Smart Sensing System for the Prognostic Monitoring of Bone Health," *Sensors*, vol. 16, p. 976, 2016.

[147] M. S. Abdul Rahman, S. C. Mukhopadhyay, P.-L. Yu, J. Goicoechea, I. R. Matias, C. P. Gooneratne, *et al.*, "Detection of bacterial endotoxin in food: New planar interdigital sensors based approach," *Journal of Food Engineering*, vol. 114, pp. 346-360, 2013.

[148] A. Bogomolova, E. Komarova, K. Reber, T. Gerasimov, O. Yavuz, S. Bhatt, *et al.*, "Challenges of electrochemical impedance spectroscopy in protein biosensing," *Analytical chemistry*, vol. 81, pp. 3944-3949, 2009.

[149] B.-Y. Chang and S.-M. Park, "Electrochemical impedance spectroscopy," *Annual Review of Analytical Chemistry*, vol. 3, pp. 207-229, 2010.

[150] C. Fernández-Sánchez, C. J. McNeil, and K. Rawson, "Electrochemical impedance spectroscopy studies of polymer degradation: application to biosensor development," *TrAC Trends in Analytical Chemistry*, vol. 24, pp. 37-48, 2005.

[151] M. E. Orazem and B. Tribollet, *Electrochemical impedance spectroscopy* vol. 48: John Wiley & Sons, 2011.

[152] J. R. Macdonald and E. Barsoukov, "Impedance spectroscopy: theory, experiment, and applications," *History*, vol. 1, p. 8, 2005.

[153] *LCR METER IM3536*. Available: https://www.hioki.com/en/products/detail/?product_key=5824

[154] E. P. Randviir and C. E. Banks, "Electrochemical impedance spectroscopy: an overview of bioanalytical applications," *Analytical Methods*, vol. 5, pp. 1098-1115, 2013.

[155] M. E. E. Alahi, X. Li, S. Mukhopadhyay, and L. Burkitt, "A Temperature Compensated Smart Nitrate-Sensor for Agricultural Industry," *IEEE Transactions on Industrial Electronics*, 2017.

[156] A. I. Zia, S. C. Mukhopadhyay, P.-L. Yu, I. H. Al-Bahadly, C. P. Gooneratne, and J. Kosel, "Rapid and molecular selective electrochemical sensing of phthalates in aqueous solution," *Biosensors and Bioelectronics*, vol. 67, pp. 342-349, 2015.

[157] A. M. Syaifudin, K. Jayasundera, and S. Mukhopadhyay, "A novel planar interdigital sensor based sensing and instrumentation for detection of dangerous contaminated chemical in seafood," in *Instrumentation and Measurement Technology Conference, 2009. I2MTC'09. IEEE*, 2009, pp. 701-706.

[158] T. Islam, Z. U. Rahman, and S. C. Mukhopadhyay, "A novel sol–gel thin-film constant phase sensor for high humidity measurement in the range of 50%–100% RH," *IEEE Sensors Journal*, vol. 15, pp. 2370-2376, 2015.

[159] T. Ramulu, R. Venu, B. Sinha, B. Lim, S. Jeon, S. Yoon, *et al.*, "Nanowires array modified electrode for enhanced electrochemical detection of nucleic acid," *Biosensors and Bioelectronics*, vol. 40, pp. 258-264, 2013.

[160] K. Cammann, B. Ross, A. Katerkamp, J. Reinbold, B. Gründig, and R. Renneberg, "Chemical and biochemical sensors," *Ullmann's Encyclopedia of Industrial Chemistry*, 1994.

[161] M. E. Tess and J. A. Cox, "Chemical and biochemical sensors based on advances in materials chemistry," *Journal of pharmaceutical and biomedical analysis*, vol. 19, pp. 55-68, 1999.

[162] S. Shtykov and T. Y. Rusanova, "Nanomaterials and nanotechnologies in chemical and biochemical sensors: capabilities and applications," *Russian Journal of General Chemistry*, vol. 78, pp. 2521-2531, 2008.

[163] E. Stern, A. Vacic, C. Li, F. N. Ishikawa, C. Zhou, M. A. Reed, *et al.*, "A Nanoelectronic Enzyme-Linked Immunosorbent Assay for Detection of Proteins in Physiological Solutions," *small*, vol. 6, pp. 232-238, 2010.

[164] S. Paulie, H. Perlmann, and P. Perlmann, "Enzyme-linked Immunosorbent Assay," *eLS*, 2003.

[165] S. D. Gan and K. R. Patel, "Enzyme immunoassay and enzyme-linked immunosorbent assay," *Journal of Investigative Dermatology*, vol. 133, p. e12, 2013.

[166] W. Putzbach and N. J. Ronkainen, "Immobilization techniques in the fabrication of nanomaterial-based electrochemical biosensors: A review," *Sensors*, vol. 13, pp. 4811-4840, 2013.

[167] R. Nojdelov and S. Nihtianov, "Capacitive-sensor interface with high accuracy and stability," *Instrumentation and Measurement, IEEE Transactions on*, vol. 58, pp. 1633-1639, 2009.

[168] C. Hsu and F. Mansfeld, "Technical note: concerning the conversion of the constant phase element parameter Y0 into a capacitance," *Corrosion,* vol. 57, pp. 747-748, 2001.

[169] L. D. Bolisay, J. N. Culver, and P. Kofinas, "Molecularly imprinted polymers for tobacco mosaic virus recognition," *Biomaterials,* vol. 27, pp. 4165-4168, 2006.

[170] F. Trotta, E. Drioli, C. Baggiani, and D. Lacopo, "Molecular imprinted polymeric membrane for naringin recognition," *Journal of membrane science,* vol. 201, pp. 77-84, 2002.

[171] M. Odabaşi, R. Say, and A. Denizli, "Molecular imprinted particles for lysozyme purification," *Materials Science and Engineering: C,* vol. 27, pp. 90-99, 2007.

[172] H. Huo, H. Su, and T. Tan, "Adsorption of Ag+ by a surface molecular-imprinted biosorbent," *Chemical Engineering Journal,* vol. 150, pp. 139-144, 2009.

[173] B. Sellergren, "Direct drug determination by selective sample enrichment on an imprinted polymer," *Analytical chemistry,* vol. 66, pp. 1578-1582, 1994.

[174] L. Ye and K. Haupt, "Molecularly imprinted polymers as antibody and receptor mimics for assays, sensors and drug discovery," *Analytical and bioanalytical chemistry,* vol. 378, pp. 1887-1897, 2004.

[175] G. Vlatakis, L. I. Andersson, R. Müller, and K. Mosbach, "Drug assay using antibody mimics made by molecular imprinting," 1993.

[176] T. Takeuchi, T. Mukawa, J. Matsui, M. Higashi, and K. D. Shimizu, "Molecularly imprinted polymers with metalloporphyrin-based molecular recognition sites coassembled with methacrylic acid," *Analytical chemistry,* vol. 73, pp. 3869-3874, 2001.

[177] P. T. Vallano and V. T. Remcho, "Affinity screening by packed capillary high-performance liquid chromatography using molecular imprinted sorbents: I. Demonstration of feasibility," *Journal of Chromatography A,* vol. 888, pp. 23-34, 2000.

[178] Y. Li, Q. Ma, Z. Liu, X. Wang, and X. Su, "A novel enzyme-mimic nanosensor based on quantum dot-Au nanoparticle@ silica mesoporous microsphere for the detection of glucose," *Analytica chimica acta,* vol. 840, pp. 68-74, 2014.

[179] A. Ersöz, V. G. Gavalas, and L. G. Bachas, "Potentiometric behavior of electrodes based on overoxidized polypyrrole films," *Analytical and bioanalytical chemistry,* vol. 372, pp. 786-790, 2002.

[180] E. Hedborg, F. Winquist, I. Lundström, L. I. Andersson, and K. Mosbach, "Some studies of molecularly-imprinted polymer membranes in combination with field-effect devices," *Sensors and actuators A: Physical,* vol. 37, pp. 796-799, 1993.

[181] T. áL Panasyuk and L. áM Sergeeva, "Conductimetric sensor for atrazine detection based on molecularly imprinted polymer membranes," *Analyst,* vol. 124, pp. 331-334, 1999.

[182] C. Malitesta, I. Losito, and P. G. Zambonin, "Molecularly imprinted electrosynthesized polymers: new materials for biomimetic sensors," *Analytical Chemistry,* vol. 71, pp. 1366-1370, 1999.

[183] P. Andrea and M. Stanislav, "A solid binding matrix/molecularly imprinted polymer-based sensor system for the determination of clenbuterol in bovine liver using differential-pulse voltammetry," *Sensors and Actuators B: Chemical,* vol. 76, pp. 286-294, 2001.

[184] Z. Cheng, E. Wang, and X. Yang, "Capacitive detection of glucose using molecularly imprinted polymers," *Biosensors and Bioelectronics,* vol. 16, pp. 179-185, 2001.

[185] J. Yin, G. Yang, and Y. Chen, "Rapid and efficient chiral separation of nateglinide and its l-enantiomer on monolithic molecularly imprinted polymers," *Journal of Chromatography A,* vol. 1090, pp. 68-75, 2005.

[186] H. Yan and K. H. Row, "Characteristic and synthetic approach of molecularly imprinted polymer," *International journal of molecular Sciences,* vol. 7, pp. 155-178, 2006.

[187] P. K. Owens, L. Karlsson, E. Lutz, and L. I. Andersson, "Molecular imprinting for bio-and pharmaceutical analysis," *TrAC Trends in Analytical Chemistry,* vol. 18, pp. 146-154, 1999.

[188] M. Kempe and K. Mosbach, "Receptor binding mimetics: A novel molecularly imprinted polymer," *Tetrahedron Letters,* vol. 36, pp. 3563-3566, 1995.

[189] S. Rimmer, "Synthesis of molecular imprinted polymer networks," *Chromatographia,* vol. 47, pp. 470-474, 1998.

[190] K. Hirayama, Y. Sakai, K. Kameoka, K. Noda, and R. Naganawa, "Preparation of a sensor device with specific recognition sites for acetaldehyde by molecular imprinting technique," *Sensors and Actuators B: Chemical,* vol. 86, pp. 20-25, 2002.

[191] F. Dickert, P. Lieberzeit, and M. Tortschanoff, "Molecular imprints as artificial antibodies—a new generation of chemical sensors," *Sensors and Actuators B: Chemical,* vol. 65, pp. 186-189, 2000.

[192] P. S. Sharma, F. D'Souza, and W. Kutner, "Molecular imprinting for selective chemical sensing of hazardous compounds and drugs of abuse," *TrAC Trends in Analytical Chemistry,* vol. 34, pp. 59-77, 2012.

[193] I. Chianella, M. Lotierzo, S. A. Piletsky, I. E. Tothill, B. Chen, K. Karim, *et al.*, "Rational design of a polymer specific for microcystin-LR using a computational approach," *Analytical chemistry,* vol. 74, pp. 1288-1293, 2002.

[194] L. Ye and K. Mosbach, "Molecularly imprinted microspheres as antibody binding mimics," *Reactive and Functional Polymers,* vol. 48, pp. 149-157, 2001.

[195] N. Lavignac, C. J. Allender, and K. R. Brain, "Current status of molecularly imprinted polymers as alternatives to antibodies in sorbent assays," *Analytica Chimica Acta,* vol. 510, pp. 139-145, 2004.

[196] F. Liu, X. Liu, S.-C. Ng, and H. S.-O. Chan, "Enantioselective molecular imprinting polymer coated QCM for the recognition of l-tryptophan," *Sensors and Actuators B: Chemical,* vol. 113, pp. 234-240, 2006.

[197] P. Spégel, L. Schweitz, and S. Nilsson, "Molecularly imprinted polymers in capillary electrochromatography: recent developments and future trends," *Electrophoresis,* vol. 24, pp. 3892-3899, 2003.

[198] N. Ul-Haq and J. K. Park, "Optical resolution of phenylalanine using D-Phe-imprinted poly (acrylic acid-co-acrylonitrile) membrane—Racemate solution concentration effect," *Polymer Composites,* vol. 29, pp. 1006-1013, 2008.

[199] A. Ellwanger, C. Berggren, S. Bayoudh, C. Crecenzi, L. Karlsson, P. K. Owens, *et al.*, "Evaluation of methods aimed at complete removal of template from molecularly imprinted polymers," *Analyst,* vol. 126, pp. 784-792, 2001.

[200] H. Khan and J. K. Park, "The preparation of D-phenylalanine imprinted microbeads by a novel method of modified suspension polymerization," *Biotechnology and Bioprocess Engineering,* vol. 11, pp. 503-509, 2006.

[201] B. R. Hart, D. J. Rush, and K. J. Shea, "Discrimination between enantiomers of structurally related molecules: separation of benzodiazepines by molecularly imprinted polymers," *Journal of the American Chemical Society,* vol. 122, pp. 460-465, 2000.

[202] A. Kugimiya, J. Matsui, T. Takeuchi, K. Yano, H. Muguruma, A. Elgersma, *et al.*, "Recognition of sialic acid using molecularly imprinted polymer," *Polymer—Plastics Technology and Engineering,* vol. 28, pp. 2317-2323, 1995.

[203] A. Sarhan and G. Wulff, "On polymers with enzyme-analogous structure. 14. Stereospecific binding by amide bonding or electrostatic interaction," *Makromolekulare Chemie-Macromolecular Chemistry and Physics,* vol. 183, pp. 1603-1614, 1982.

[204] L. I. Andersson, "Molecular imprinting: developments and applications in the analytical chemistry field," *Journal of Chromatography B: Biomedical Sciences and Applications,* vol. 745, pp. 3-13, 2000.

[205] J. Svenson, J. G. Karlsson, and I. A. Nicholls, "1H nuclear magnetic resonance study of the molecular imprinting of (−)-nicotine: template self-association, a molecular basis for cooperative ligand binding," *Journal of Chromatography A,* vol. 1024, pp. 39-44, 2004.

[206] D. A. Spivak, "Optimization, evaluation, and characterization of molecularly imprinted polymers," *Advanced Drug Delivery Reviews,* vol. 57, pp. 1779-1794, 2005.

[207] B. Ekberg and K. Mosbach, "Molecular imprinting: A technique for producing specific separation materials," *Trends in Biotechnology,* vol. 7, pp. 92-96, 1989.

[208] B. Sellergren, "Molecular imprinting by noncovalent interactions. Enantioselectivity and binding capacity of polymers prepared under conditions favoring the formation of template complexes," *Die Makromolekulare Chemie,* vol. 190, pp. 2703-2711, 1989.

[209] H. Kim and D. A. Spivak, "New insight into modeling non-covalently imprinted polymers," *Journal of the American Chemical Society,* vol. 125, pp. 11269-11275, 2003.

[210] M. Esfandyari-Manesh, M. Javanbakht, F. Atyabi, A. Badiei, and R. Dinarvand, "Effect of porogenic solvent on the morphology, recognition and release properties of carbamazepine-molecularly imprinted polymer nanospheres," *Journal of Applied Polymer Science,* vol. 121, pp. 1118-1126, 2011.

[211] G. Wulff, A. Sarhan, and K. Zabrocki, "Enzyme-analogue built polymers and their use for the resolution of racemates," *Tetrahedron Letters,* vol. 14, pp. 4329-4332, 1973.

[212] P. Li, F. Rong, and C. Yuan, "Morphologies and binding characteristics of molecularly imprinted polymers prepared by precipitation polymerization," *Polymer international,* vol. 52, pp. 1799-1806, 2003.

[213] J. Wang, P. A. Cormack, D. C. Sherrington, and E. Khoshdel, "Monodisperse, molecularly imprinted polymer microspheres prepared by precipitation polymerization for affinity separation applications," *Angewandte Chemie International Edition,* vol. 42, pp. 5336-5338, 2003.

[214] A. G. Mayes and K. Mosbach, "Molecularly imprinted polymer beads: suspension polymerization using a liquid perfluorocarbon as the dispersing phase," *Analytical Chemistry,* vol. 68, pp. 3769-3774, 1996.

[215] X. Shen, T. Zhou, and L. Ye, "Molecular imprinting of protein in Pickering emulsion," *Chem. Commun.,* vol. 48, pp. 8198-8200, 2012.

[216] M. W. Noh and D. C. Lee, "Synthesis and characterization of PS-clay nanocomposite by emulsion polymerization," *Polymer Bulletin,* vol. 42, pp. 619-626, 1999.

[217] A. Ersöz, A. Denizli, A. Özcan, and R. Say, "Molecularly imprinted ligand-exchange recognition assay of glucose by quartz crystal microbalance," *Biosensors and Bioelectronics,* vol. 20, pp. 2197-2202, 2005.

[218] C. Wang, A. Javadi, M. Ghaffari, and S. Gong, "A pH-sensitive molecularly imprinted nanospheres/hydrogel composite as a coating for implantable biosensors," *Biomaterials,* vol. 31, pp. 4944-4951, 2010.

[219] A. V. Mamishev, K. Sundara-Rajan, Y. Fumin, D. Yanqing, and M. Zahn, "Interdigital sensors and transducers," *Proceedings of the IEEE,* vol. 92, pp. 808-845, 2004.

[220] T. Coan, G. S. Barroso, G. Motz, A. Bolzán, and R. A. F. Machado, "Preparation of PMMA/hBN composite coatings for metal surface protection," *Materials Research,* vol. 16, pp. 1366-1372, 2013.

[221] H.-C. Wang, A. Zyuzin, and A. V. Mamishev, "Measurement of coating thickness and loading using concentric fringing electric field sensors," *IEEE Sensors Journal,* vol. 14, pp. 68-78, 2014.

[222] A. Azmi, A. A. Azman, K. K. Kaman, S. Ibrahim, S. C. Mukhopadhyay, S. W. Nawawi, *et al.,* "Performance of Coating Materials on Planar Electromagnetic Sensing Array to Detect Water Contamination," *IEEE Sensors Journal,* 2017.

[223] J. Snoeijer, J. Ziegler, B. Andreotti, M. Fermigier, and J. Eggers, "Thick films of viscous fluid coating a plate withdrawn from a liquid reservoir," *Physical review letters,* vol. 100, p. 244502, 2008.

[224] S. Krishnan, C. J. Weinman, and C. K. Ober, "Advances in polymers for anti-biofouling surfaces," *Journal of Materials Chemistry,* vol. 18, pp. 3405-3413, 2008.

[225] A. E. Nel, L. Mädler, D. Velegol, T. Xia, E. M. Hoek, P. Somasundaran, *et al.*, "Understanding biophysicochemical interactions at the nano–bio interface," *Nature materials,* vol. 8, pp. 543-557, 2009.

[226] M. L. Yola, T. Eren, and N. Atar, "A sensitive molecular imprinted electrochemical sensor based on gold nanoparticles decorated graphene oxide: Application to selective determination of tyrosine in milk," *Sensors and Actuators B: Chemical,* vol. 210, pp. 149-157, 2015.

[227] A. Aghaei, M. R. M. Hosseini, and M. Najafi, "A novel capacitive biosensor for cholesterol assay that uses an electropolymerized molecularly imprinted polymer," *Electrochimica Acta,* vol. 55, pp. 1503-1508, 2010.

[228] S. Viswanathan, C. Rani, S. Ribeiro, and C. Delerue-Matos, "Molecular imprinted nanoelectrodes for ultra sensitive detection of ovarian cancer marker," *Biosensors and Bioelectronics,* vol. 33, pp. 179-183, 2012.

[229] M. Nebi and D. Peker, "Effect of Heat Treatment on the Structural Properties of TiO2 Films Produced by Sol-Gel Spin Coating Technique," in *Journal of Physics: Conference Series,* 2016, p. 012026.

[230] S. Ilican, "Structural, Optical and Electrical Properties of Erbium-Doped ZnO Thin Films Prepared by Spin Coating Method," *Journal of Nanoelectronics and Optoelectronics,* vol. 11, pp. 465-471, 2016.

[231] M. Wong, R. Ishige, K. L. White, P. Li, D. Kim, R. Krishnamoorti, *et al.*, "Large-scale self-assembled zirconium phosphate smectic layers via a simple spray-coating process," *Nature communications,* vol. 5, p. 3589, 2014.

[232] Y. Guo, W. Li, H. Yu, D. F. Perepichka, and H. Meng, "Flexible Asymmetric Supercapacitors via Spray Coating of a New Electrochromic Donor–Acceptor Polymer," *Advanced Energy Materials,* vol. 7, 2017.

[233] D. Grosso, "How to exploit the full potential of the dip-coating process to better control film formation," *Journal of Materials Chemistry,* vol. 21, pp. 17033-17038, 2011.

[234] S. H. Chaki, M. Deshpande, and J. P. Tailor, "Characterization of CuS nanocrystalline thin films synthesized by chemical bath deposition and dip coating techniques," *Thin Solid Films,* vol. 550, pp. 291-297, 2014.

[235] R. Ashiri, A. Nemati, and M. S. Ghamsari, "Crack-free nanostructured BaTiO 3 thin films prepared by sol–gel dip-coating technique," *Ceramics International,* vol. 40, pp. 8613-8619, 2014.

[236] X. Zhang, H. Ye, B. Xiao, L. Yan, H. Lv, and B. Jiang, "Sol− gel preparation of PDMS/Silica hybrid antireflective coatings with controlled thickness and durable antireflective performance," *The Journal of Physical Chemistry C,* vol. 114, pp. 19979-19983, 2010.

[237] C. Alexander, H. S. Andersson, L. I. Andersson, R. J. Ansell, N. Kirsch, I. A. Nicholls, *et al.*, "Molecular imprinting science and technology: a survey of the literature for the years up to and including 2003," *Journal of molecular recognition,* vol. 19, pp. 106-180, 2006.

[238] A. Bossi, F. Bonini, A. Turner, and S. Piletsky, "Molecularly imprinted polymers for the recognition of proteins: the state of the art," *Biosensors and Bioelectronics,* vol. 22, pp. 1131-1137, 2007.

[239] G. Díaz-Díaz, D. Antuña-Jiménez, M. Carmen Blanco-López, M. Jesús Lobo-Castañón, A. J. Miranda-Ordieres, and P. Tuñón-Blanco, "New materials for analytical biomimetic assays based on affinity and catalytic receptors prepared by molecular imprinting," *TrAC Trends in Analytical Chemistry,* vol. 33, pp. 68-80, 2012.

[240] K. Hsieh, B. S. Ferguson, M. Eisenstein, K. W. Plaxco, and H. T. Soh, "Integrated electrochemical microsystems for genetic detection of pathogens at the point of care," *Accounts of chemical research,* vol. 48, pp. 911-920, 2015.

[241] D. A. Cook, K. J. Sorensen, R. A. Nishimura, S. R. Ommen, and F. J. Lloyd, "A comprehensive information technology system to support physician learning at the point of care," *Academic Medicine,* vol. 90, pp. 33-39, 2015.

[242] J. Sun, Y. Xianyu, and X. Jiang, "Point-of-care biochemical assays using gold nanoparticle-implemented microfluidics," *Chemical Society Reviews,* vol. 43, pp. 6239-6253, 2014.

[243] R. Sista, Z. Hua, P. Thwar, A. Sudarsan, V. Srinivasan, A. Eckhardt, *et al.*, "Development of a digital microfluidic platform for point of care testing," *Lab on a Chip,* vol. 8, pp. 2091-2104, 2008.

[244] A. K. Yetisen, M. S. Akram, and C. R. Lowe, "based microfluidic point-of-care diagnostic devices," *Lab on a Chip,* vol. 13, pp. 2210-2251, 2013.

[245] J. P. Lafleur, A. Jönsson, S. Senkbeil, and J. P. Kutter, "Recent advances in lab-on-a-chip for biosensing applications," *Biosensors and Bioelectronics,* vol. 76, pp. 213-233, 2016.

[246] G. Luka, A. Ahmadi, H. Najjaran, E. Alocilja, M. DeRosa, K. Wolthers, *et al.*, "Microfluidics integrated biosensors: a leading technology towards lab-on-a-chip and sensing applications," *Sensors*, vol. 15, pp. 30011-30031, 2015.

[247] C. Parolo, A. de la Escosura-Muniz, and A. Merkoci, "Electrochemical DNA Sensors Based on Nanoparticles," *Electrochemical Biosensors*, p. 195, 2015.

[248] Y. Uludag, E. Esen, G. Kokturk, H. Ozer, T. Muhammad, Z. Olcer, *et al.*, "Lab-on-a-chip based biosensor for the real-time detection of aflatoxin," *Talanta*, vol. 160, pp. 381-388, 2016.

[249] Y. Uludag, F. Narter, E. Sağlam, G. Köktürk, M. Y. Gök, M. Akgün, *et al.*, "An integrated lab-on-a-chip-based electrochemical biosensor for rapid and sensitive detection of cancer biomarkers," *Analytical and bioanalytical chemistry*, vol. 408, pp. 7775-7783, 2016.

[250] Y. Wu, P. Xue, Y. Kang, and K. M. Hui, "based microfluidic electrochemical immunodevice integrated with nanobioprobes onto graphene film for ultrasensitive multiplexed detection of cancer biomarkers," *Analytical chemistry*, vol. 85, pp. 8661-8668, 2013.

[251] Y. Wu, P. Xue, K. M. Hui, and Y. Kang, "A paper-based microfluidic electrochemical immunodevice integrated with amplification-by-polymerization for the ultrasensitive multiplexed detection of cancer biomarkers," *Biosensors and Bioelectronics*, vol. 52, pp. 180-187, 2014.

[252] G. Korotcenkov, V. Brinzari, and B. K. Cho, "Conductometric gas sensors based on metal oxides modified with gold nanoparticles: a review," *Microchimica Acta*, vol. 183, pp. 1033-1054, 2016.

[253] D. Q. Hung, O. Nekrassova, and R. G. Compton, "Analytical methods for inorganic arsenic in water: a review," *Talanta*, vol. 64, pp. 269-277, 2004.

[254] S. M. R. Islam, D. Kwak, M. H. Kabir, M. Hossain, and K. S. Kwak, "The Internet of Things for Health Care: A Comprehensive Survey," *IEEE Access*, vol. 3, pp. 678-708, 2015.

[255] Thingspeak. (2017, 26/08/2017). *Thingspeak*. Available: https://thingspeak.com/

[256] A. Website. (2017, 26/08/2017). *Ciao*. Available: https://www.arduino.cc/en/Reference/Ciao

[257] Arduino. (2017, 4/09/2017). *Arduino Uno WiFi*. Available: https://store.arduino.cc/usa/arduino-uno-wifi

[258] A. Devices. (04/09/2017). *AD5933: Impedance Analyzer*. Available: http://www.analog.com/media/en/technical-documentation/data-sheets/AD5933.pdf

[259] A. Devices. (2017, 08/09/2017). *ADG849*. Available: http://www.analog.com/media/en/technical-documentation/data-sheets/ADG849.pdf

[260] A. Device. (2017, 08/09/2017). *Direct Digital Synthesis*. Available: http://www.analog.com/media/en/analog-dialogue/volume-38/number-3/articles/all-about-direct-digital-synthesis.pdf

[261] J. Mankar, C. Darode, K. Trivedi, M. Kanoje, and P. Shahare, "Review of I2C protocol," *International Journal*, vol. 2, 2014.

[262] Arduino. (2017). *Arduino*. Available: https://www.arduino.cc/en/Guide/Environment

[263] *UrineCartiLaps*. Available: http://peramed.com/peramed/docs/AC-10F1_EN.pdf

[264] B. Khadro, A. Betatache, C. Sanglar, A. Bonhommé, A. Errachid, and N. Jaffrezic-Renault, "Molecularly imprinted polymers (MIP) based electrochemical sensor for detection of urea and creatinine," *Sensor Letters*, vol. 9, pp. 2261-2264, 2011.

[265] M.-H. Lee, T.-C. Tsai, J. L. Thomas, and H.-Y. Lin, "Recognition of creatinine by poly (ethylene-co-vinylalcohol) molecular imprinting membrane," *Desalination*, vol. 234, pp. 126-133, 2008.

[266] P. Khashayar, H. Aghaei Meybodi, G. Amoabediny, and B. Larijani, "Biochemical markers of bone turnover and their role in osteoporosis diagnosis: a narrative review," *Recent patents on endocrine, metabolic & immune drug discovery*, vol. 9, pp. 79-89, 2015.

[267] S. Petra and A. Gerald, "Multiplexed point-of-care testing-xPOCT," *Trends in biotechnology*, 2017.

[268] F. Piraino, F. Volpetti, C. Watson, and S. J. Maerkl, "A digital–analog microfluidic platform for patient-centric multiplexed biomarker diagnostics of ultralow volume samples," *ACS nano*, vol. 10, pp. 1699-1710, 2016.

[269] F. Piraino, *Diagnostic Devices with Microfluidics*: CRC Press, 2017.

[270] C. Branger, W. Meouche, and A. Margaillan, "Recent advances on ion-imprinted polymers," *Reactive and Functional Polymers*, vol. 73, pp. 859-875, 2013.

[271] T. Alizadeh, A. N. Shamkhali, Y. Hanifehpour, and S. W. Joo, "A Ca 2+ selective membrane electrode based on calcium-imprinted polymeric nanoparticles," *New Journal of Chemistry*, vol. 40, pp. 8479-8487, 2016.